RD&E CENTER

Technical Report

No. 13315

MM&T ADVANCED BALANCING/MACHINING

CONTRACT NO. DAAE07-85-C-R163

NOVEMBER 1988

Albert Kalbfleisch
Charles Turcotte
Textron Lycoming, Stratford, CT
Dr. Alex Ballantyne
Dr. Henry Eppich
By Avco Research Laboratory Textron, Everett, MA

U.S. ARMY TANK-AUTOMOTIVE COMMAND
RESEARCH, DEVELOPMENT & ENGINEERING CENTER
Warren, Michigan 48397-5000

NOTICES

This report is not to be construed as an official Department of the Army position.

Mention of any trade names or manufacturers in this report shall not be construed as an official endorsement or approval of such products or companies by the U.S. Government.

Destroy this report when it is no longer needed. Do not return it to the originator.

REPORT DOCUMENTATION PAGE

Form Approved
OMB No 0704-0188
Exp. Date Jun 30, 1986

1a REPORT SECURITY CLASSIFICATION Unclassified	1b. RESTRICTIVE MARKINGS
2a. SECURITY CLASSIFICATION AUTHORITY	3. DISTRIBUTION/AVAILABILITY OF REPORT Approved for Public Release Distribution is Unlimited
2b. DECLASSIFICATION/DOWNGRADING SCHEDULE	
4 PERFORMING ORGANIZATION REPORT NUMBER(S)	5 MONITORING ORGANIZATION REPORT NUMBER(S) . 11315
6a NAME OF PERFORMING ORGANIZATION Textron Lycoming 6b OFFICE SYMBOL (If applicable)	7a. NAME OF MONITORING ORGANIZATION U.S. Army Tank Automotive Command
6c. ADDRESS (City, State, and ZIP Code) 550 Main Street Stratford, CT 06497-2452	7b. ADDRESS (City, State, and ZIP Code) Warren, MI 48397-5000
8a. NAME OF FUNDING/SPONSORING ORGANIZATION U.S. Army TACOM 8b. OFFICE SYMBOL (If applicable) AMSTA-TMM	9. PROCUREMENT INSTRUMENT IDENTIFICATION NUMBER DAAE07-85-C-R163
8c. ADDRESS (City, State, and ZIP Code) Warren, MI 48397-5000	10. SOURCE OF FUNDING NUMBERS PROGRAM ELEMENT NO. / PROJECT NO. / TASK NO. / WORK UNIT ACCESSION NO

11. TITLE (Include Security Classification)
MM&T Advanced Balancing/Machining (u)

12. PERSONAL AUTHOR(S) Kalbfleisch, Albert and Turcotte, Charles - Lycoming and Ballantyne, Dr. Alex and Eppich, Dr. Henry - Avco Research Laboratory

13a. TYPE OF REPORT	13b. TIME COVERED	14. DATE OF REPORT (Year, Month, Day)	15. PAGE COUNT
Final	FROM 85,10 TO 87,10	88,11	

16. SUPPLEMENTARY NOTATION
A portion of the reported effort was performed at the Avco Research Laboratory, Everett, MA.

17. COSATI CODES		
FIELD	GROUP	SUB-GROUP

18. SUBJECT TERMS (Continue on reverse if necessary and identify by block number)
Balancing, Laser, Turbine Engines, Machining, ~~Nd:YAG~~

19. ABSTRACT (Continue on reverse if necessary and identify by block number)

A laser balancing system was developed and successfully demonstrated. The system uses a pulsed Nd:YAG laser to remove metal from the part while it is rotating in the balancing machine. Computer algorithms were developed which accepted imbalance information from the balancing machine and generated firing signals for the laser. This system balanced AGT1500 compressor impellers to less than one half the allowable imbalance under full computer control. Preliminary low cycle fatigue testing showed no major differences between laser irradiated test bars and hand ground and burnished test bars.

20 DISTRIBUTION/AVAILABILITY OF ABSTRACT	21 ABSTRACT SECURITY CLASSIFICATION
☒ UNCLASSIFIED/UNLIMITED ☐ SAME AS RPT. ☐ DTIC USERS	Unclassified

22a NAME OF RESPONSIBLE INDIVIDUAL	22b TELEPHONE (Include Area Code)	22c. OFFICE SYMBOL
John Herbert	(313) 574-8718	AMSTA-TMM

DD FORM 1473, 84 MAR 83 APR edition may be used until exhausted
All other editions are obsolete

SECURITY CLASSIFICATION OF THIS PAGE

SUMMARY

Stratford Army Engine Plant (SAEP) and Avco Research Laboratory (ARL) have demonstrated the methodology and the feasibility of implementing a laser-machined balancing process that can work in a production environment to balance turbine engine components.

SAEP and ARL have worked together to complete the task of developing a computer-controlled, laser-machining balancer system. The following tasks have been completed successfully during the contract:

- SAEP provided AGT1500 impellers and Lycoming fatigue specifmens for testing during the various stages of the system development.
- ARL integrated laser, optics, computer control and balancer hardware. They also developed control software and algorithms to test hardware to do material tests.
- ARL designed and fabricated a material "spatter" removal system.
- ARL balanced the A and B planes of the AGT1500 impeller.
- SAEP has conducted metallographic examinations of irradiated impeller samples and Lycoming fatigue specimens. Life cycle tests were done on both ground and irradiated fatigue specimens.

It is recommended that some enhancements be made to the existing system with regard to reliability and ease of operation, to facilitate implementation into production. The next development phase will include increasing the number of parts and materials and also the engineering development of multiple-balance, multiple laser system capabilities.

PREFACE

We recognize the efforts of at least two other companies known to be developing laser machined balance capabilities:

- Schenck Trebel--principally in the application to the balance of gyro rotors.
- MTI--application of the technology to gyros, dental drills, impellers and shafts.

Their development programs have been directed toward small parts with simple irradiation requirements, governed by simple algorithms.

We wish to thank our project staff and the support personnel for their efforts in successfully completing this contract, including:

ARL:
Dr. Alex Ballantyne, Principle Investigator
Jim Cunningham, System Integration
Henry Eppich, Algorithm Development
Paul Gozewski, Technician

SAEP:
Phil Follo, Materials Testing
Al Kalbfleisch, Project Leader
Jerry Pedrosa, Project Manager
Charles Turcotte, MM&T Program Manager
Don Wilson, Materials Testing
Rolf Paulson, Materials Engineer
Ramesh Mehta, Staff Engineer

TABLE OF CONTENTS

TABLE OF CONTENTS (Continued)

LIST OF ILLUSTRATIONS

LIST OF ILLUSTRATIONS (Continued)

LIST OF ILLUSTRATIONS (Continued)

1.0. INTRODUCTION

This final report, prepared by Stratford Army Engine Plant (SAEP) and Avco Research Laboratory, Inc. (ARL) for (DAAE07-85-C-R163) the U.S. Army Tank-Automotive Command (TACOM), describes the development of a cost-effective laser machining process for the balancing of AGT1500 impellers.

The high operating speeds of current gas turbine engines make the vibratory stresses associated with rotor imbalance a major concern. Higher power-to-weight ratios planned for advanced engines will make this an even more critical issue in the future. The currently established manufacturing procedures for the AGT1500 engine involve the balancing of rotating components on an iterative basis. The rotating components are balanced on a machine which uses computer-based diagnostics to identify the amount and location of material which must be removed to bring the part within specifications. The part is then marked, removed from the balance machine and material is taken off at a separate work station by hand grinding. The part is then rechecked on the balance machine and reground in an iterative manner until it is within design tolerances.

Balance completion time for the above process ranges from minutes to days depending on the condition of the components and the skill and experience of the operators. In addition to being time consuming, the process is subject to errors with regard to the actual location and amount of materials removed. The result may be a final inspection component having an unnecessarily large amount of material removed due to the trial-and-error nature of the process. This can lead to future problems if a component must be balanced a number of times during its lifetime. Finally, future engine design, because of higher operating speeds, will have even tighter balance specifications and physically smaller components. This may create material removal tolerances which are beyond those achievable by the current hand grinding process.

It is clear from the above discussion that a fully automated, precision, integrated balancer/material removal system provides significant manufacturing benefits for the AGT1500 and future production engines. It will improve productivity, permit the use of less skilled personnel, and significantly reduce labor costs and balance time. In addition, it will improve part quality in the areas of precision, repeatability, and lower scrappage rates.

An integrated, computer-controlled laser/balance machine is the most attractive approach for an advanced, automated gas turbine component balancing system. This is because lasers lend themselves to the rapid, easily controlled and precise removal of material.

Based on the above discussion, it became clear that the following items needed to be addressed for an AGT1500 laser balance system:

- Demonstrate the balancing of a disk, with particular attention to control of the melted material.

- Tailor the geometry of the material removal region to simulate hand grinding geometry and thereby reduce stress concentrations.

- Demonstrate that none of the AGT1500 alloys of interest will experience microstructural material damage, which would have a significant, detrimental effect on the structural integrity of the components.

- Demonstrate the operation of an automated prototype unit with due consideration to safety and the anticipated skill of operators.

2.0. OBJECTIVES

The objective of this contract is to develop a computer-controlled, laser-machining balancer system. Specifically:

- Provide AGT1500 impellers and Lycoming fatigue specimens for testing during the various stages of the system development.

- Develop control software and algorithms in order to integrate laser, optics, computer control and balancer hardware.

- Design and fabricate a material "spatter" removal system.

- Balance the A and B planes of the AGT1500 impeller.

- Conduct metallographic examinations of irradiated impeller samples and Lycoming fatigue specimens. Perform life cycle tests on both hand ground and irradiated "Test Bars."

3.0. CONCLUSIONS

All of the objectives outlined in Section 2 were met. The feasibility of laser machining parts, while spinning on the balance machine, is now proven. The materials testing shows material properties and life cycle properties, comparable to the hand ground samples.

4.0. RECOMMENDATIONS

The experience resulting from achieving our objectives demonstrated the need for some enhancements, which would improve productivity, during system operation namely, the incorporation of remote video focus and alignment systems that can be operated from a control console. They would provide more accurate and rapid completion of the part setup process.

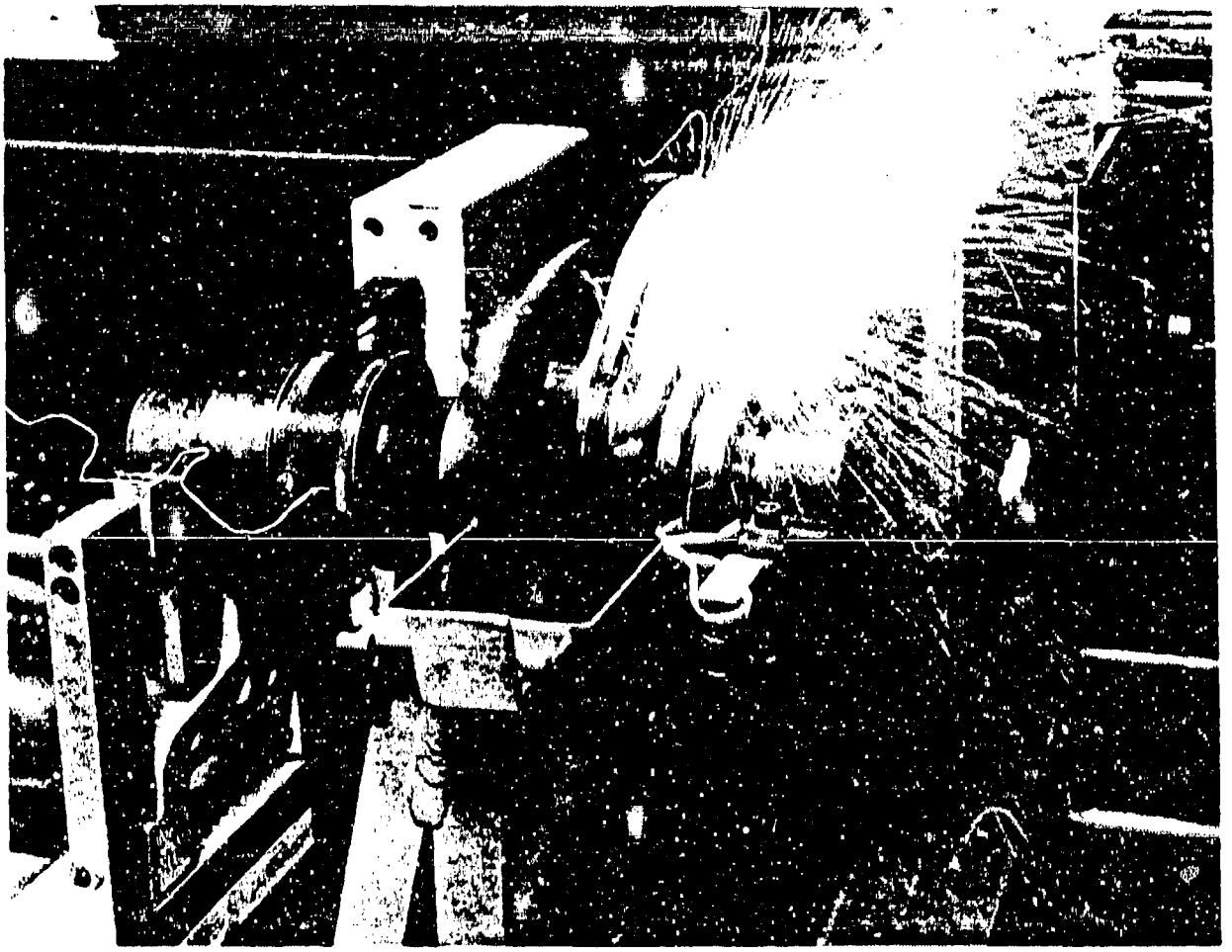

Figure 3-1. Irridation of B-Plane

Figure 3-2. Irridation of A-Plane

5.0. DISCUSSION

5.1. System Design and Fabrication

5.1.1. Design Methodologies. The laser-machined balancing system, as pointed out in the introduction, is able to take advantage of several appropriate technologies. This enables the system to be implemented with "off-the-shelf" components. The keys to achievement of the desired goals are those of system integration and of methodology development for the laser system to emulate conventional hand grinding and perform, under fully automated conditions, controlled and desirable mass removal.

The design methodology is illustrated schematically in Figure 5-1. Knowledge of the laser surface interaction phenomenology, the balance machine operating conditions, along with specification of requirements and adequate diagnostics, enabled an optimal removal operation to be defined. Under these guidelines it was possible to define an overall system concept based upon several key requirements:

- The majority of the system components were to be easily available from commercial vendors and specifically take advantage of the existing balance machine technology and equipment available at SAEP.
- The system was required to be flexible in operation, allowing for changes in procedures, geometries and programming.
- The control and computational elements of the process should be under the direction of a single, unified process controller.

The overall system layout is illustrated in Figure 5-2. It can be seen to resolve into four key elements: existing balance machine hardware, laser and control hardware, system software, and finally, part specifications and sequencing. The existing hardware consisted of the actual balance machine and also of its associated microprocessor and diagnostic equipment. This provides the basic information upon which the automated laser balancing system relies--imbalance angle and amount, the rotational speed and a reference timing marker. The laser system, consisting of a short pulse laser of sufficient power, is required to be fired under the control of a timing and synchronization system that uses data from the balancer via a digital interface. The delivery of the laser energy to the correct location on the rotor requires a motorized traverse assembly with its associated optics. The hardware structure of the system requires substantial software support in order to carry out the balancing procedure. This includes software elements to control the firing of the laser, control the motion of the optics, define and control the location of the beam focus with respect to the rotor surface, and most importantly, define the mass removal from the rotor via suitable algorithms. All of this software requires procedural information in order to operate--this includes, geometry and past

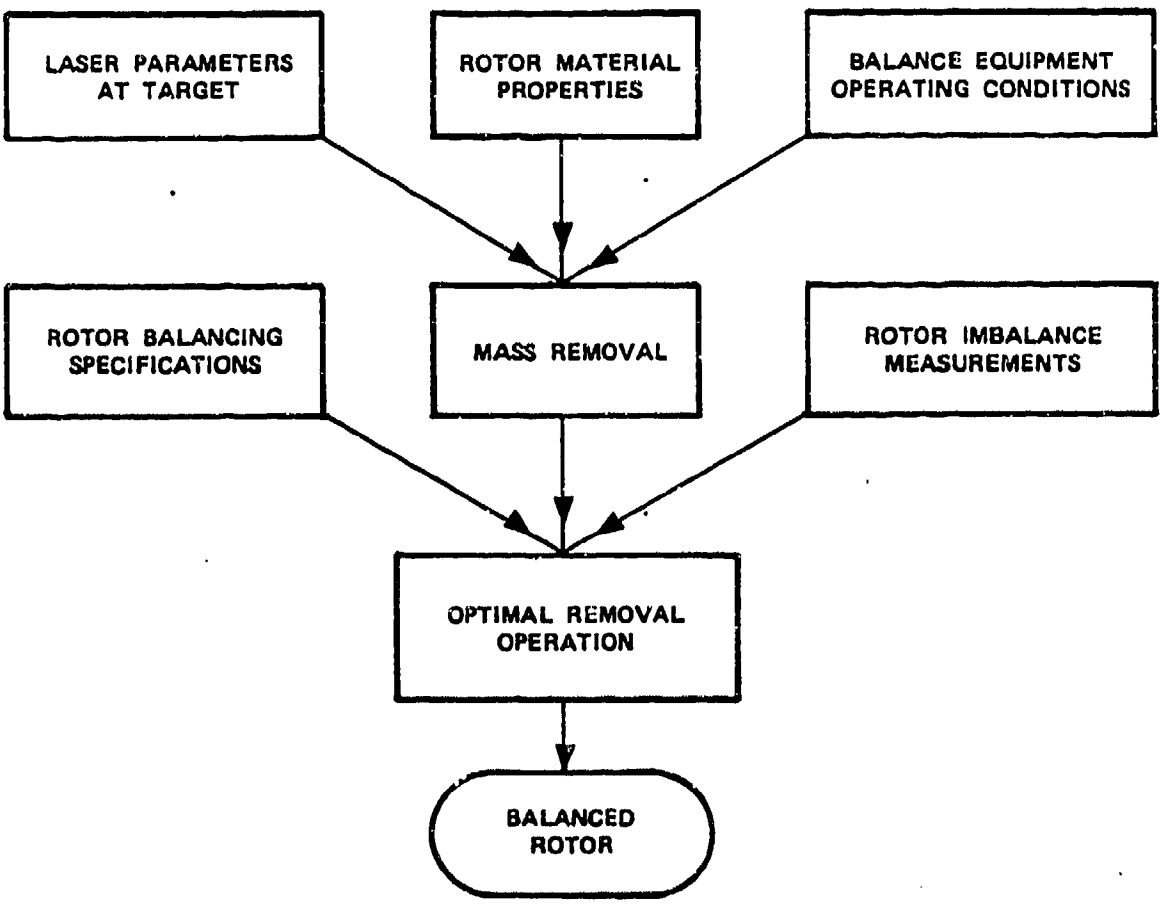

Figure 5-1. Laser Balance Design Methodology

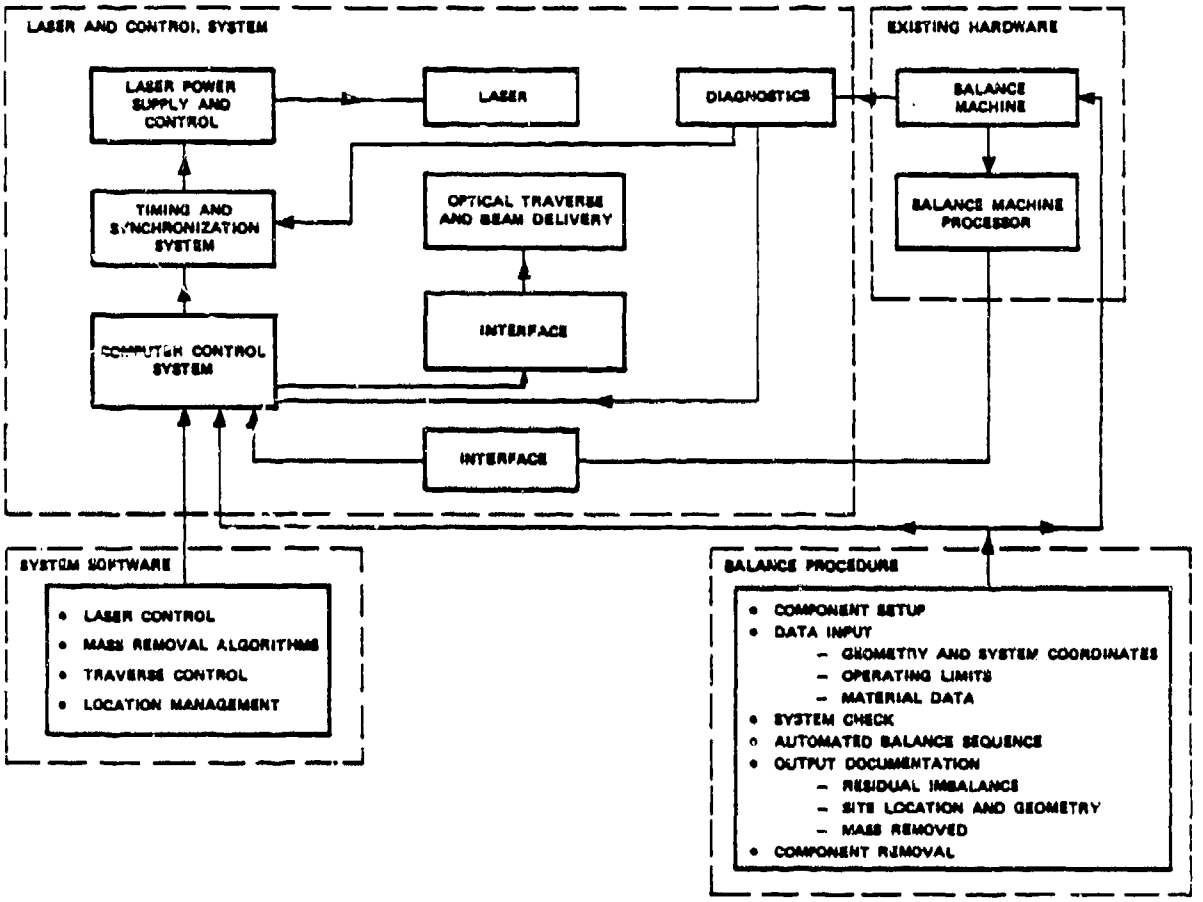

Figure 5-2. Conceptual Framework for System Design

specific data, balancing sequence specification, documentation requirements, as well as calibration and check-out diagnostic requirements.

The following sections describe each of these elements in more detail. The hardware structure is then discussed, with the procedural and algorithm structure following in Section 5.2.

5.1.2. Laser Selection. The requirements necessitate the use of a pulsed laser for optimum mass removal and balancing. A Neodymium-YAG Laser is the most appropriate choice at this time, with its range of operating pulse repetition frequencies exceeding the present balance procedure requirements (15-25 Hz, or 900-1,500 r/min). This enables mass removal to be performed in as efficient a manner as is possible, with a laser pulse coinciding with each rotor revolution. The laser selected as having the necessary requirements is a Control Laser Model 440-B High-Energy System, which is a nominal 200-watt average power system.

The rational for the 200-watt system was that of its being the smallest adequate system to deliver enough energy per pulse that can remove mass from the rotor at its nominal required balancing speed. The laser, with its 13-Joule, 0.65-msec pulse and with the system-imposed focusing optic constraints, is capable of providing a reasonable mass removal efficiency, (see Figure 5-3). The preferred region, to operate the laser, would be near (above) the small spot limit; but not into the plasma ignition area of the curve. In addition, with the inferred mass removal efficiency, the estimated balancing timescales are typically better than those achievable with conventional procedures.

This laser potentially offered some other advantages, which were explored. Its controller, a Laserbrain Microcomputer controller, has the capability of being internally programmed to control up to a five-axis traverse system with an RS232 interface capability. Unfortunately, this was found not to be adaptable to real-time uploading from an external computer and could, therefore, not be used to provide optical system position control.

The major issue with laser selection proved to be, as expected, the accurate control of laser firing time. Under the constraints of a rotating target, with a spatial error in burn location of one laser spot diameter, the requirement becomes 50usec jitter in firing time. Using the Laserbrain external trigger circuit was not adequate, even with software modification. A modification was proposed by Control Laser, providing direct triggering of the laser itself, giving a jitter of 10usec.

The external control interface delivered by Control Laser was found to present a potentially fatal flaw. The operation of the laser under external control, requires that some of the internal system safety

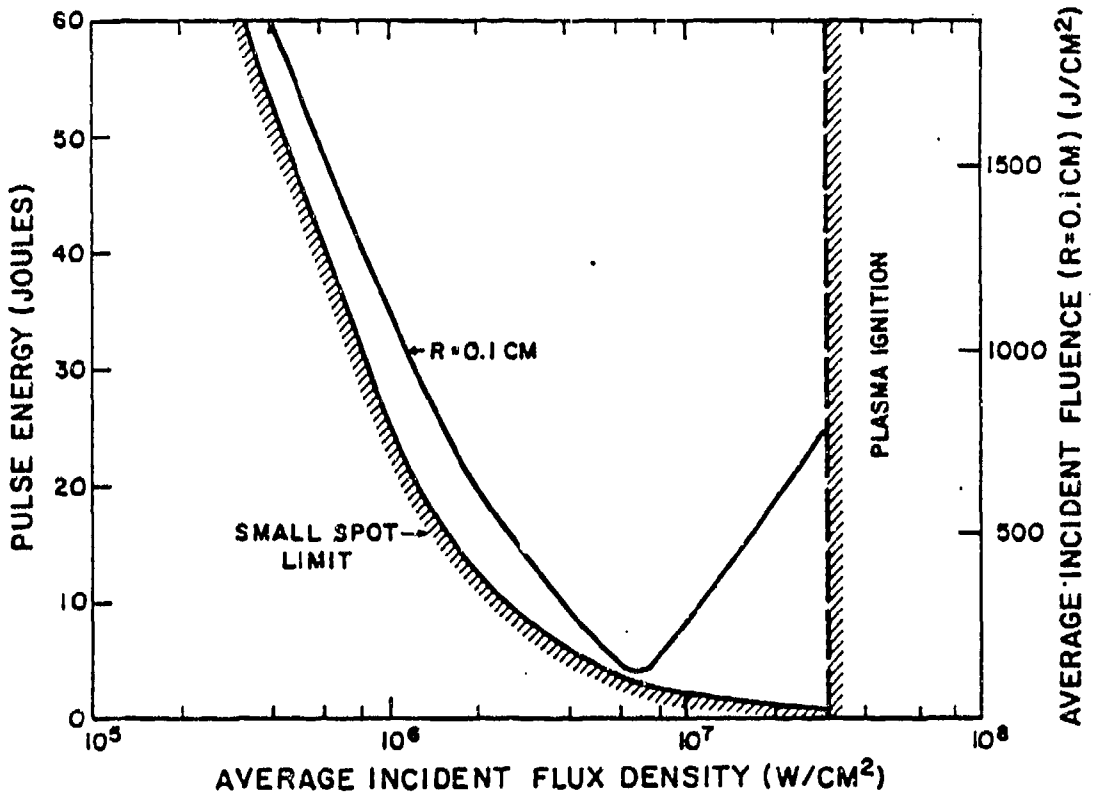

Figure 5-3. Pulse Energy Requirements for Efficient Mass Removal

interlocks be defeated. In particular, this offered the potential for damage of the power supply modules if an accidental external trigger signal were sent to the controller when the laser high-voltage system was inoperative. As this could be a forced situation, when the laser external safety interlock switches were opened (as for example, a consequence of an external door being opened), it was perceived as a threat to laser system integrity. Considerable effort was expended in the provision of an adequate interlock system that would prevent the transmission of external control signals unless the high-voltage system was energized. This necessitated the modification of the controller interface board (Figure 5-4) to provide an Electronic Industry Standard for Digital I/O Volt (TTL) output to the computer, appraising it of the HV status. The first implementation of this was found to have a flaw, as the HV status indication could be circumvented by external safety switch cut-out. This was replaced by use of the HV simmer voltage status indicator which truly reflected the power condition of the capacitor bank.

The control lines go through two opto-isolator stages, one within the laser and one in the computer rack. This helps reduce any laser-generated noise being picked up by the wiring and input into the computer backplane.

5.1.3. Balance Machine Selection. The balance machine selected for this program was a Gilman Gesholt, model #3S machine, equipped with a BP2020 microprocessor system. This machine is a soft bearing system, driven by a constant speed motor via belt drive. This machine is of the type used at SAEP for balancing of the components chosen for study under this program (i.e., the high-pressure compressor impeller on the AGT1500 engine). The calculated resolution for this machine, using the test rotor/impeller is .0064 gm-in.

5.1.4. Computer Selection. The approach taken for design of the control and computational aspects of the system was predicated upon a key technology. This is the availability of numerous interfacing and control products compatible and specifically designed for IBM compatible personal computers. This provides us with a cost-effective solution and a large degree of flexibility in layout and specific interfacing systems. The computer system chosen is a Compaq Deskpro 286 personal computer (PC) with 512 Kilobyte (KB) memory and 30 Megabyte (MB) hard disk. The selection of the Compaq system was predicated upon benchmarking various IBM compatible machines at ARL. The Compaq system was found to be typically more than twice as fast as its IBM equivalent. In view of the 'real-time' computing requirement for the process, it was clear that computer speed was potentially rate limiting for the overall system performance and defined our selection of the Compaq machine.

5.1.5. Optical System.

5.1.5.1 Methodology. Optical system design is a key factor in the design of the complete, integrated system. This is illustrated in

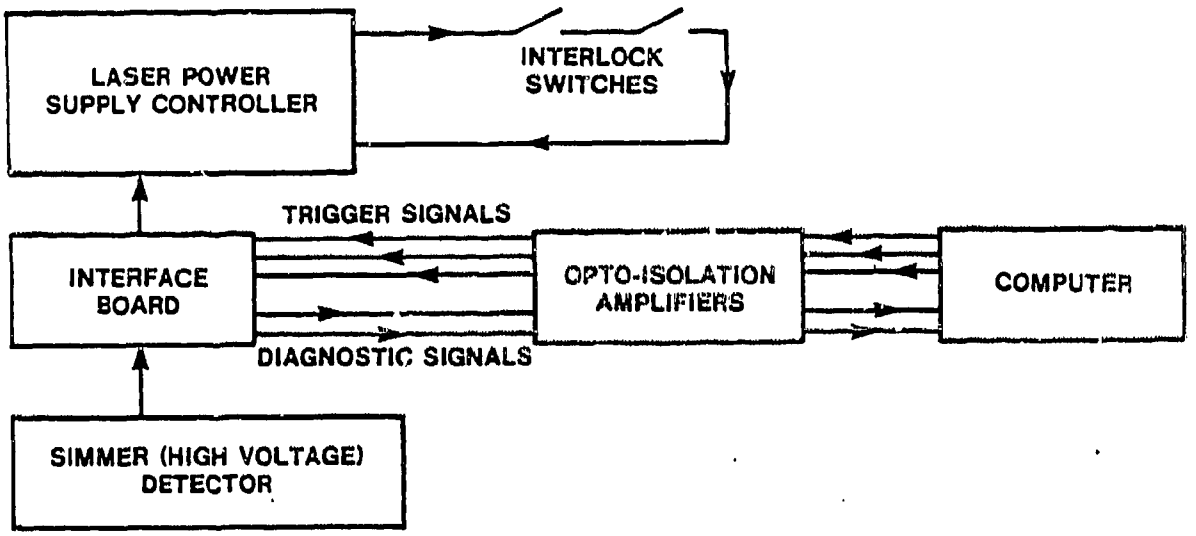

Figure 5-4. Laser Interlock System Schematic

Figure 5-5. The driving issues for optical design are the specifications upon balance system operation such as laser timing and targeting resolution. Additionally, the layout of the component to be balanced upon the balancing machine impacts the design of the optical system. The test program envisaged the balancing of the AGT1500 High-

Pressure Compressor Impeller, which requires two-plane balancing and has two distinct balance mass removal site geometries.

The design of the optical system is a necessary prerequisite for the design of many other components in the balancing system. Once an optical design methodology has been determined, the mechanical layout of the whole system can be defined and designed. The access of the optics to the mass removal target zones impacts the operational sequencing and targeting location control. The optical design impacts the specification of the traverse system and its controller requirements, of the overall system computer and software needs.

The design of the optical system has, therefore, been a primary element of the program, in that many of the other design choices and decisions are predicated upon it.

5.1.5.2. Opto-mechanical system. The preliminary design concept, as given in the proposed program documentation called for a two-head optical system (Figure 5-6), with one optical head for each of the two balancing planes. This was rejected, as a system of choice for the initial stages of development, although it was considered an effective solution for long-term implementation. The chosen approach to this problem, reduces cost and overall control requirements by minimizing the software and mechanical complexity of the system, while allowing the system to demonstrate contract specified tasks. The system installed at this time consists of a traversable single-head layout (Figure 5-7) with a selectable final optical focusing element.

The single-head optical system implies a translation of the optical assembly from one side of the rotor to the other. The timescale for this operation is typically 140 seconds, whereas the typical irradiation time is 300-900 seconds.

The original design concept called for each individual traverse assembly to have a four-axis capability (three translation and one rotation). The requirements for the resolution of the translation stages are based upon a fractional laser spot diameter positioning increment of 0.1 spot diameters. This corresponds to a 50-um (0.002-inch) resolution/step limit for the translation stages. The axial stages parallel to the rotation axis (X axis) consist of a long stage for gross relocation from one side of the turbine component to the other, plus a shorter, final high-resolution/step Y-axis stage (perpendicular to the rotation axis) and the Z-axis stage (vertical). This reduces the system complexity as well as the computer/interface design requirements. This traversing system is adequate for most irridation geometries (Figure 5-8).

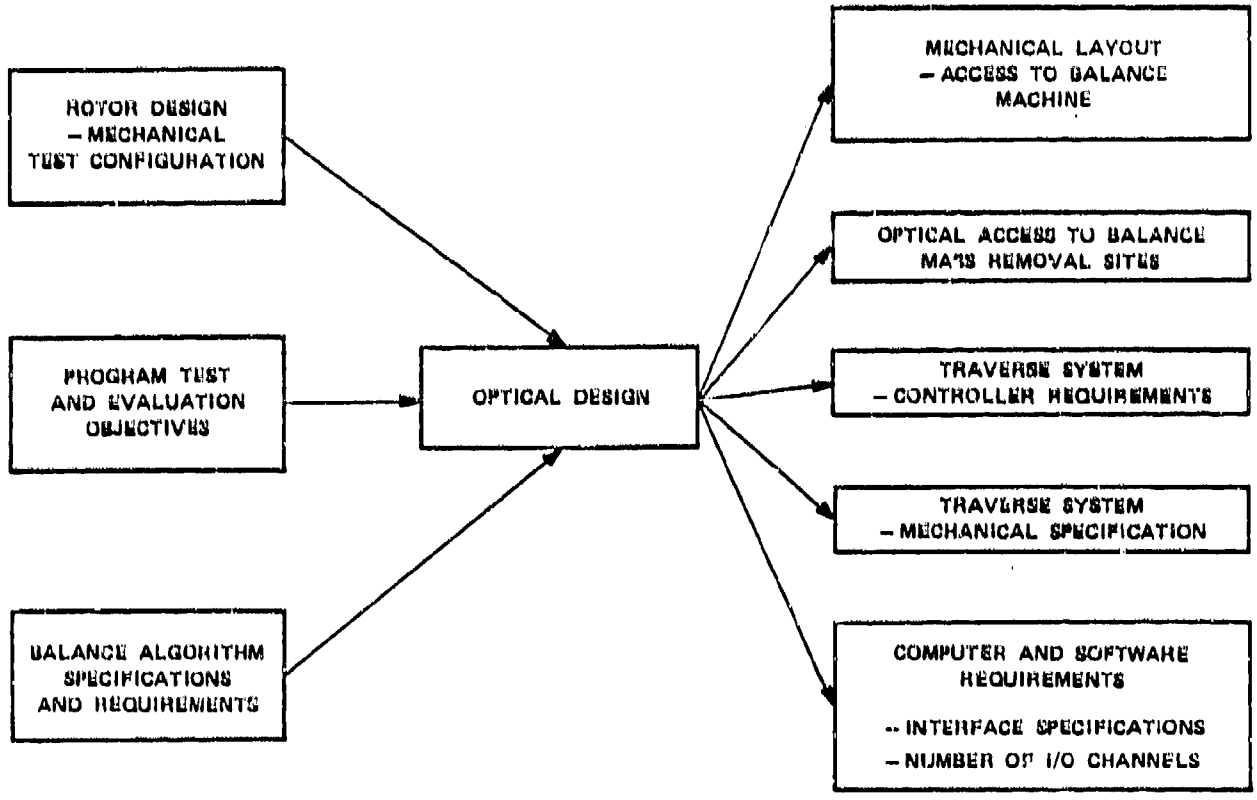

Figure 5-5. Optical Design Methodology

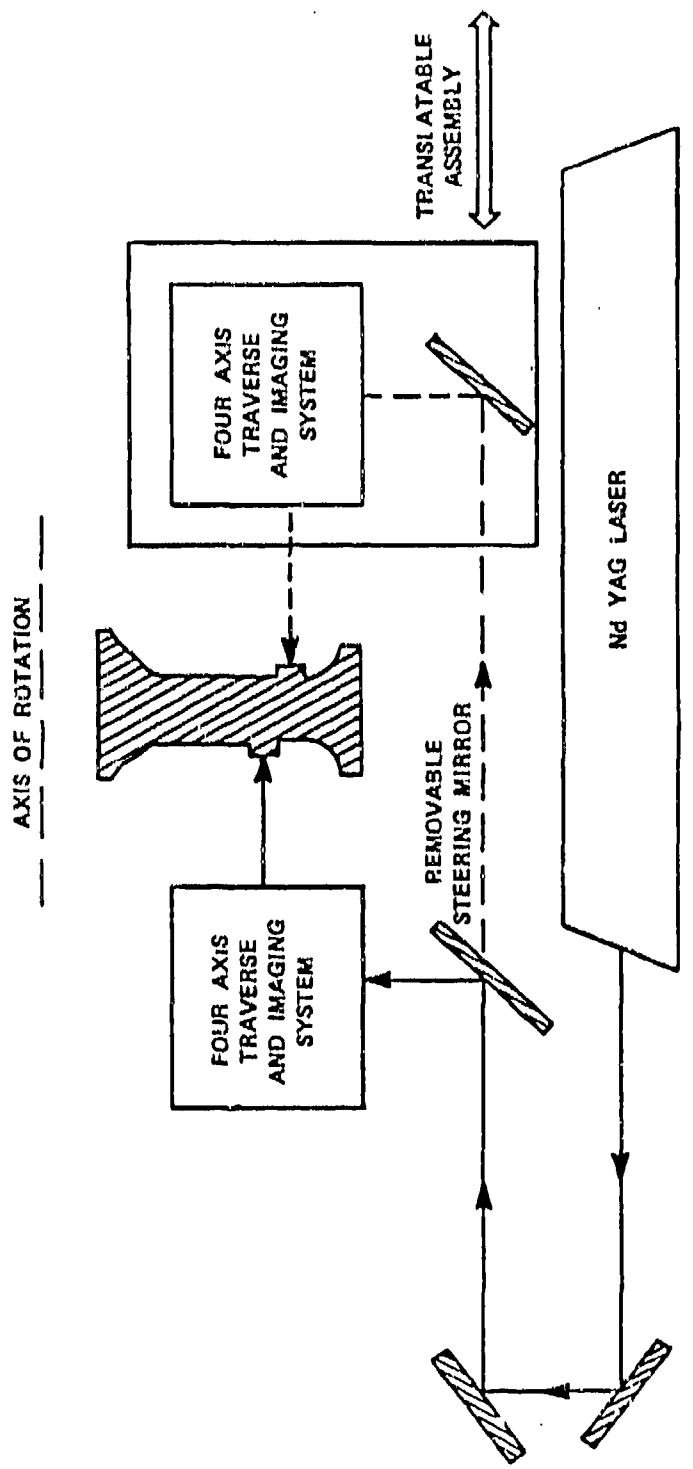

Figure 5-6. Original Optical Layout Concept

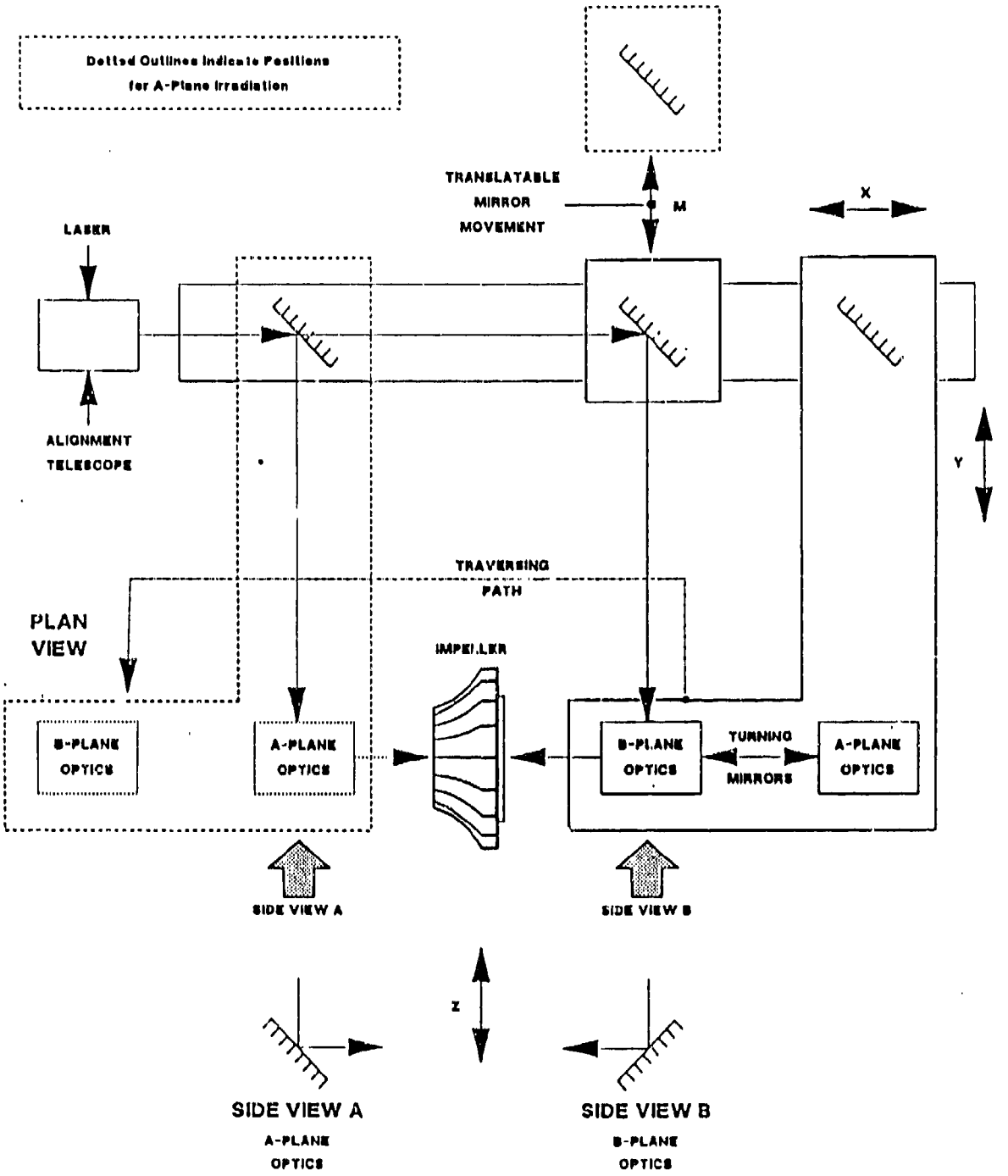

Figure 5-7. Optical System Layout

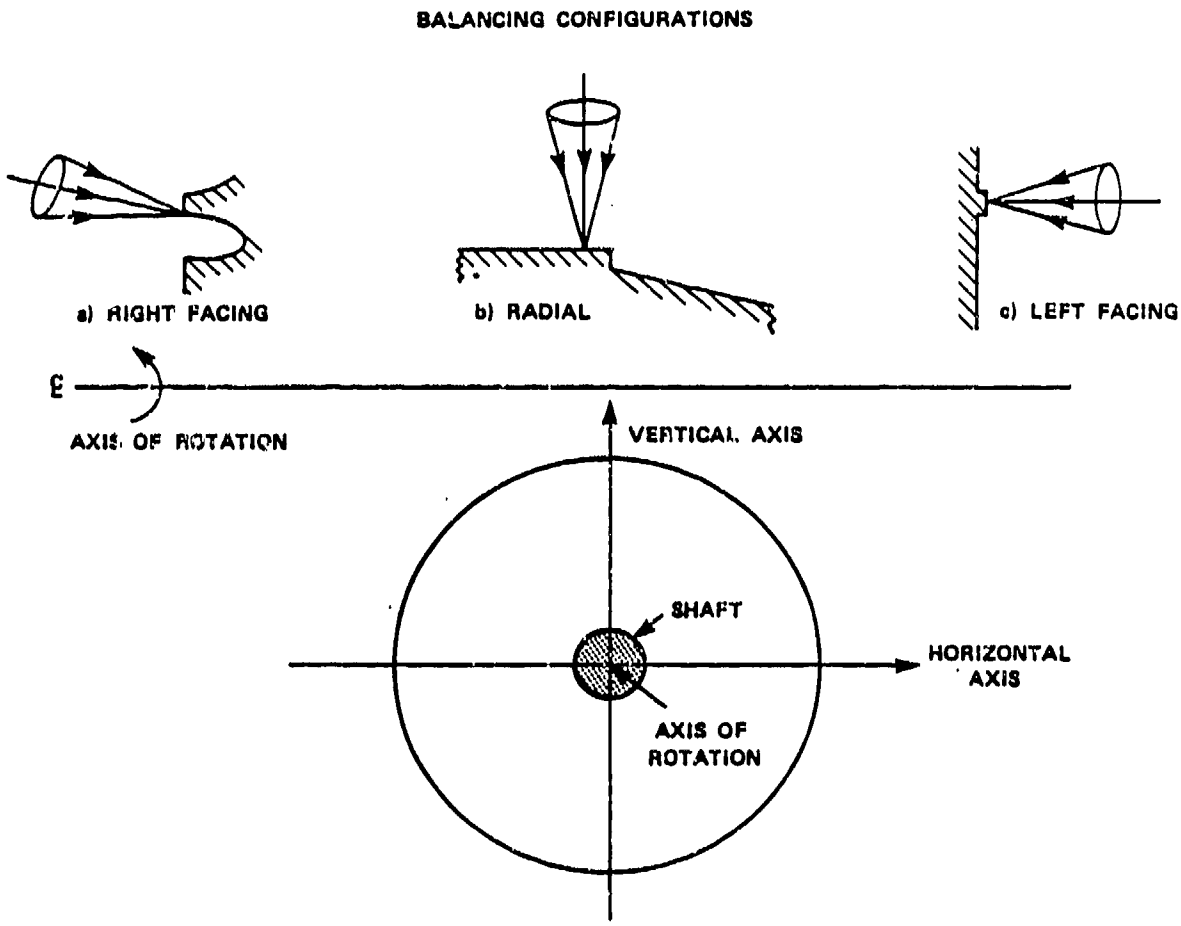

Figure 5-8. Optical Targeting Geometrics

Originally it was believed that it was attractive to use a rotational stage at the focusing optical element, so that the beam can be directed in either +X or -X directions by mirror rotation. In the case of radial focusing, as required by some balancing assemblies, such as the high-pressure compressor assembly, the final mirror can be removed to achieve the same results. As it was not intended to test in this configuration during this program, it did not appear necessary to install a motor-driven mirror translation assembly with its attendant cost and complexity. In fact, it became apparent that both for this program and later stages of implementation in production, the use of several different final focusing assemblies, as opposed to a single, multi-purpose and fully automated assembly, was more attractive in terms of both cost and flexibility.

It became clear that the potentially wide range of balance configurations and component requirements would require a range of final focusing concepts. For the purposes of this program, two different geometries became necessary. The use of a selectable beam path option, through use of a removable mirror, became an attractive approach to mounting both left-and right-facing assemblies on one transverse system (Figure 5-7).

5.1.5.3. System layout. The positioning of the optical bench affects accessibility, compactness and necessary floor area. At this time accessibility would appear to be more attractive. The optical bench is required to support both the optical and traverse assemblies as well as the laser head. The laser is 73 inches in length, and is thus the key element to the size of optical table needed for the apparatus, giving a 6- by 4-foot overall dimension. The optical table, in addition to its role as mounting plane for the optics, must also act as a vibration isolation system for the optics. Typically, resonant frequencies of large-area honeycomb optical tables are of 1-10 Hz. In view of the balance machine operating frequencies of 15-25 Hz, it behooves us to obtain an isolation between floor-transmitted vibrations and the optical table. This was to be obtained through the use of pneumatic isolation mounts, with response frequencies of 1-2 Hz, which provides significant damping to the motor-driven vibrations. At the start of the program it was not clear whether an isolation system was completely warranted. For the modest cost, however, it reduced the impact of potential vibration hazard and allowed baseline data to be obtained for future implementation evaluations. It was found on testing throughout the program that little vibration coupling occurred between the optics and the balancer. The system could be successfully operated with the pneumatic damping system disabled. The removal of the system has some advantages in the long term for overall system alignment stability and elimination of possible operator error. However, it is also important to consider the benefits it allows to some aspects of system alignment.

5.1.6. Control System.

5.1.6.1. Methodology. A schematic of the control system and diagnostics is shown in Figure 5-9. The required interfaces for the systems include the laser trigger system, stepping motor drives, the balance machine microprocessor, linear and rotary encoders. These have been implemented using off-the-shelf equipment.

The balance machine microprocessor, a Gisholt BP2020, has optional cards for computer interfacing. Originally it was intended to use an available parallel interface, but in discussions with Gisholt engineers, it was recommended that a serial interface be used as this offers a simpler and more easily debugged approach. This was installed along with an output for the photodiode reference timing signal that is required both by the BP2020 and by the laser trigger.

The motion control is provided through the use of plug-in controller boards in the PC chassis. Two boards can control up to four motors. The power drivers for the motors are mounted in an external rack.

The control computer requires data from the balancer to define angle and firing timing. This is provided by photodiode and encoder signals. This proved to be a key technical issue in this program and is more fully discussed in a later section.

5.1.6.2. Laser trigger system. As described earlier, the major issue with regard to irradiation of the target was that of accurate firing time control. The spatial error in burn location has to be controlled to less than a spot diameter, which translates to less than a 50-usec jitter. This was accomplished by means of an interface between computer and laser controller. The efficient use of this system depends upon the accurate reading of angular location from the spinning rotor in order to deliver the laser energy at the correct location on the rotor circumference.

Our design of choice early in the program was that of using a rotary encoder, mounted on the motor shaft, in association with the angular reference signal generated by the balancer photodiode. Early development problems prompted use of a purely photodiode-based system early in the program while these problems were being addressed. A schematic of the two systems is shown in Figure 5-10. The data from the rotary encoder and photodiode was to be used by a computer-mounted counter board that would initiate a trigger signal on reaching a predefined count (equivalent to a predetermined delay time or angle.)

The counter board worked well with a dummy load (oscilloscope) when operated with the vendor's test software, (in BASIC) but failed completely with our own software (in Fortran and Assembler). This, of course, led to a serious look at our software for problems--none were obvious. Further checking with the vendor's software showed that a "permanent" frequency setup established within the BASIC program would disappear erratically after leaving BASIC and typing on the keyboard. Putting the chip select line of the counter chip on an oscilloscope

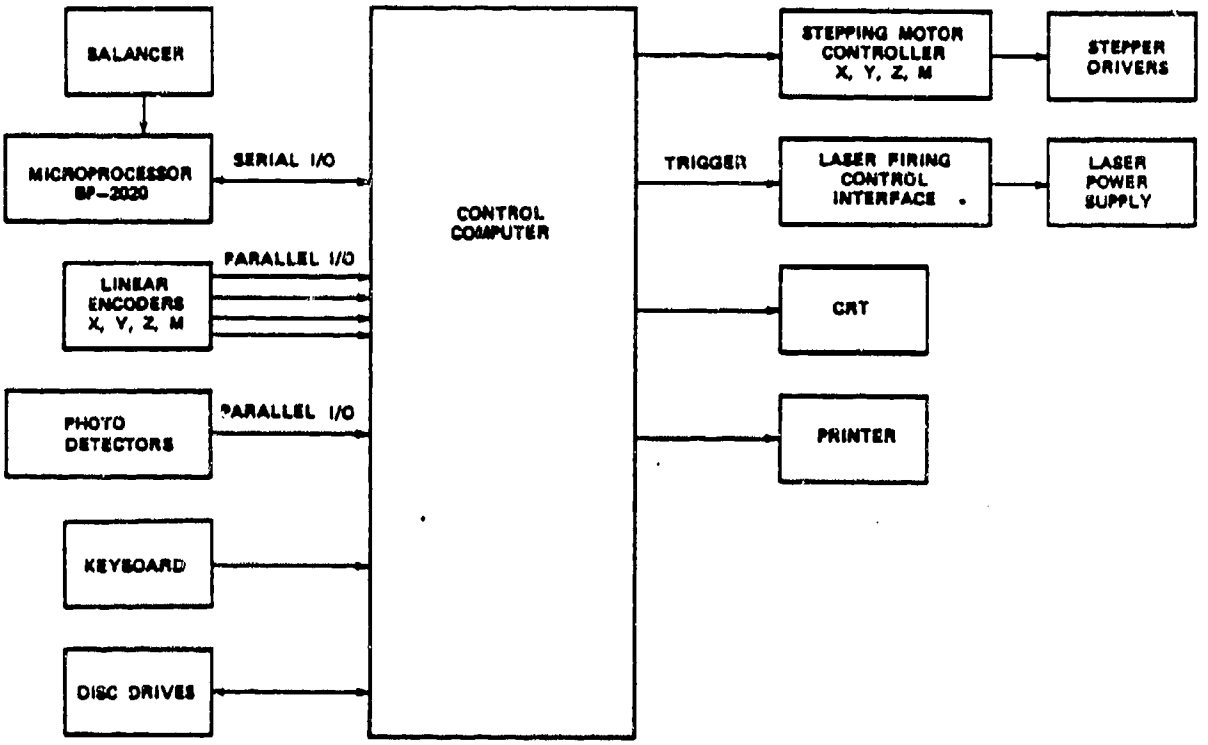

Figure 5-9. Control System Schematic

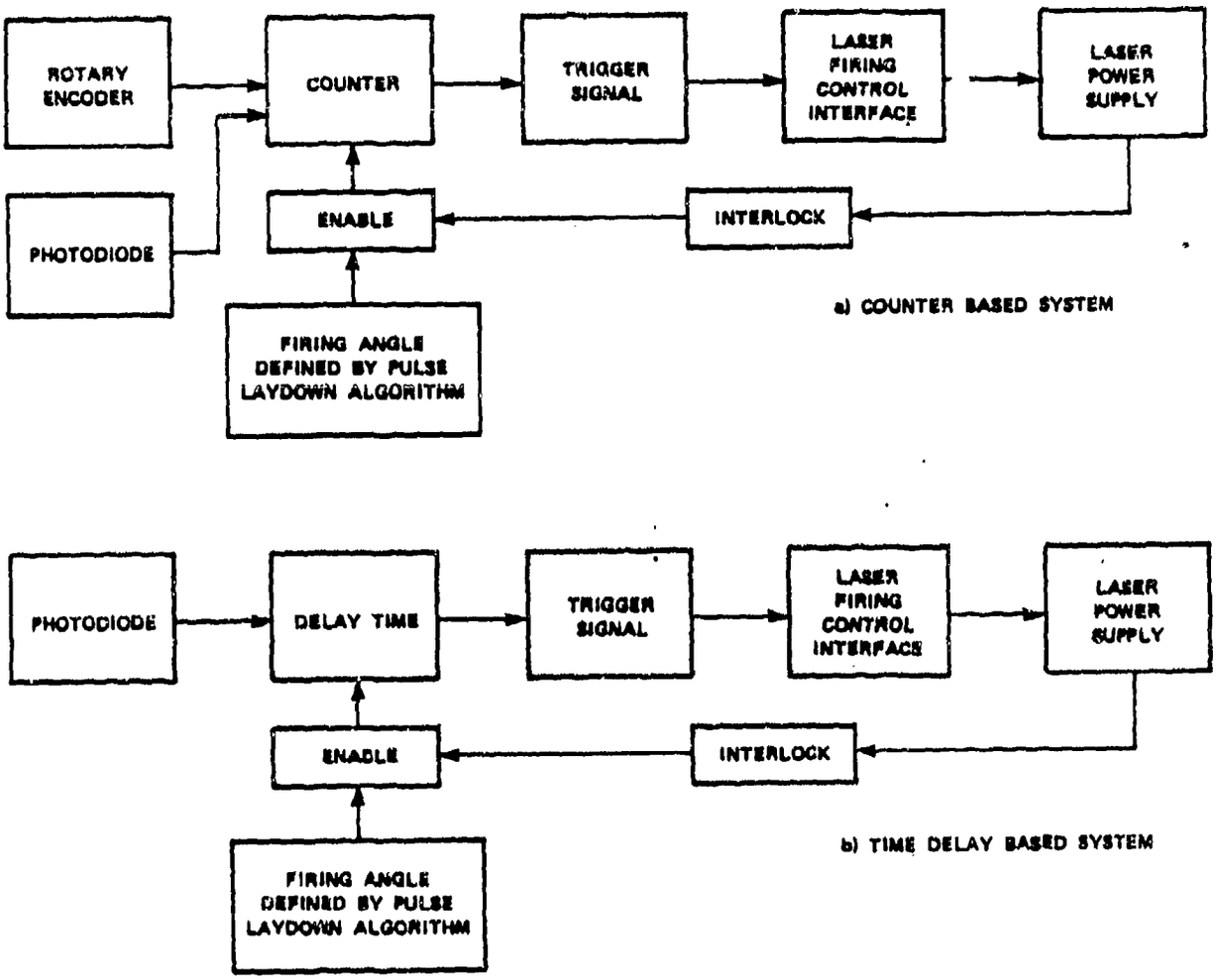

Figure 5-10. Laser Trigger System Schematics

showed it was being selected for all I/O operations. The board was sent back to the vendor for warrantee service. The vendor later said we had the wrong hardware revision level for an IBM AT compatible machine, which gives improper timing and shows up as a chip select problem.

In the meantime, a parallel I/O board was setup and the fire angle calculated by time delay after waiting for a photodiode zero crossing. This setup worked well, although it produced about a 65-usec (0.3^{o}) timing variance due to the software loop. Much of the test data accumulated on the program was obtained using the time delay system.

However, problems with the counter-based system were not eliminated on installation of the corrected hardware revisions. These problems were found to be twofold. Although the system was found to perform well during dummy testing, the actual tests with the laser showed two faults. The major problem was that of false firing occasioned by a noise generated by laser firing. It was found to be inherent in the counter board, (high impedance input) that appeared possible to fix with some effort. The more damaging problem was that of jitter, which appeared to be a result of belt slippage. As the photo detector is mounted on the rotor and the encoder on the motor shaft, the potential for error is greater than that possible with the delay timing system. Typical low-frequency oscillations in rotor speed were $\pm$0.2.%. The high inertia of the rotor enables a single rotation of the disc to have little change in surface speed. However, belt slippage of the motor appears to have a more damaging effect on the counter timing (a $\pm$1.5% error in motor speed from load to no load). The success of the delay timing system in earlier testing made it appear a better solution, provided one major constraint could be overcome.

The difficulty of using the time delay system, in a generalized sense, is that of the sequenced time delays in the system. The charging of the laser, operation of the software, and waiting for the photodiode signal required a certain minimum time. If the firing angle was less than 45^{o}, a delay equivalent to one revolution was needed, thereby halving the laser firing rate. This was solved by using two photodiode signals, approximately 180^{o} out of phase (Figure 5-11). The second signal is taken, via one bit on a parallel I/O board directly to the computer. At the start of each run, the two signals are compared and an offset angle computed. This prevents errors, due to setup or misalignment from impacting the system performance. Based upon the required delay angle for each pulse, as defined by the pulse laydown algorithm, the correct photodiode signal is chosen, the delay time calculated, and the trigger signal sent to the laser. This produces a continuously variable firing angle capability that allows for once per rotation laser firing.

The laser firing system necessitates several sequential timing marks.

(1) Charge signal, followed by a 12.5-msec charge time.

(2) Delay time prior to firing ($\geq$0.2 msec).

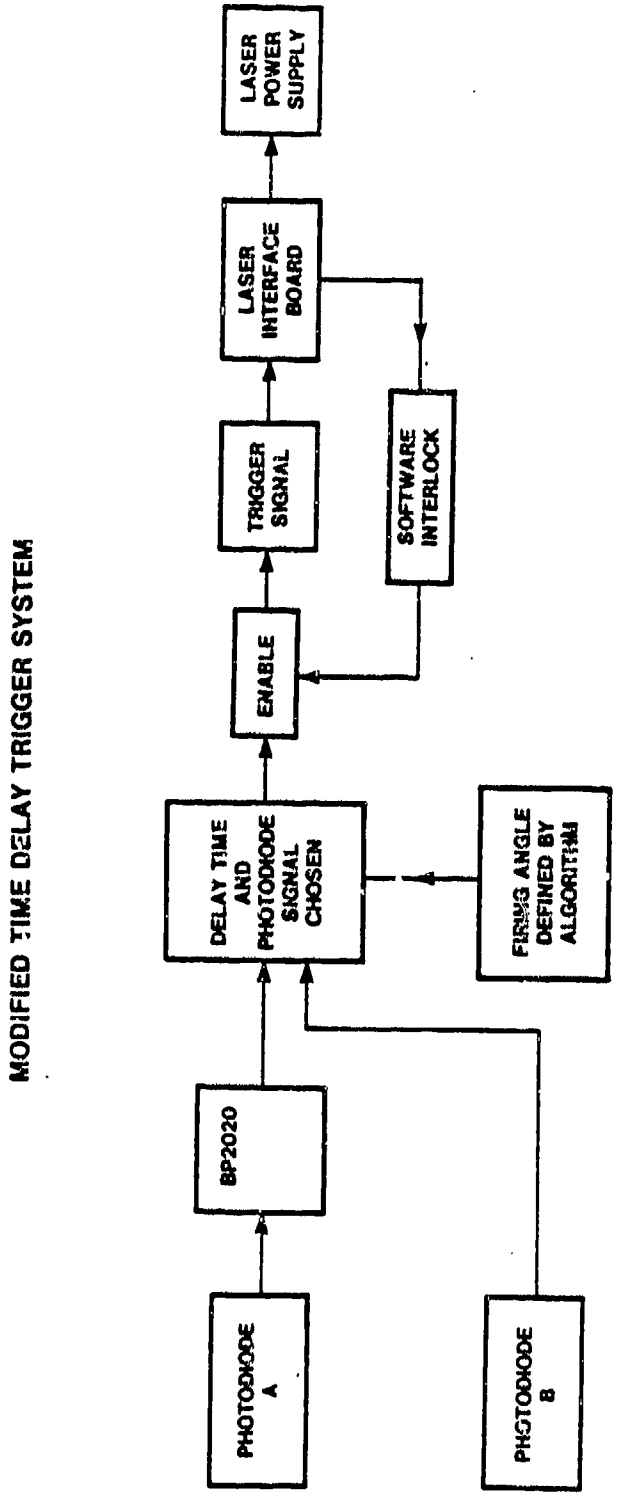

Figure 5-11. Operational Laser Trigger System Layout

(3) Firing signal (0.5 msec).

(4) Firing system decay time ($\geq$7.5 msec).

Thus, it can be seen that in its simplest form, if the desired angle corresponds to a time 8 msec (45^0) after the zero degree, or reference, marker, then two revolutions of the rotor would be required for each laser firing. However, a secondary reference marker is derived from the other photodiode, corresponding to 180^0 relative to the zero mark. This then allows a firing of the laser every rotation, with triggering, by primary marker for angles between 46 and 225^0 and via the secondary marker for 226 to 45^0.

5.1.6.3. Traverse system. The traverse system consists of four Design Component Industries (DCI) precision cross slides capable of 0.001-inch resolution with zero backlash. They are driven by standard 12v-dc stepper motors. The axial or X-stage is capable of 24-inch translation which allows the stage to be operated in both A-and B-plane modes. The lateral stage (Y-axis) has 12-inch movement, whereas the vertical (Z-axis) and mirror mounts have 8-inch motion capability. The slides are equipped with DRC linear encoders that are interfaced with the computer via BEI interfaces and parallel I/O boards.

The traversing system is controlled by Rogers Laboratories motor controller boards mounted in the PC. The motors are powered by 12v-dc supplies through rack-mounted driver boards. The four channel controller consists of two separate two-channel driver boards.

5.1.7. System Integration. The optics, traverse assemblies and balance machine were integrated to provide a usable package. The major point of opto-mechanical integration is that of overall alignment. The axial (x-axis) and rotation axes have to be parallel. This is especially important for removal of material from sacrificial areas that have any axial extent (such as the impeller A-plane). This was achieved by use of mechanical centering via the traverses on either end of balancing arbor. Horizontal alignment required small movement of the balance machine, whereas vertical alignment could be achieved using the pneumatic vibration isolation system. The optical system has been fully integrated with the balancer and laser system. The mounting plates for all the optical components were fabricated to facilitate flexibility and ease of modification. A view of the system can be seen in Figure 5-12. This shows the traverses, mirror and lens mounts assembled and ready for testing. The optics have not been masked in this view, allowing ease of access. During melt removal a masking system is implemented. Obviously, during a full operational test in a production line environment, further system enclosure is necessary.

Optical system alignment required the centering of the beam on each of the reflective mirror elements over its range of traverse. As the alignment He-Ne laser is colinear with the Nd:Yag beam this procedure is straight-forward. A view of the optical system can be seen in Figure 5-

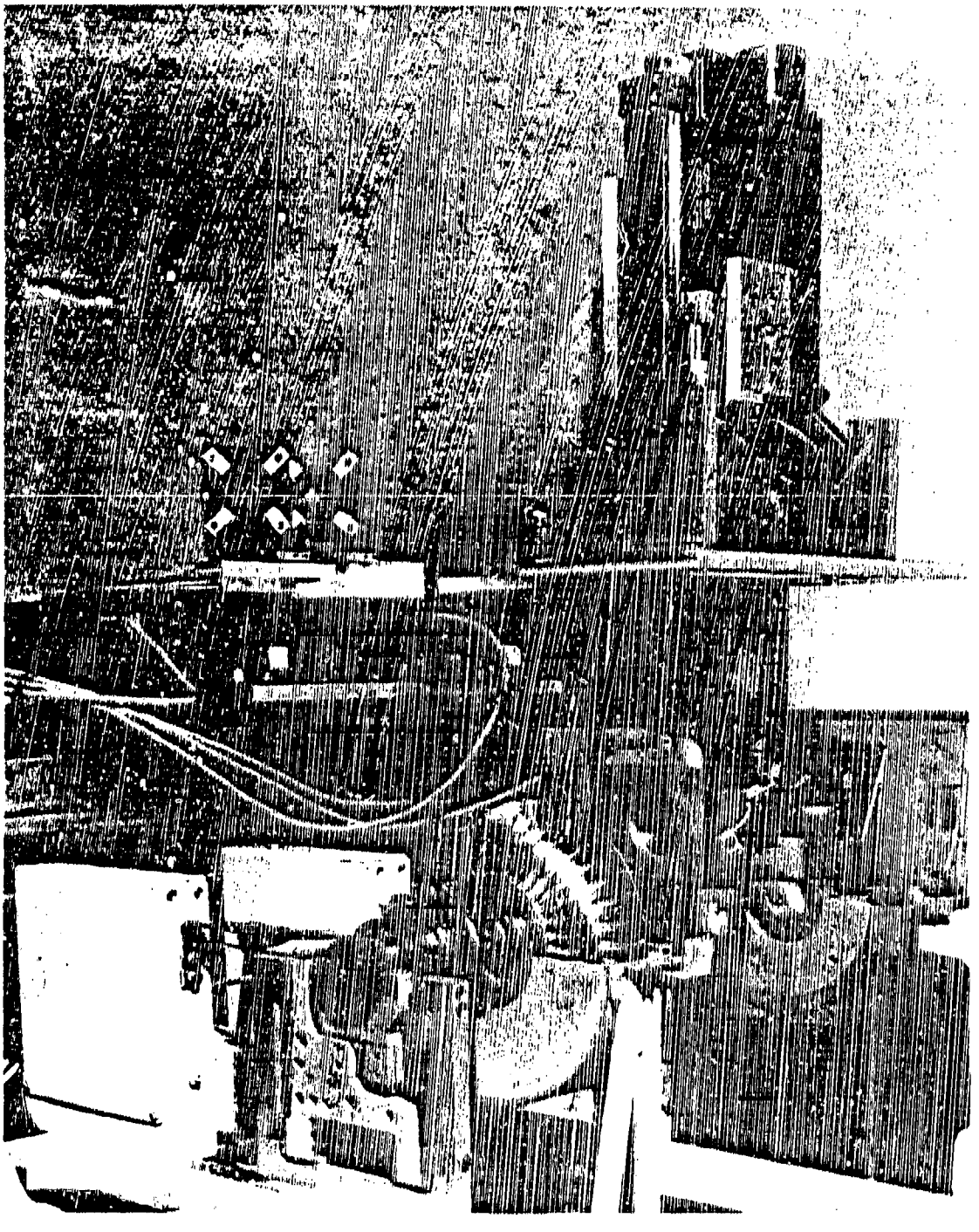

Figure 5-12. Optical System Layout

13. Alignment masks are used to position the He:Ne alignment laser beam on each optical element. The alignment procedure has been found to be quite rapid, and more importantly, the alignment has been found to be rugged and stable.

There is some beam splash arising out of reflection from the glass cover plate protecting the focusing lens, which requires some masking. This cover plate is necessary to prevent long-term buildup of metal droplets on the high-quality antireflection coated lens. The plate, being a 2x2-inch microscope slide, is easily and cheaply replaced.

The major issues of integration are those of software integration, which are addressed in the Section 5.2. However, the hardware issues that had to be resolved were those of wiring and power. The system electronic components were mounted in a standard 19-inch rack. The trigger system for the laser required use of series of opto-isolators, both on the rack and also on the laser interface card to prevent noise-related problems. Most of the wiring system was implemented using quick connecting components that allowed for flexibility and ease of modification, which proved necessary at early stages of the program.

5.1.8. Focusing Optics. The focusing optics delivers the laser energy to the target zone on the sacrificial surface. This requires as short a focal length convex lens as is possible to be used. This aids in the efficient use of energy to maximize the removal of melt from the surface. The physical constraints upon the system, imposed by arbor, bearing size and location, mounting bracket and transducer housings, and physical size limits of optical mounts and traverse elements, makes for some problems in efficient optic design.

The B-plane configuration is relatively straightforward. The laser beam is rotated through 90^{0} by a turning flat and focused normally onto the surface by a 10- to 12-cm focal length lens (Figure 5-14). It is difficult to make this any shorter in focal length because of arbor and bearing constraints as well as the desire to include a melt splash collection system on the optical assembly (see next section).

The A-plane provided severe difficulty in obtaining an adequate optical assembly. The requirement for the burn to impinge on the inside edge of the recessed sacrificial area provided little opportunity to select a simple and efficient geometry. An axial system, such as that used for the B-plane is not possible, as the axial width of the burn zone (0.5-inch), in association with its small maximum radial depth (0.070-inch), leads to a masking of the laser beam prior to reaching maximum burn depths. The tilting of the beam off axis to avoid this problem was inhibited by the length and shape of the arbor on that side of the rotor. The only geometry that allows access over the entire required area is a two-plane tilted arrangement. This is shown schematically in Figure 5-15. The beam is tilted downwards and laterally, to pass over the inner hub region of the rotor and impinge on the sacrificial surface near to the horizontal plane of the rotor axis

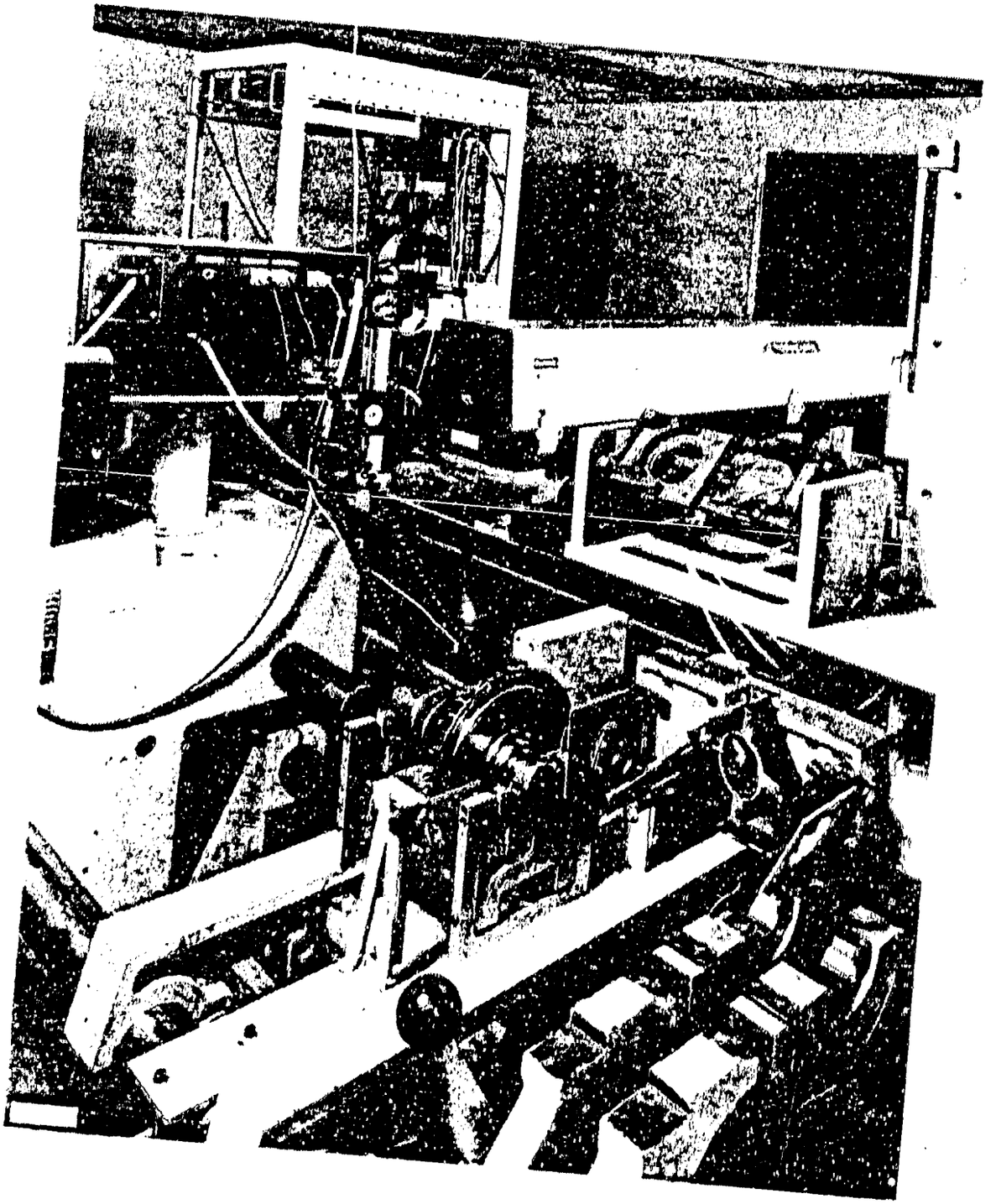

Figure 5-13. Optical and Traverse System

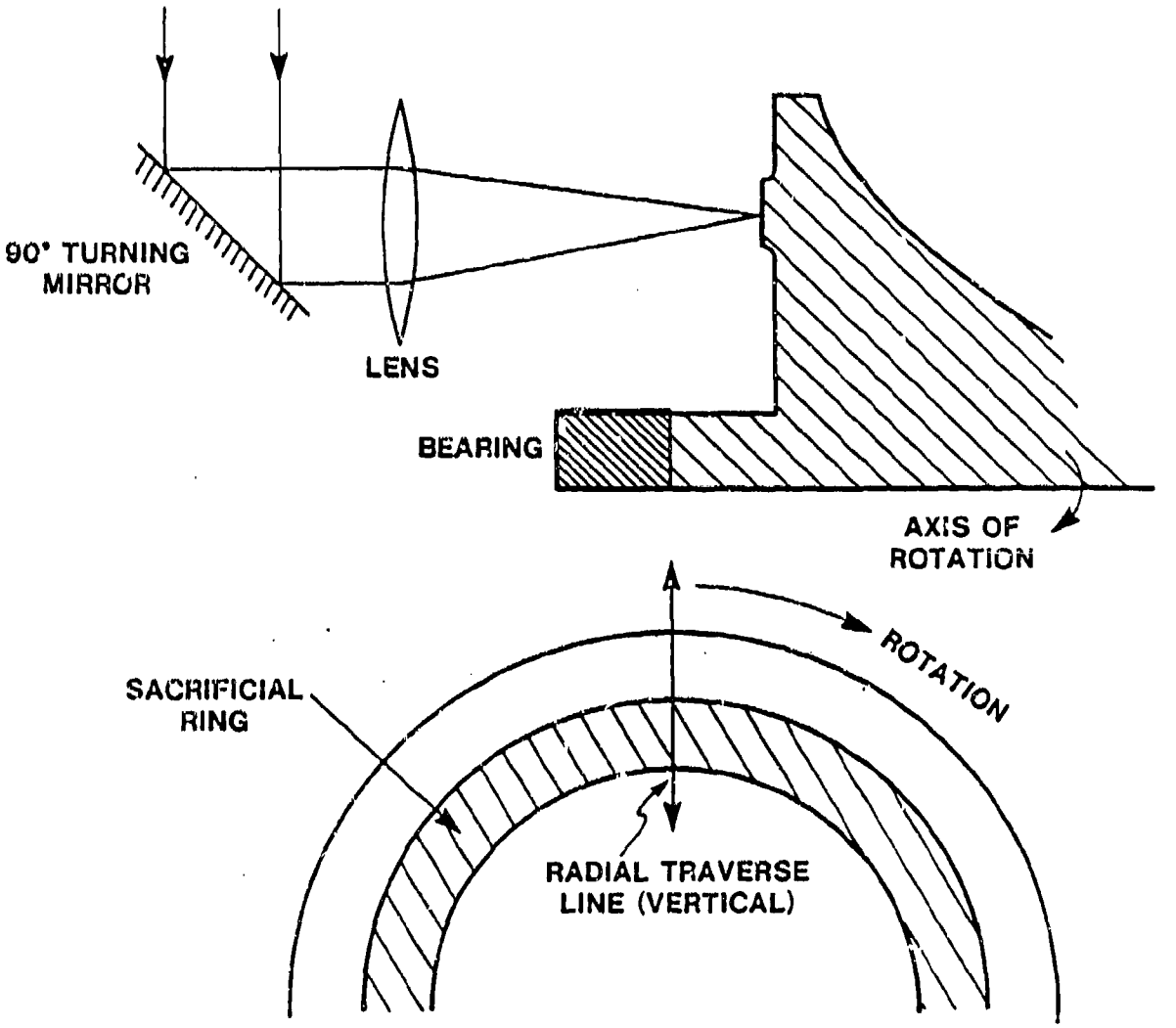

Figure 5-14. B-Plane Focusing Optics

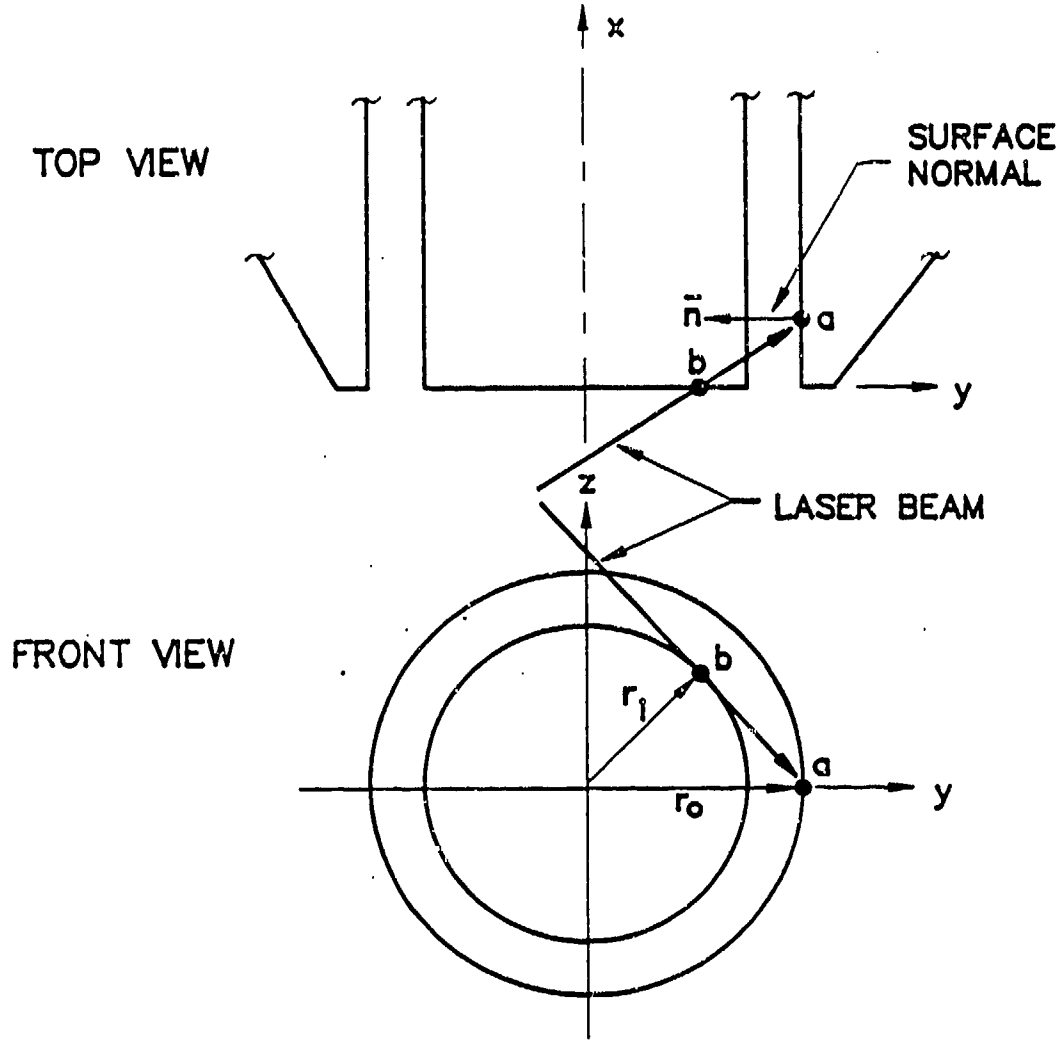

Figure 5-15. A-Plane Access Issues

(point a). However, due to possible interaction of the beam by the hub (at point b) the actual burn location is offset from the horizontal, by approximately 30^{o}. The configuration is obtained through use of a 45^{o} lateral rotation of the beam and a 20-degree downward tilt (Figure 5-16).

It should be noted that there is a major difference in these two optical configurations. The B-plane optics are arranged such that the direction of motion sensitivity of the balancer transducers (Y-axis in optical coordinates) can cause only small perturbations in the firing delay time, and not in focus or radial burn location. This is the optimum geometry with small and random errors occurring in the firing pattern. However, the optical access constraints placed on the A-plane geometry puts the laser focal region in the worst possible position with respect to motion of the rotor due to imbalance forces. This offers the potential for some defocusing errors to occur as the motion of the rotor is maximized relative to the optical axis.

5.1.9. Melt Removal System. Initial testing showed that melt splash was potentially a problem with respect to contamination of optical surfaces as well as to the bearings. For B-plane operations there is little problem with redeposition on the rotor. The A-plane has a more significant problem with deposited material owing to its confined location.

An inspection of the trajectories of melt off of the B-plane showed a predisposition to a tangential spread of particles in the rotational direction. Vapor debris and some particulates were directed back along the beam path (Figure 5-17). This lead to the implementation of a two-part collection system. Clearly, no physical contact could be allowed between the rotating elements of the system and an optically mounted collector. An optically mounted element was designed, consisting of an inner optical protection screen and an outer melt splash suction box (Figure 5-18). The inner cone allows the focusing lens to be protected from vapor and debris. It includes a glass slide cover plate to absorb any residual debris and protect the lens coatings from damage. Being a low-cost consumable item, it suffers from thermal stress failure if uncooled. The air jet, therefore, serves two purposes; it cools the cover plate and prevents debris from entering the cone by acting as an air curtain. The outer melt splash collector is connected by a commercial vacuum cleaner. The axial spray of particulates is collected by the suction system and filtered out in the vacuum cleaner. The tangential spray of particulates could not be collected in this device. It was found that the pre-existing safety housing for the rotor could serve a dual purpose. The shield is used to protect against ballistic damage from a damaged rotor and external interference of objects with the spinning rotor. It provides a closed environment around the rotor, except for arbor access and now for laser access. By adding a suction port to the casing, it can be used to extract particulate material. This has been done and the combined elements of the system work well in removing debris.

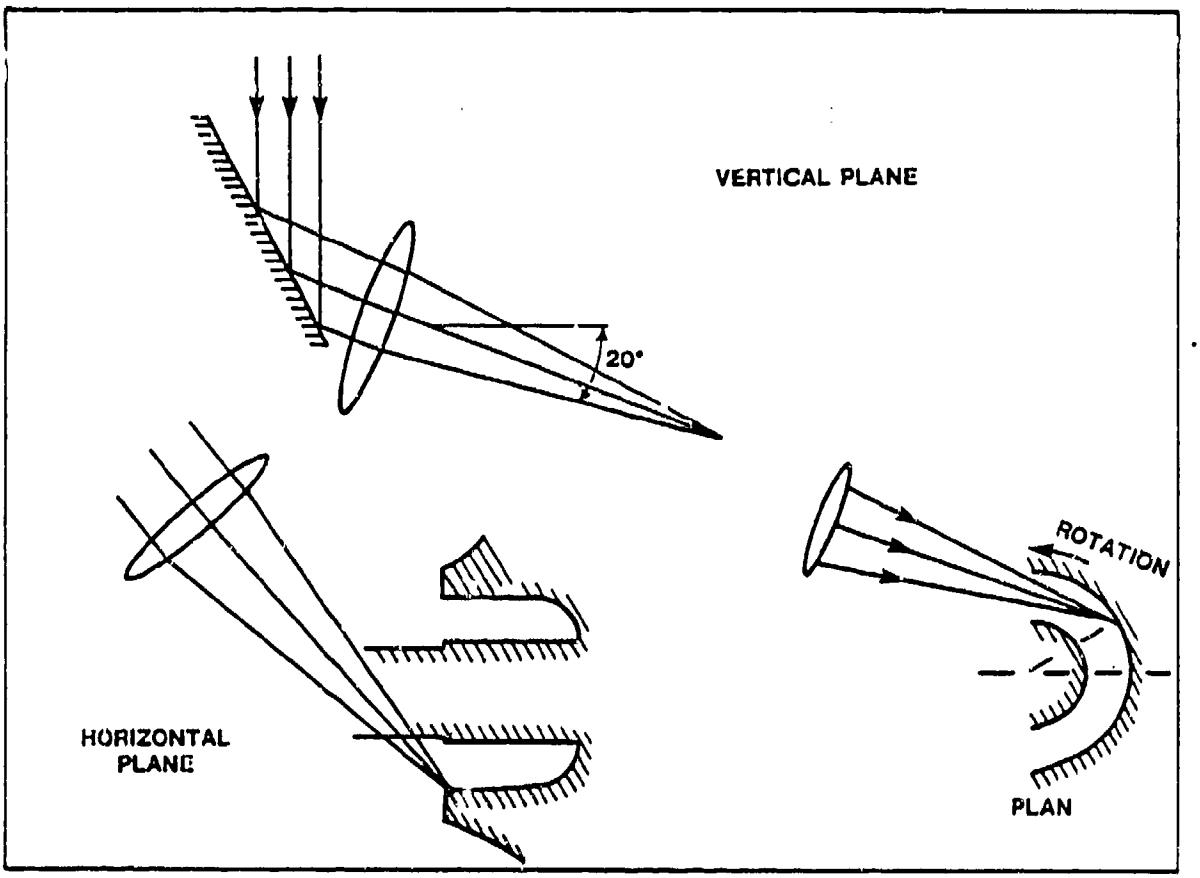

Figure 5-16. A-Plane Focusing Optical Geometry

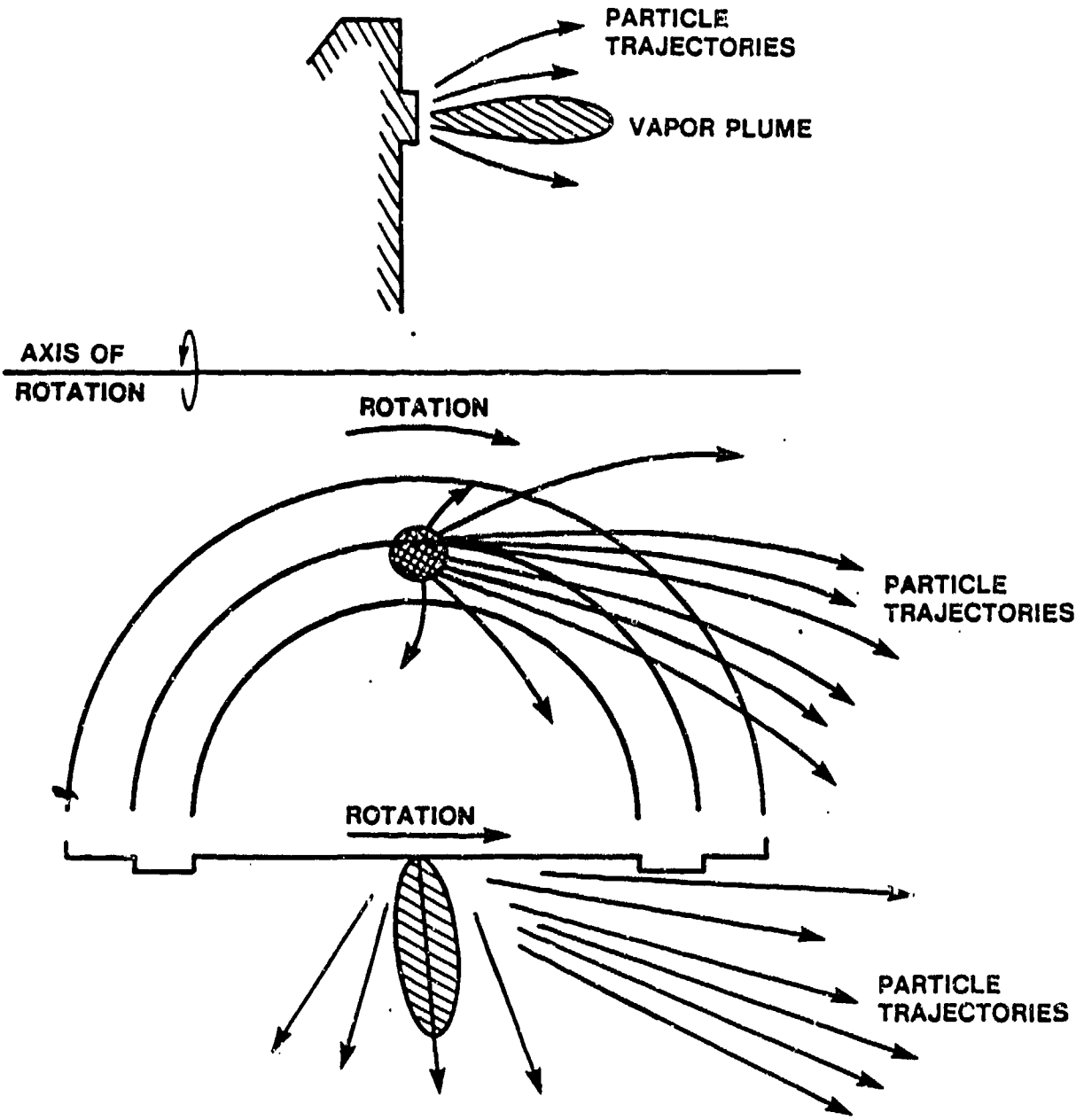

Figure 5-17. Melt Splash Trajectories

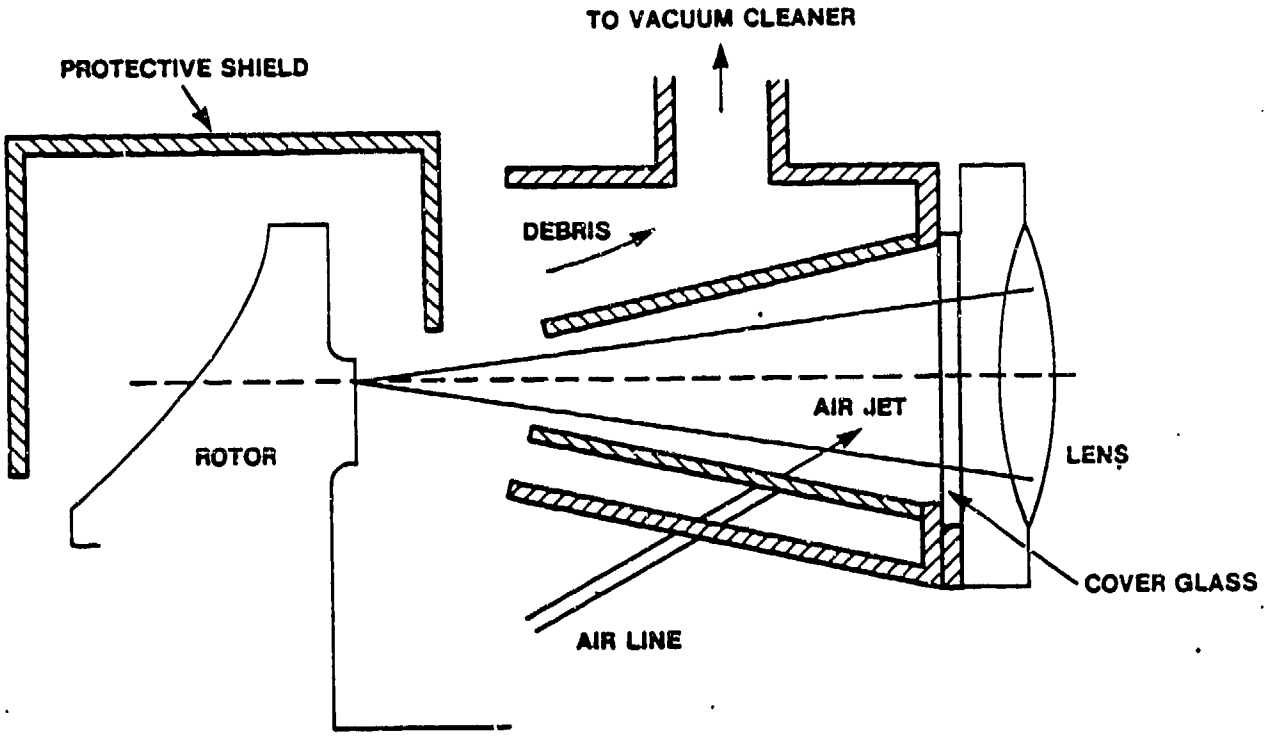

Figure 5-18. Melt Splash Collection System

An obvious question that had to be considered was that of possible interaction between the suction system and the balancer. Clearly, if the balancer readings are altered by the operation of the suction system, the design would be unusable. This was tested, and no significant variation in balancer reading could be found.

The A-plane collection of debris was found to be a significant problem, by virtue of limitations imposed upon optical access. It is not felt that this is insurmountable, and more is said of this in the implementation plan. It was felt that it would be unnecessary and inefficient use of funds to work on a solution for the existing geometric configuration; rather, an A-plane workable approach should be developed, as part of the implementation effort.

5.1.10. Enclosure. A Class IV safety enclosure was constructed around the balancer, optics, optics bench and laser head to contain all laser emissions. The size of this enclosure could be significantly reduced by the removal of the optics bench and repackaging of the optics and laser head.

5.1.11. Fatigue Test Bar Rig. The key parameters of interest, for the testing of standard Lycoming Fatigue Specimens test bars, are those of maintaining a comparable thermal history between rotor irradiation conditions and those chosen for the test specimens. This means that peak temperatures, irradiation time scales and surface velocity have to be matched. Needless to say, it is difficult to fully simulate the behavior of a large-diameter rotor, by means of a small diameter test piece, primarily from the viewpoint of potential notch generation, which becomes dominant in the case of a small-diameter test bar. A close simulation can be achieved; however, if the objective is to examine the impact of surface heat-affected material upon overall material performance. A diagram of the fatigue sample irradiation rig is show in Figure 5-19.

The approach taken to obtaining a reasonable simulation was that of mounting the test bars on a jig coupled to a high-speed pneumatic rotary grinder. This jig allowed the bar to be aligned and held firmly on axis while rotating at 15,000 ($\pm$100) r/min. The laser was then aligned with the centerline of the test piece and focused to the desired flux intensity level. The flux intensity, which defines the thermal history for a given local residence time, was adjusted by suitably defocusing the laser with respect to the surface. The calculated maximum temperature for a given amount of defocus is shown in Figure 5-20. If one determines the independent variables, i.e., defocus distances for the bar and impeller, for the same thermal history (ΔT), it can be seen that matching between the impellers and the test bars is quite good. This was verified by examination of the impeller and test bar microstructures. The major issue with the above approach is that of obtaining a uniform heat-affected zone around the periphery of the test piece. Each pulse produces a surface burn zone approximately 60 degrees in extent. The nonuniformity of each burn in terms of spatial thermal

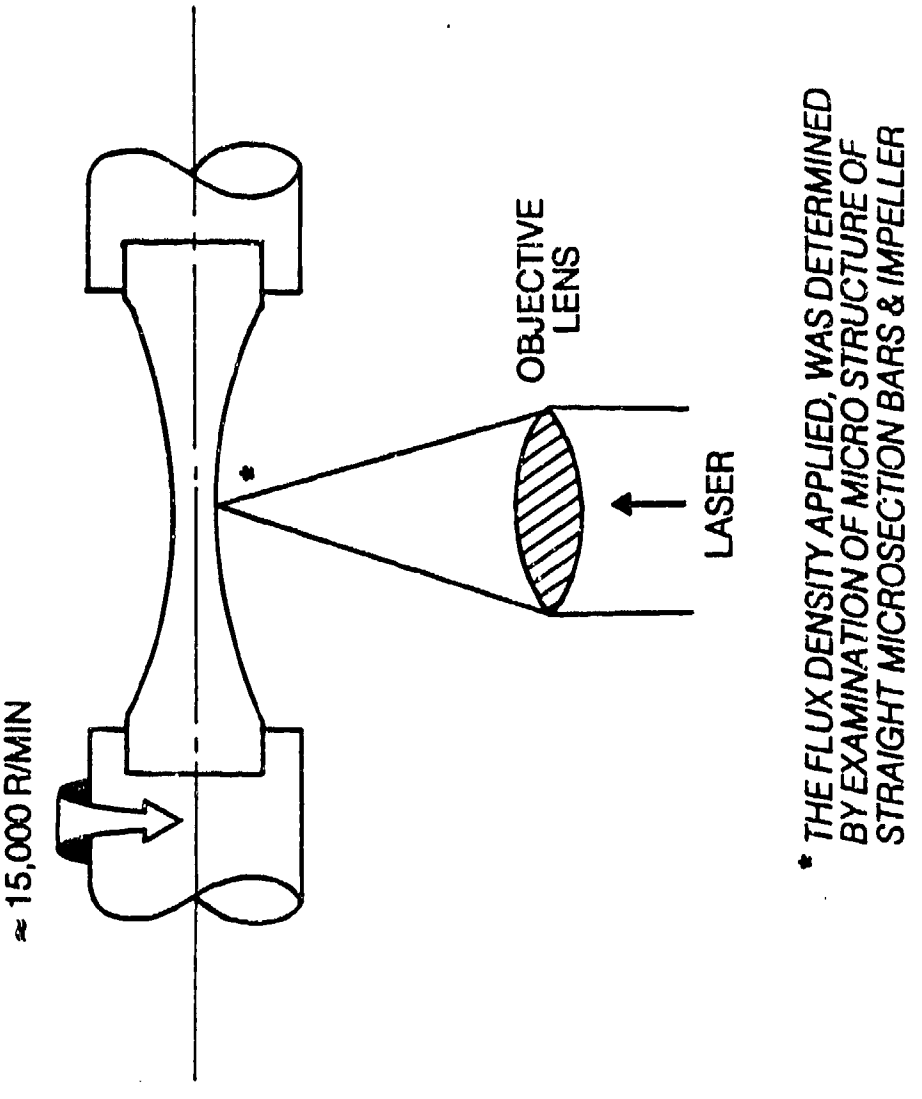

Figure 5-19. Diagram of Specimen Irradiation Rig

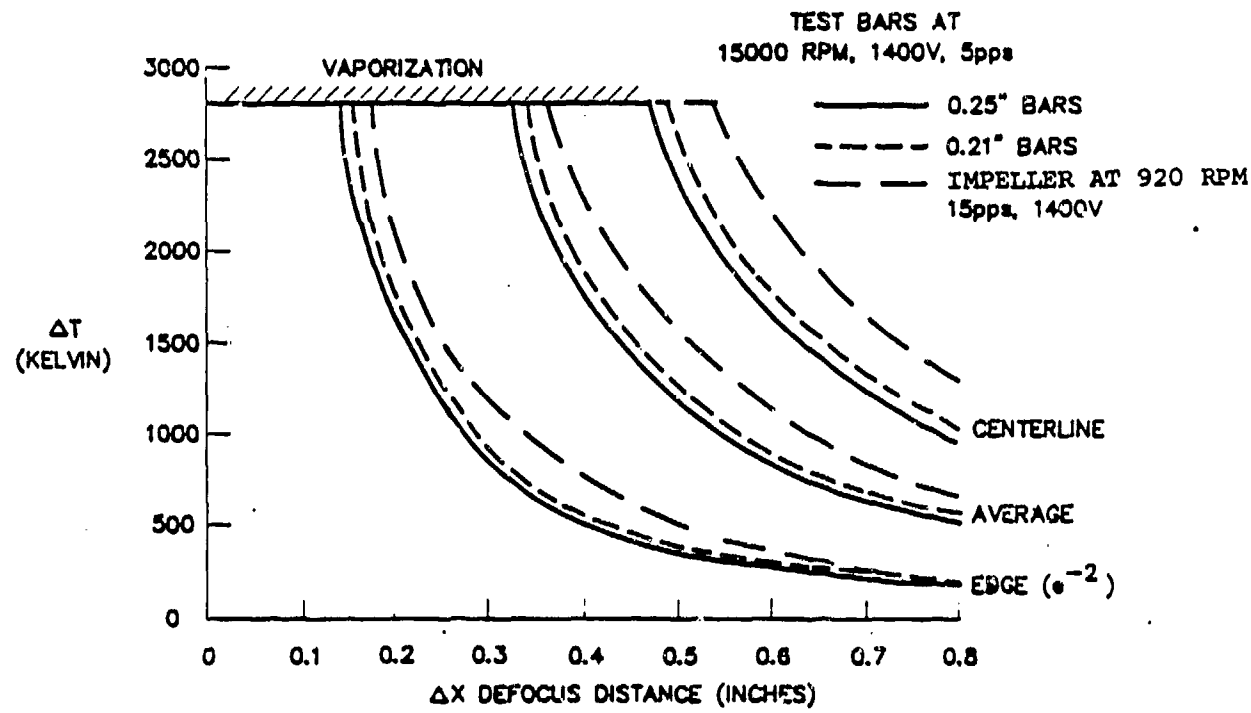

Figure 5-20. Thermal History of Rotors and Test Bars

history was counteracted on the basis of multiple burns at any given circumferential location. The wide mismatch between laser repetition frequency and rotational speed, allows a random laydown of pulses that will tend towards uniformity of surface condition with multiple irradiation over a pulse train of 50-100 pulses. Clearly, as the laser is focused, this will lead to deep burn scars. However, under defocusedconditions, the surface can still be heated to vaporization, with little mass removal occurring.

5.2. Software Algorithm Development and Testing

5.2.1. Software Methodology. The majority of code development for this program uses Fortran-77. A Macro Assembler compiler has been installed for I/O (Input/Output) with external devices. An operating system (MS-DOS) and a full screen editor (SPF) have also been installed.

The software structure for the program has been broken down into three major elements (Figure 5-21):

- The algorithm part fulfills most of the logic and computational requirements.
- Hardware interface routines.
- System and component configuration files.

All the subroutines reside in either a software (SW) or hardware (HW) library. The underlying methodology of subroutine structure is that of providing the most generally applicable coding which requires minimal changes to alter the process of balancing in any given situation. Thus, for example, at the present level of code evolution, the data file containing all the relevant physical parameters for a specific rotor geometry and balancing procedure includes two variables, "jgeom" and "jplane." These two variables are used as internal logic controls to direct the process as required by a given part. Although not fully generalized at this time, it can be easily modified or extended as new components, new balance machine configurations and system procedural improvements are included.

Two versions of the algorithm structure were developed. The first worked well, but was not as efficient in terms of elapsed time as was believed possible nor was it a generic part type code. Consequently, another version was developed to enhance the performance and versatility.

In the following sections, the formulation, structure and testing of the software will be described.

5.2.2. Laser Balancing Algorithm Development. The goal of this aspect of the Laser Balancing Project was to develop a software algorithm which, on the basis of information received from a Gisholt 3S balancing

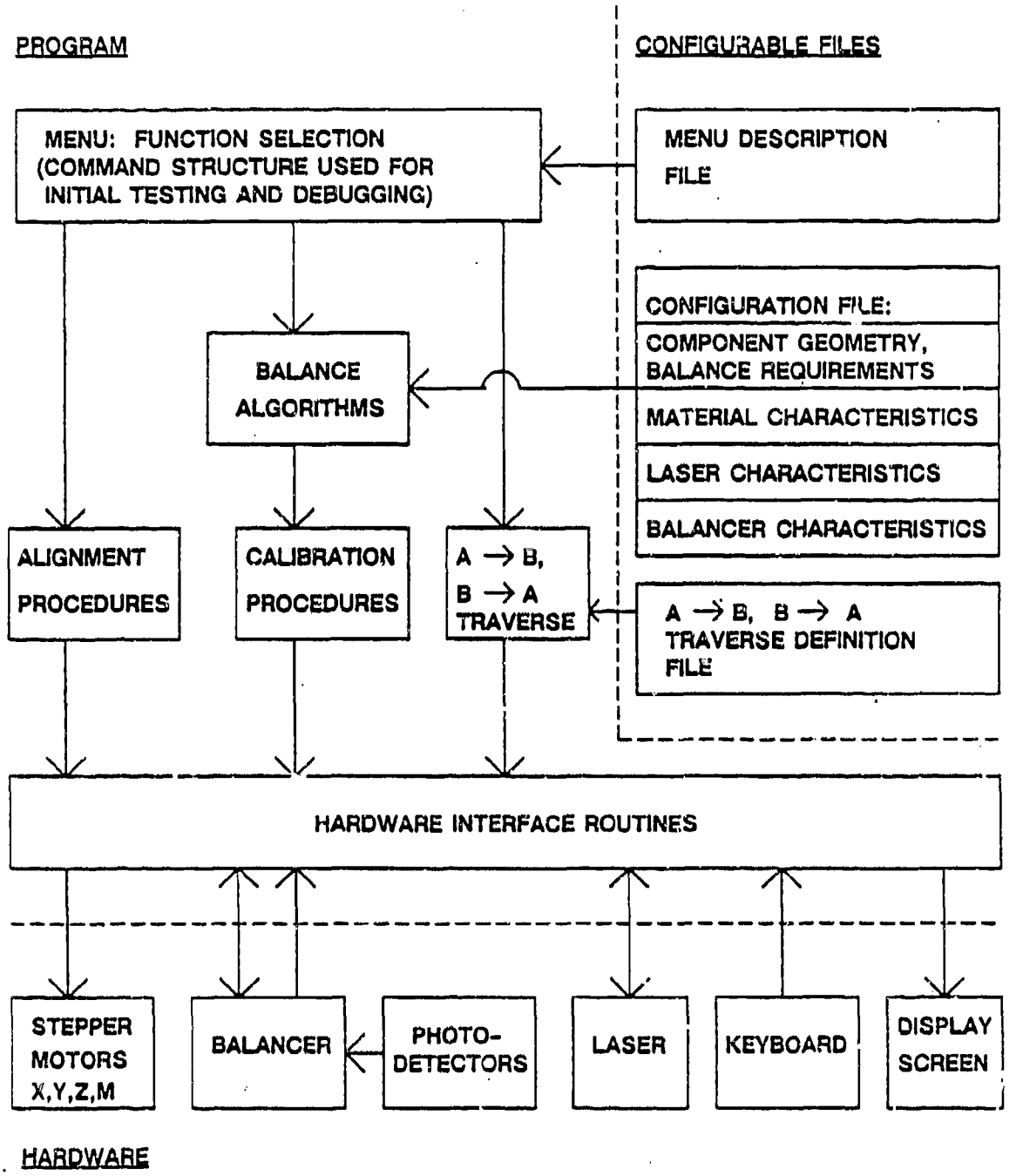

Figure 5-21. Software Structure

machine, defines and controls the placement of laser pulses needed to balance a given turbine component. Analysis to date has been focused on a specific turbine component, namely the impeller assembly of the AGT1500 turbine engine. Initial formulation was directed at the B-plane geometry. This mass removal site can be characterized as being an annular ring lying in a plane which is normal to the axis of rotation of the impeller. This situation was chosen for analysis because it is geometrically simple, thereby allowing attention to be focused on developing pulse pattern optimization strategies, automatic correction

schemes (if the process begins to deviate from an idealized path), etc., rather than compounding the problem with difficulties associated with complex geometries. On the basis of experience gained so far, however, it can be said that these strategies and schemes form the basis for mass removal algorithms which are applicable to other mass removal sites, even those with complex geometries.

The strategy and constraints for balancing the B-plane of the AGT1500 impeller assembly can be listed as follows:

- If $R\Delta M$ is the magnitude of the measured mass moment imbalance, then the plane does not need balancing if the measured value of $R\Delta M$ is less than 0.5 g-in;
- The impeller is rejected if the measured value for $R\Delta M$ is greater than 45.0 g-in;
- The maximum depth of the mass removal region normal to the B-plane cannot exceed 0.100 in;
- The ends of the mass removal region (i.e., in the circumferential direction) must have a radius of curvature which yields acceptable stress concentration levels, and;
- The circumferential and radial pulse increments, which regulate pulse overlap, must be small enough so as to yield acceptable stress concentration levels due to modulations in the floor of the resulting burn region.

In general, the strategy is one in which material is removed from the component one layer at a time until the criteria for balance is achieved. Before removing any material, however, a pulse pattern for each layer is defined such that the collective mass moment generated by all layers matches the mass moment measured by the balancing machine. It should be noted that the circumferential length of each layer decreases from one layer to the next so as to yield burn region ends with a known radius of curvature (S_e), and pulse overlapping in both the circumferential and radial pulse overlap increments, then the quantities ΔC, ΔR, and S_e, which are specified parameters, will be used to control stress concentration levels generated by the burn geometry.

If the actual mass removed per pulse were known exactly beforehand, and the laser and remaining components of the system performed ideally, the component would be in balance after removing material according to the initial overall pulse pattern. Since the mass removed per pulse is not known exactly beforehand and the system, in general, will not perform ideally, an automatic correction scheme must be incorporated in the mass removal algorithm. With this understanding, the mass removal process proceeds as follows:

(1) Estimate the mass removed per pulse;

(2) Determine the number of layers to be removed and generate the initial pulse pattern for each layer;

(3) Remove one layer of material;

(4) Based on the difference between the mass moment measured before and after removing a layer, calculate the actual mass removed per pulse;

(5) Generate new pulse patterns for the remaining layers based on the actual mass removed per pulse;

(6) If the indicated angular location of the mass removal location has changed, remove the next layer at the new angular location;

(7) Repeat steps (3) through (6) until all layers have been removed. Since this procedure is inherently self correcting, the component will be in balance after all layers have been removed.

By correctly setting the parameters ΔC, ΔR, and S_e, stress concentration levels can be reduced to acceptable levels. For example, if S_e is specified as 1 cm and material is removed to a depth of 0.254 cm, which is the maximum allowable burn depth for the B-plane of the impeller, Peterson[1] shows that this will lead to a stress concentration factor of roughly two, due to end effects. If ℓ_p is defined as the circumferential length of a single-pulse burn and w_p is the corresponding width, preliminary modeling shows for $\Delta C/\ell_p = 0.25$ and $\Delta R/w_p = 0.50$ that modulations in the floor of the resulting burn region are minimal and stress concentration levels due to this should not be a problem. For c defined as circumferential distance at a given radial location, ℓ_c as the total circumferential length of a burn region, y as the radially averaged burn depth, and y_{max} as the maximum allowable burn depth, Figure 5-22 presents a circumferential burn profile for a single

---

[1] Peterson, R.E., "Stress Concentration Factors," John Wiley & Sons, New York, N.Y., p.33 (1974).

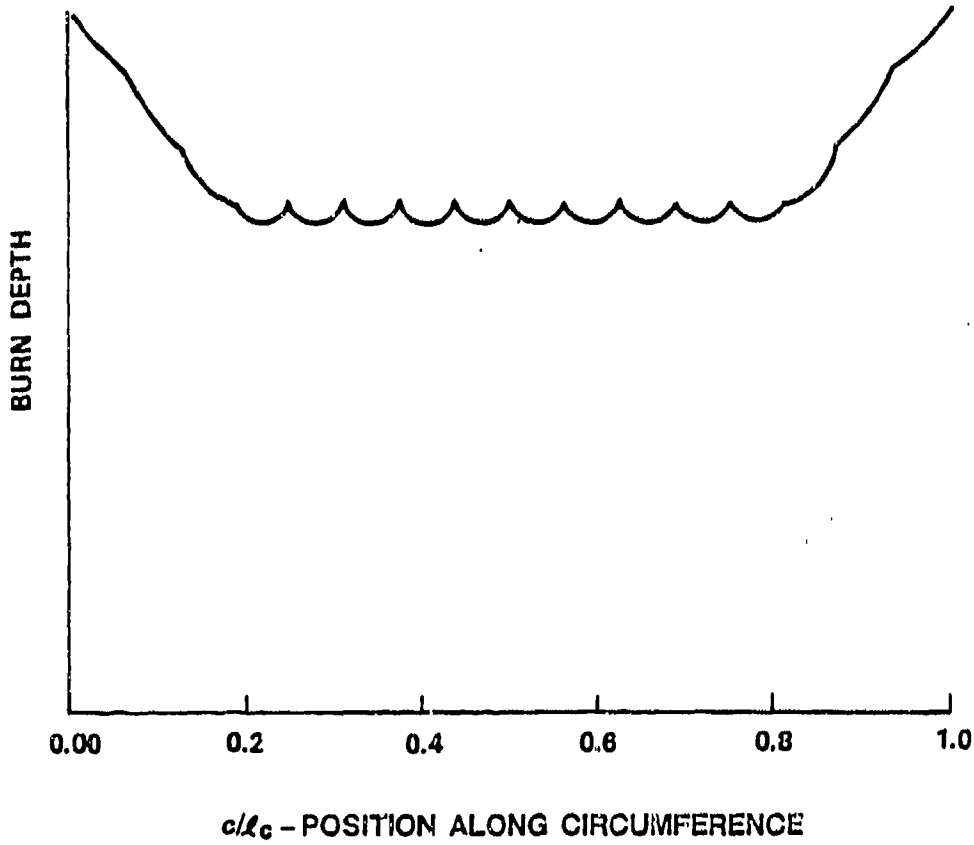

Figure 5-22. Single Layer, Circumferential Burn; $\Delta C/\ell_p = 0.25$, $\Delta R/w_p = 0.50$

layer burn for $\Delta C/\ell_p = 0.25$ and $\Delta R/w_p = 0.50$. Figure 5-23 gives the same type of distribution but for $\Delta C/\ell_p = 1.00$, and $\Delta R/w_p = 0.50$. Based on a parametric study of burn profiles generated by varying $\Delta C/\ell_p$ over the range $0.25 < \Delta C/\ell_p < 1.00$ and $\Delta R/w_p$ over the range $0.25 < \Delta R/w_p < 2.00$, it was found that values of $\Delta C/\ell_p$ 0.25 and $\Delta R/w_p = 0.50$ should yield a burn region floor which is relatively smooth.

In order to generate the distributions given in Figures 5-22 and 5-23 and the initial and updated pulse patterns for the mass removal algorithm, it was necessary to develop a geometric model for a single-pulse burn, which is shown in Figure 5-24. For pulses having a triangular pulse shape, which is typical of pulsed Neodymium-YAG laser (at the pulse duration of interest), and for laser pulses striking a surface rotating about an axis parallel to the optical axis of the laser, the circumferential profile of a single pulse burn can be modeled as a trough of constant curvature, S_p. In the radial direction, however, the profile is assumed to be modeled adequately by means of a truncated Gaussian profile. Currently, expressions relating single-pulse burn length (ℓ_p) and width (w_p) to angular rotation speed (Ω), radial location (R), pulse length time (τ_p), and vaporization time (τ_v) have been obtained. Based on the single-pulse burn model given in Figure 5-24, the radius of curvature (S_p), has been related to the pulse width, burn width and mass removed per pulse. Thus an analytic model has been developed which is a function of angular rotation speed (Ω), radial location (R), pulse length (τ_p), vaporization time (τ_v), and mass removed per pulse (Δm_p).

By applying this model and the idea of superposition, the effects of pulse overlap have been studied. This was the procedure used to generate the distributions in Figures 5-22 and 5-23. Furthermore, the key element necessary for generating the initial and updated pulse patterns, which is layer mean-thickness (h_m), has been derived based on the single-pulse model and superposition principle. In general, h_m is found to be a function of $\Delta C/\ell_p$, $\Delta R/w_p$, Δm_p, and material density (ρ).

With expressions relating ℓ_p, w_p, and h_m to the angular rotation speed, radial location, pulse length, vaporization time, and mass removed per pulse, it became possible to define three different geometries, based on the initial measured mass moment imbalance ($R\Delta M$), to use when defining the number of layers to be removed, the number and location of pulses in each layer, and the circumferential length of each layer. For iron and the operating conditions: Ω = 900 RPM, R = 60 mm, τ_p = 0.65 ms, τ_v = 0.06 ms, and Δm_p = 1 mg, which are characteristic of the system being developed, Figure 5-25 defines the regions in which a particular mass removal cut geometry should be used, while Figure 5-26 gives the details concerning each of the three possible regimes. As can be seen, an optimal cut geometry can be selected based on the measured mass moment imbalance ($R\Delta M$).

Once having identified an optimal geometry for mass removal based on ($R\Delta M$), it is a reasonably straightforward process to generate a pulse

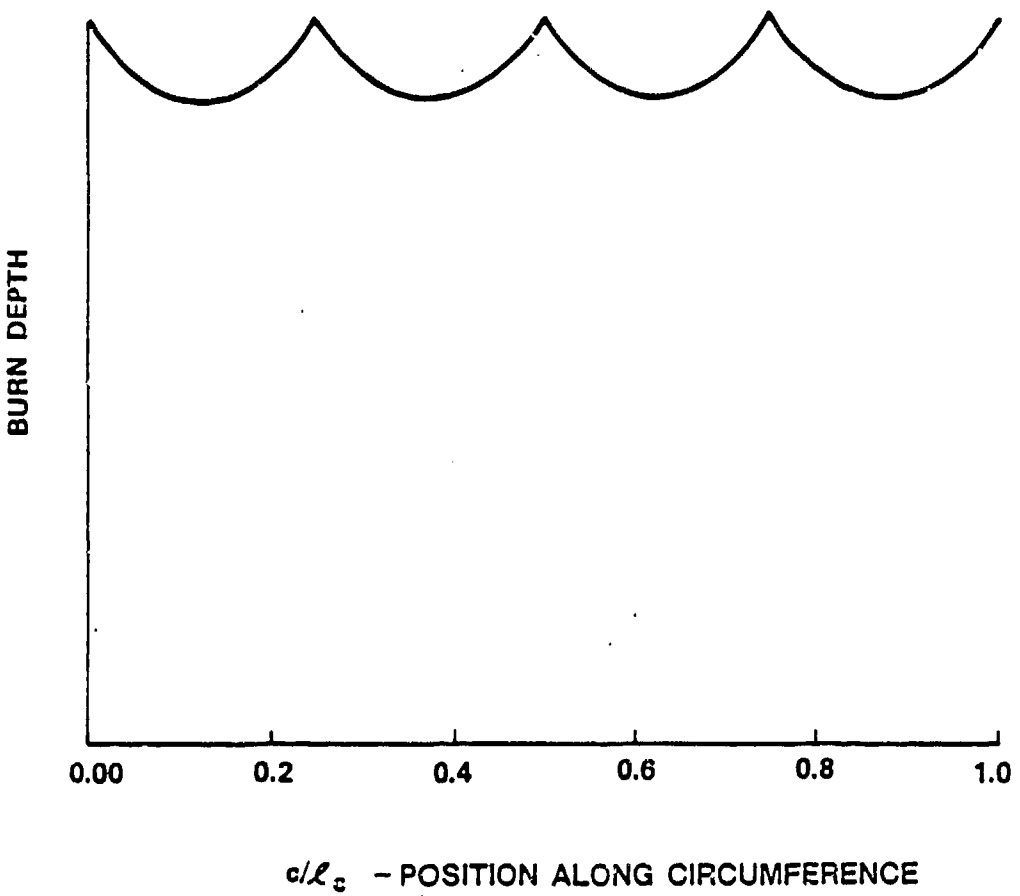

Figure 5-23. Single Layer Circumferential Burn; $\Delta C/\ell_p = 1.0$, $\Delta R/w_p = 0.50$

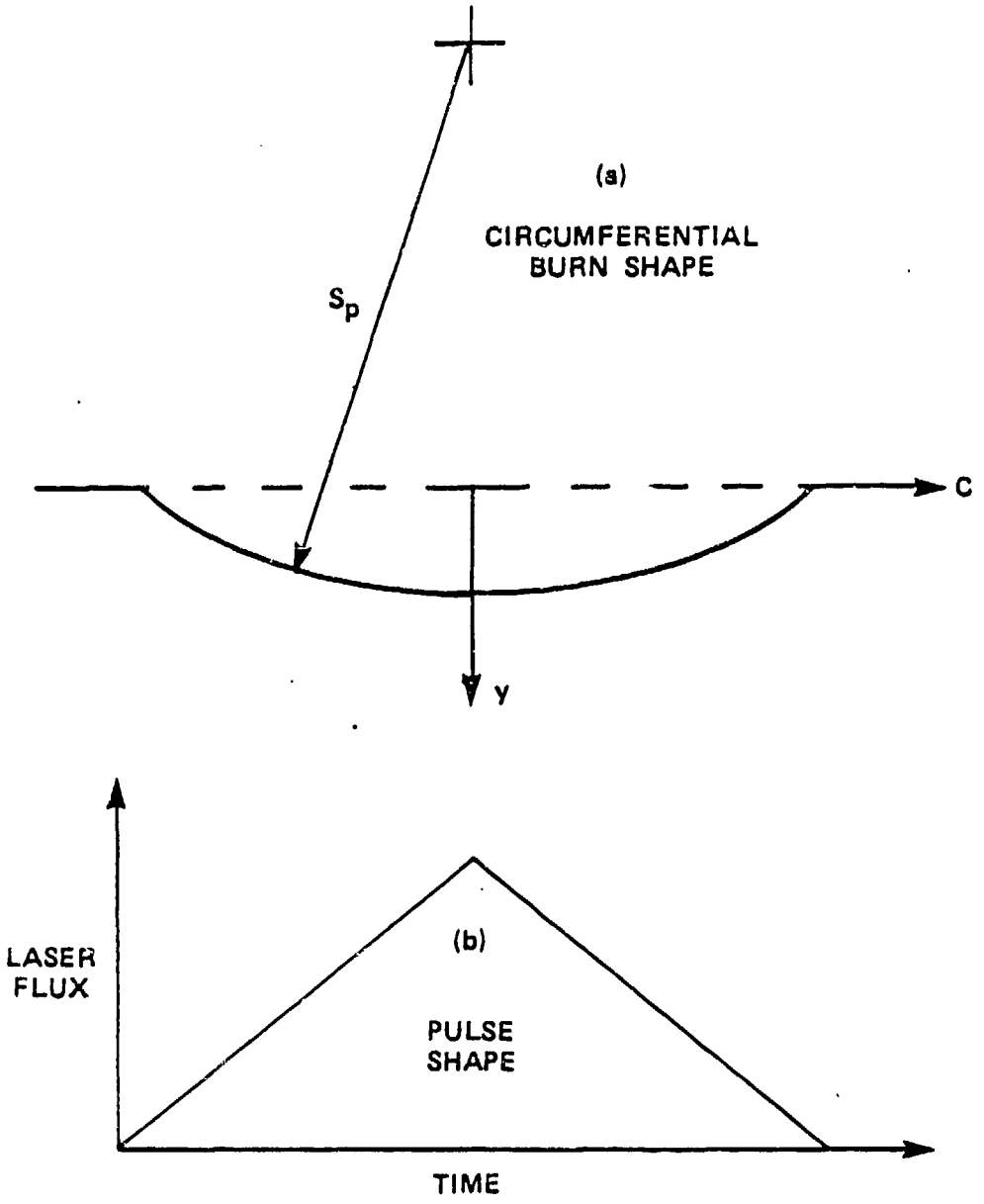

Figure 5-24. Single Pulse, Geometric Burn Model

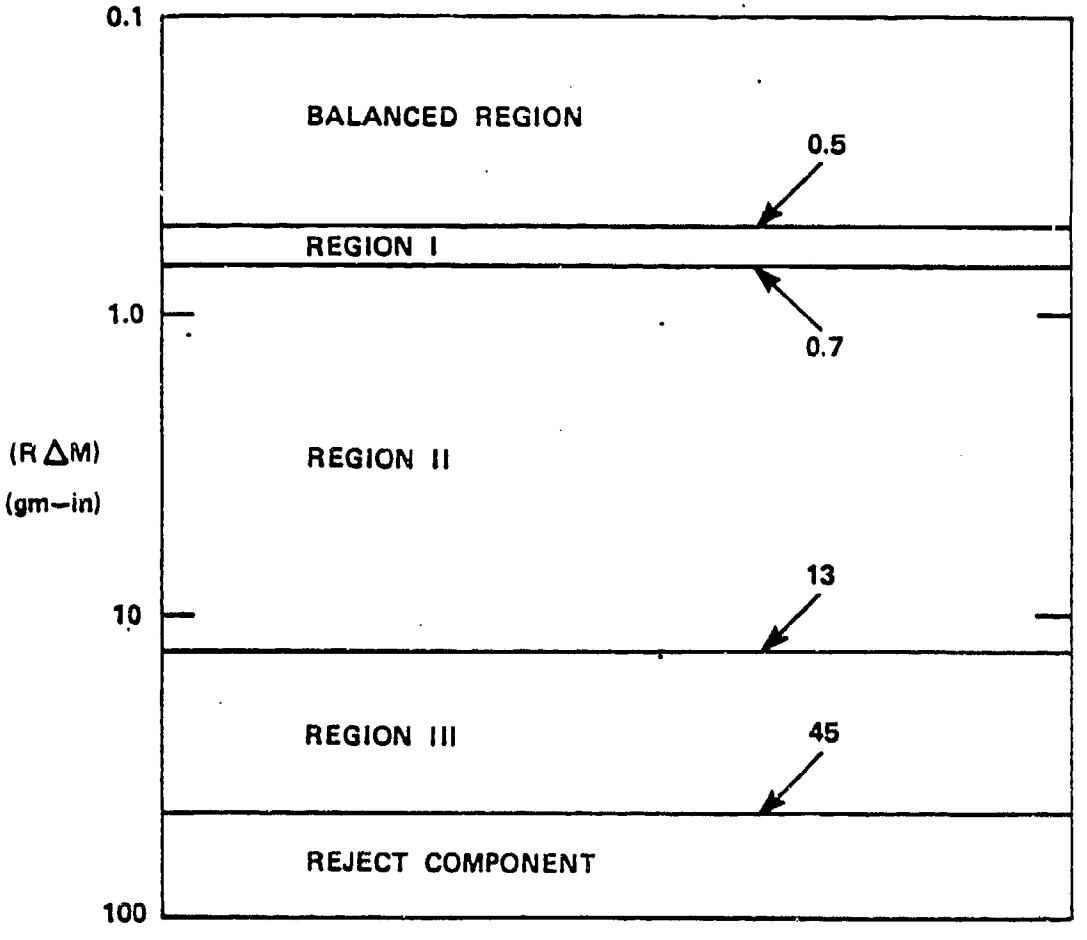

Figure 5-25. Typical Mass Moment Limits for B-Plane Geometry

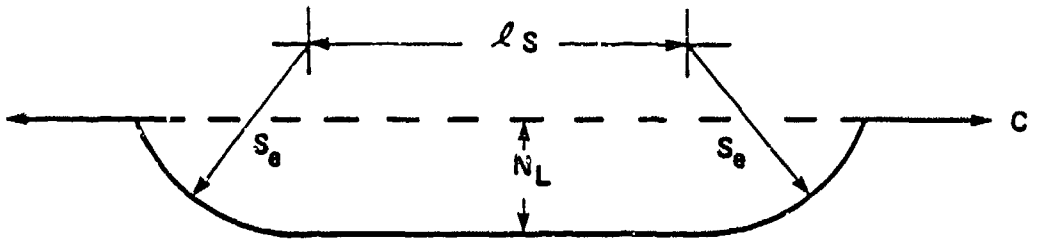

THE GEOMETRICS FOR REGIONS I THROUGH III ARE DEFINED BY:

REGION I:	$N_L = 1$	(FIXED)
	$\ell_s < 2\ell_p$	(VARIABLE)
REGION II:	$1 < N_L < (N_L)_{MAX}$	(VARIABLE)
	$\ell_s = 2\ell_p$	(FIXED)
REGION III:	$N_L = (N_L)_{MAX}$	(FIXED)
	$\ell_s > 2\ell_p$	(VARIABLE)

NOTE: N_L = NUMBER OF LAYERS

$(N_L)_{MAX}$ = MAXIMUM NUMBER OF LAYERS (= MAXIMUM ALLOWABLE BURN DEPTH/LAYER MEAN-THICKNESS)

ℓ_p = LENGTH OF SINGLE PULSE BURN

Figure 5-26. Definition of Burn Geometries and Regimes for B-Plane

pattern for each layer so that the collective mass moment generated by all layers matches the initial measured mass imbalance.

The automatic correction component of the algorithm serves two purposes. First, it determines the actual mass removed per pulse by operating on the difference between the mass moment imbalances measured before and after the removal of each layer of material. Knowledge of the actual mass removed per pulse is necessary in order to construct pulse patterns for the remaining layers that will yield a balanced component once finished. Second, if the angular location of the imbalance changes during the mass removal process, the automatic correction scheme determines new angular locations for the remaining layers so that their removal will yield a balanced component.

During the mass removal process, the pulse patterns for layers which have not been removed must be updated in order to account for variations in the mass removed per pulse and drift in imbalance angular location. This part of the code is referred to as the pulse pattern update component.

In this formulation, the initial pulse pattern generator, automatic correction, and pulse pattern update components, have been integrated to form the actual mass removal algorithm for the B-plane of the AGT1500 impeller assembly. Preliminary tests have shown that the mass removal algorithm will yield good pulse pattern results when the initial (estimated) mass per pulse is in error relative to the actual mass being removed per pulse by as much as a factor of two (either high or low).

5.2.3. Initial Software Integration. One of the key features of the software structure is the ability to use parts of it in a 'debugging' mode, with simple, one-line commands, in order to assess the operational characteristics of mass removal from a spinning rotor. This enabled testing of pulse overlapping, control routines, time delay changes between pulses and assessment of target response.

The program for testing and balancing is called "lbal." It is structured to easily add and delete test routines as the need arises. Some of the routines (and command lines) used are:

ru #st, stinc
: fire laser and step radially

as #ang, %ang, #st, stinc
: fire laser, sweeping through #ang of %ang degrees within radial sweep of #st steps of stinc increment.

mi #ang, %ang, #st, stinc, #ast, astinc
: same as "as" except loop "as" within set of axial steps.

bp
: balance the B-plane with the full algorithm (calls up the menu structure).

ba

read and print the balancer data.

al

alignment: display the positions of the four axes and move them using the keyboard arrow keys.

Other commands set laser parameters such as charging time, post-fire delays, etc.

The software is split into three major levels (Figure 5-21):

(1) operator interface--command or menu input and interpretation.

(2) balancing algorithm--a higher level of the balancing process--theoretical calculations and pulse pattern configurations are performed. Calls lower level routines to perform hardware functions.

(3) hardware functions--routines provide a simple interface for operating the laser, steppers and balancer. Includes:

FAZX - fire laser at array of angles within array of radial positions at given axial position.

BREAD - read balancer angles and amounts.

STEP - move axis N number of steps.

STEPOS - read current axes positions.

Option "bp" of main program "lbal" transfers control of the system to the B-plane mass removal algorithm. This algorithm balances the B-plane of the impeller by removing material under computer control, i.e., computer control of movement of system optics and laser firing based on information read by the computer from the balancing machine.

The first layer of material is removed carefully by applying one or two radial burns at a time. A radial burn is generated by first setting the laser beam at the outer radial edge of the mass removal region, then firing the laser, stepping the laser beam toward the inner radial edge of the mass removal region by one-half beam diameter, and repeating the first-step procedure until reaching the inner radial edge of the burn region (Figure 5-27). The first layer removal process begins by applying two radial burns that straddle the angular location, α, of the mass moment imbalance. These radial burns are separated by a preset angular increment $\Delta\alpha$. In the application of subsequent radial burns, two radial burns are applied at angular locations shifted $\Delta\alpha$ away from the radial line defined by α relative to the last applied radial burns. If α changes enough after application of any pair of radial burns, only

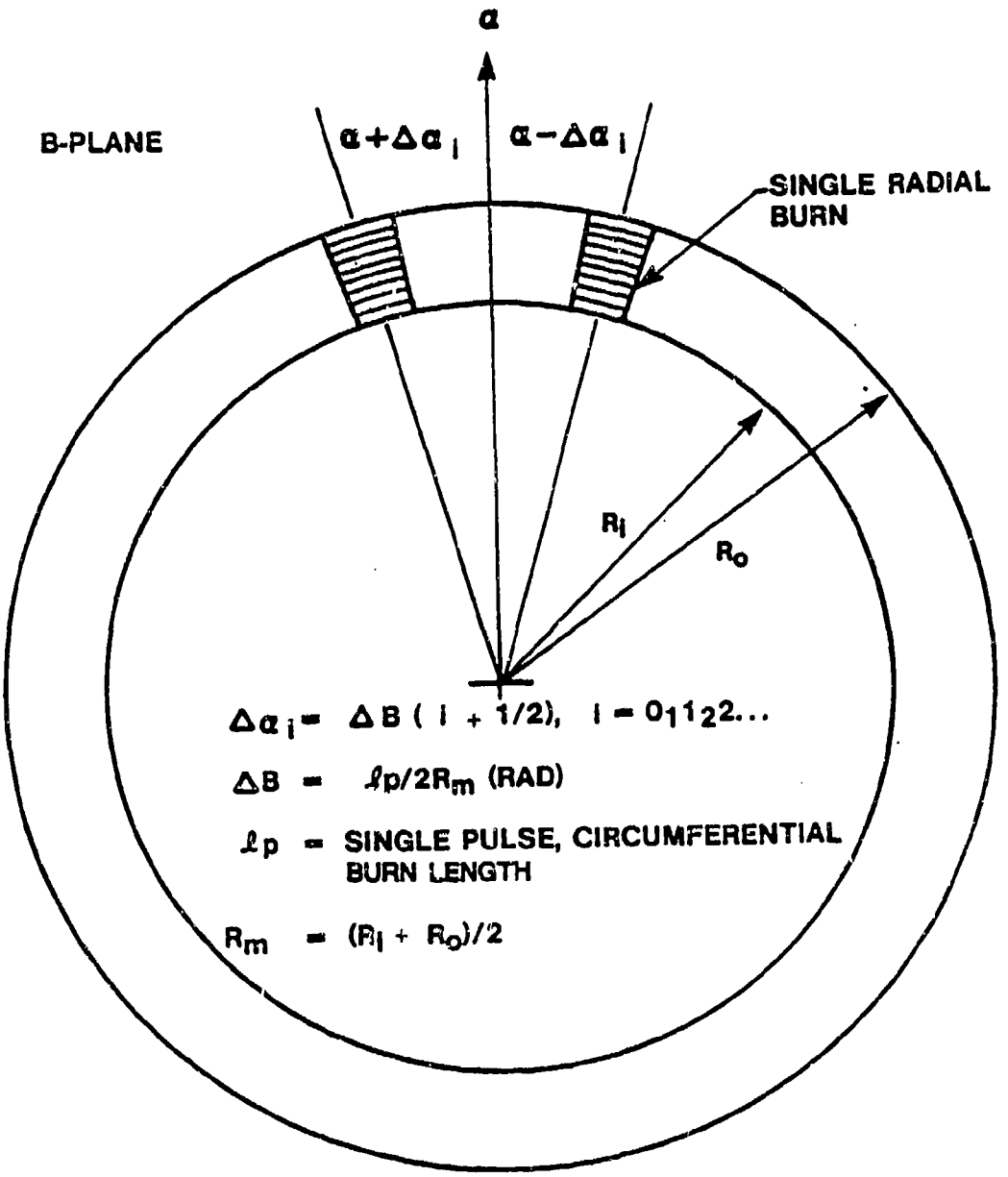

Figure 5-27. First Layer Removal Geometry

one radial burn is applied on the next pass in order to maintain the initial measured value for α. Thus, if there is discrepancy between the measured and actual angular location of the mass moment imbalance, this procedure will correct for the error. This process is terminated when either the change in measured mass moment is greater than the estimated mass moment for the first layer or the number of radial burns exceeds the number estimated for the first layer.

The above procedure is inherently slow because the laser beam is being moved between laser pulses, thus the laser will not fire during every revolution of the component, and the balancing machine is being read after every pair of radial burns, which requires 10 seconds each time. Thus, if this procedure is applied to a first layer that has a relatively long arc length, removal of the first layer may consume an unacceptable amount of time.

This problem was corrected, after initial testing and evaluation, by terminating the above procedure when the change in the mass moment imbalance of the first layer exceeds 0.5 g-in. For typical operating conditions, this requires 400 laser pulses. This number of pulses is sufficient to provide a statistically accurate value for the mass removal per laser pulse. Once an accurate value for the mass removed per pulse is known, the entire pulse pattern can be updated and the remainder of the first layer can be removed in a more efficient manner.

Since the surface generated by laser mass removal is granular, it has been found necessary to perform a post-balance procedure which smooths the surface. Smoothing is obtained by defocusing the laser relative to the surface and applying a pattern of laser pulses which covers the region where material has been removed.

5.2.4. Mass Removal Tests.

5.2.4.1 Introduction. A large set of tests was performed on several test rotors to find the performance levels of the traverse and pulse timing control software, in addition to a preliminary investigation of burn quality and laydown pattern optimization. In the following sections, we address the procedures followed in these tests and discuss the results and their implications.

5.2.4.2. Test procedur s. As part of the software development it became apparent that several test routines would be necessary in order to assess the performance of the control system. These routines were described in the previous section. The impact of the routines was important for determining time effective subsystem actuation procedures. The two baseline mass removal routines are:

(1) Radial step and fire combination firing at a specified angular position, over a defined number of steps (routine "ru").

(2) Circumferential step and fire combination over a defined angular range followed by a radial step increment. The procedure is then repeated as many times as is necessary to traverse across a defined distance (routines "as" and "ml").

The testing of these procedures clearly demonstrated the limitations of Number 1 in terms of time averaged mass removal rate. Procedure Number 1 limited effective pulse repetition frequencies to less than 2 Hz, owing to the mechanical acceleration limited stepping rates imposed by torque considerations on the motors. The angular firing control requirements of Number 2 are, however, only limited by computer software timescales, and in consequence provide, therefore, a much higher average firing rate, matching the rotation rate.

It was found that Number 1 provides a key function in determining the initial parameters for the balancing procedure during first layer removal as described earlier. In general, Number 2 was used to provide the highest achievable mass imbalance correction rates.

The tests described in the following sections were performed on the B-plane of the AGT1500 impeller rotor. The optical axis for traversing during a run is that along a radial line through the rotor, which for practical reasons is the vertical axis.

5.2.4.3. Single layer tests. A series of burns were carried out in order to assess the impact of several operational parameters. Figures 5-28 and 5-29 illustrate the impact of the first of these which is the radial pulse overlap. Figure 5-27 shows a radial traverse of nominally identical pulses. The incremental displacement between pulses is a nominal half spot radius (0.005 in.). The burn shows clear circumferential striations. In Figure 5-28 the interpulse displacement is three-quarters of the spot diameter (0.015 in.), which yields a more clearly and more deeply modulated burn.

Figure 5-30 illustrates the impact of circumferential overlap on a traverse identical to that in Figure 5-28. In this case the longitudinal overlap is approximately one half the burn length. It is clear that the circumferential striations of a single row of burns are reduced significantly by circumferential overlapping. This particular burn consisted of a series of sequential radial burns of the Number 1 type.

Figure 5-31 is an example of a Number 2-type burn with radial stepping between a series of circumferential pulses. In this case, there is evidence of circumferential striations, but considerably muted as compared to that of Figure 5-28. As a consequence of post-removal surface treatment, however, a surface wave structure of order of this incremental circumferential offset is apparent. This muting is also to be seen in Figure 5-32 which is identical in terms of pulse pattern geometry to that of Figure 5-28, but with an additional pass of

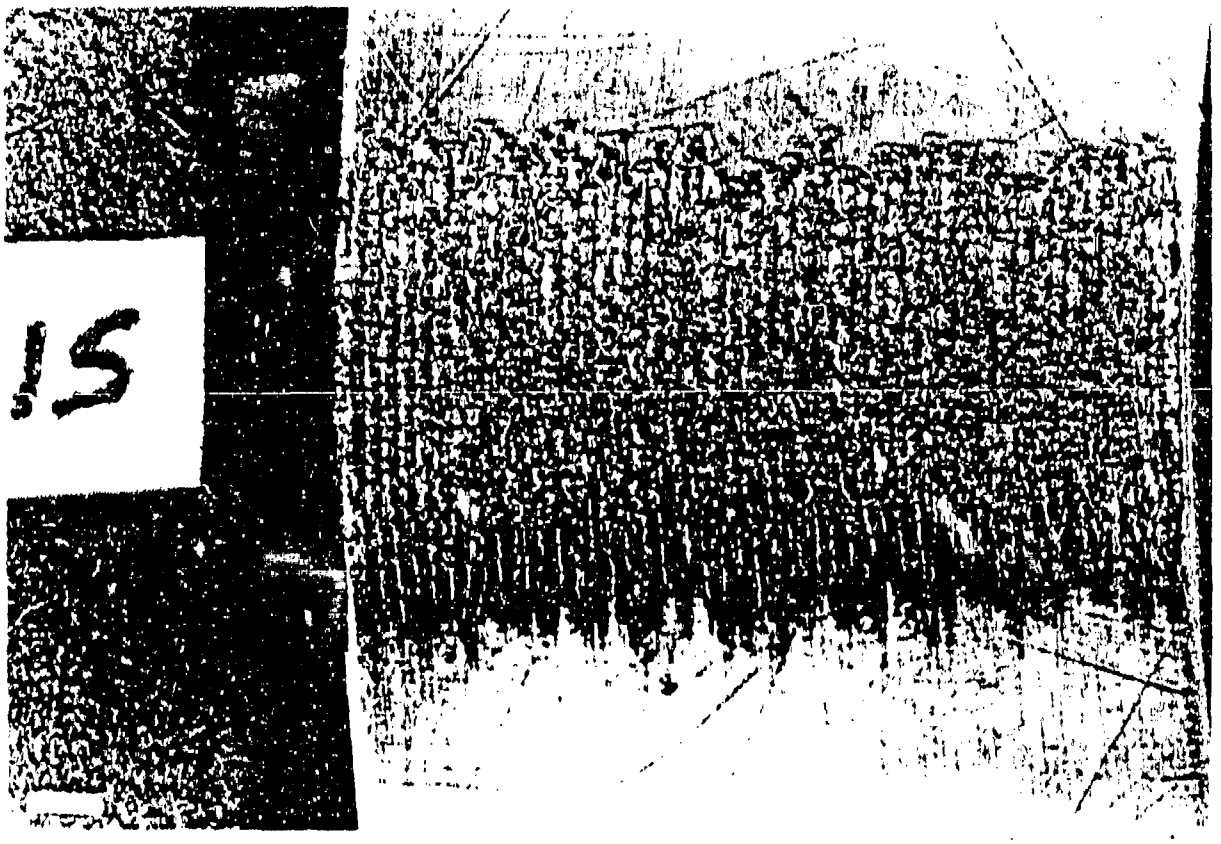

Figure 5-28. Radial Burn Sequence -- Steps at 0.005-in Intervals.

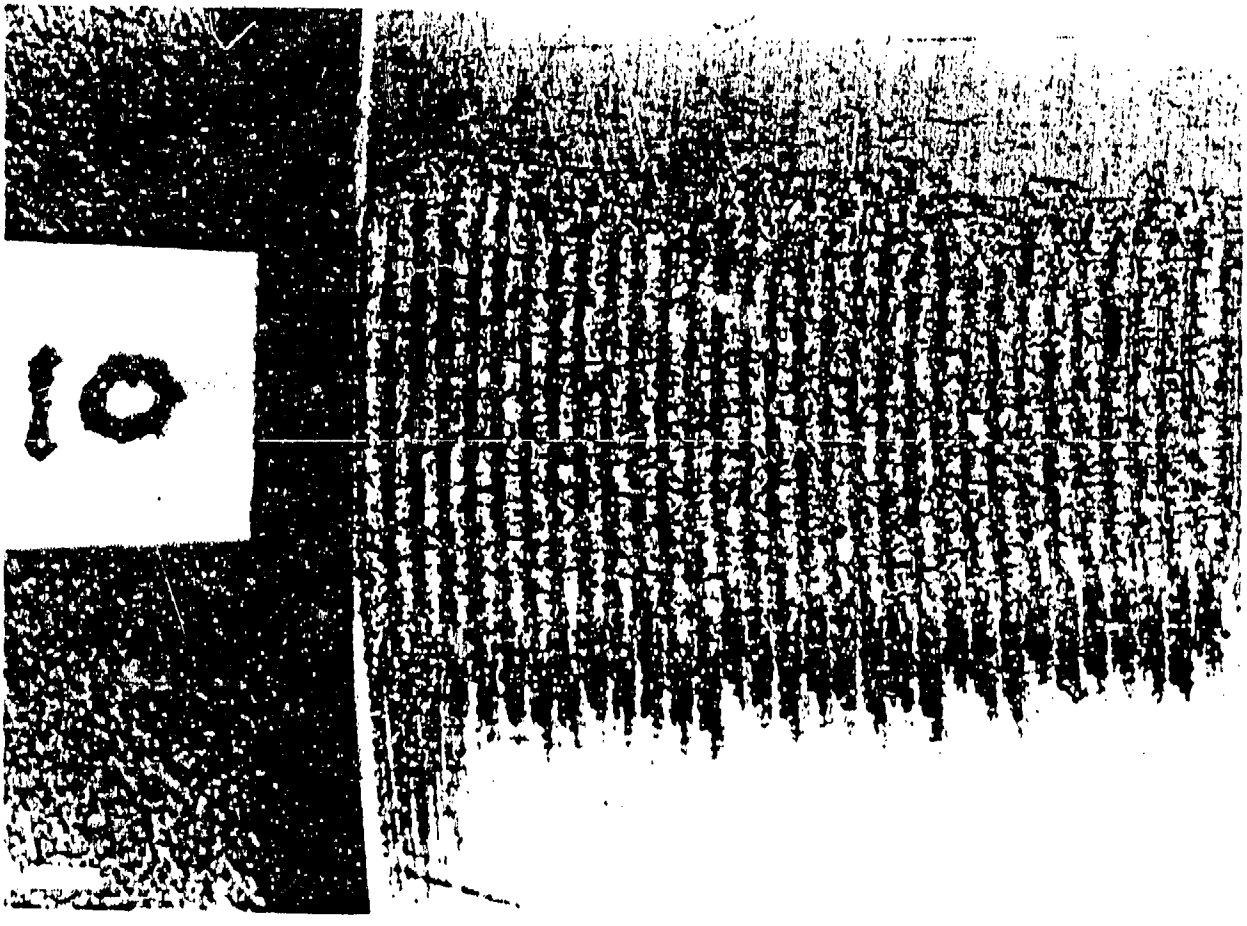

Figure 5-29 Radial Burn Sequence -- Steps at 0.015-in Intervals.

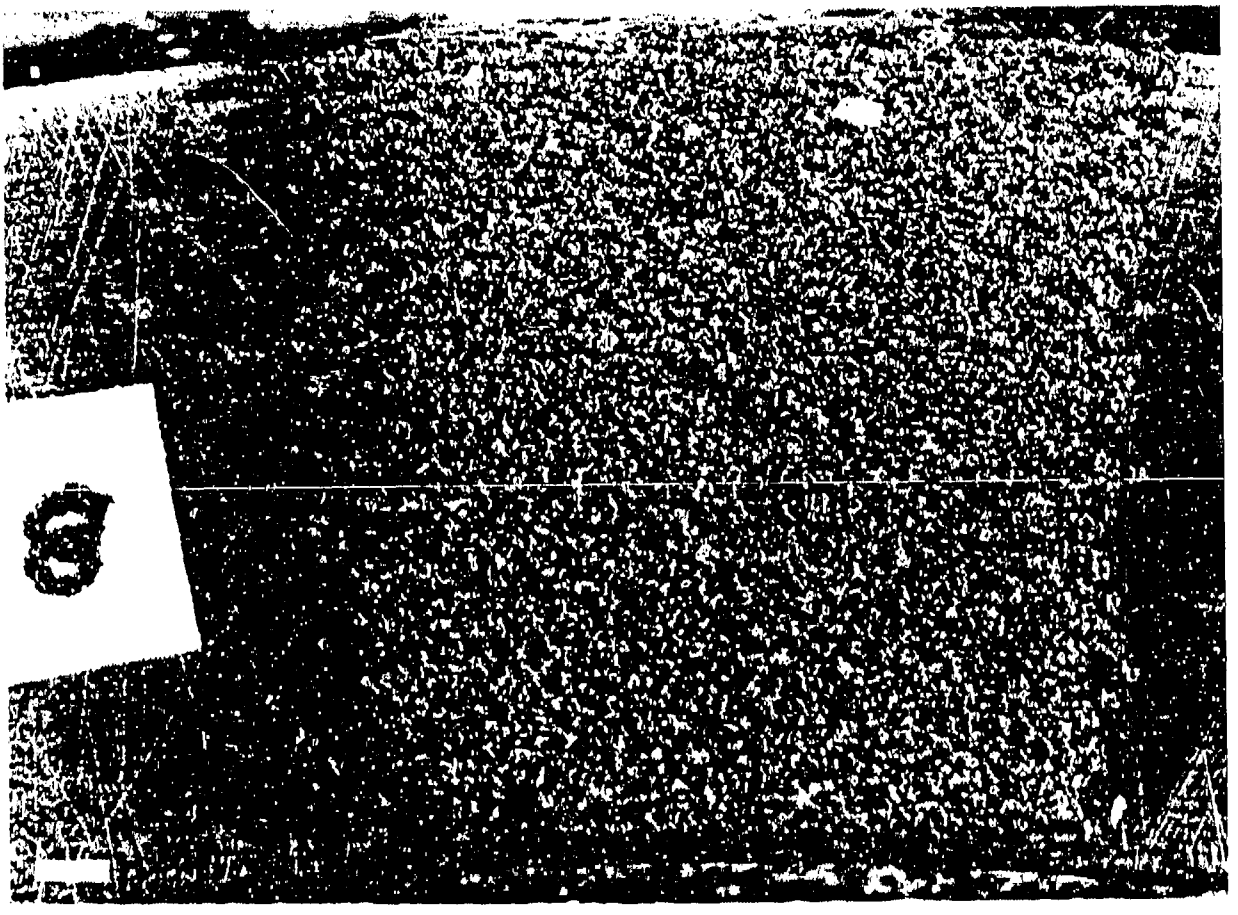

Figure 5-30. Impact of Circumferential Overlap--0.005-in. Radial Step

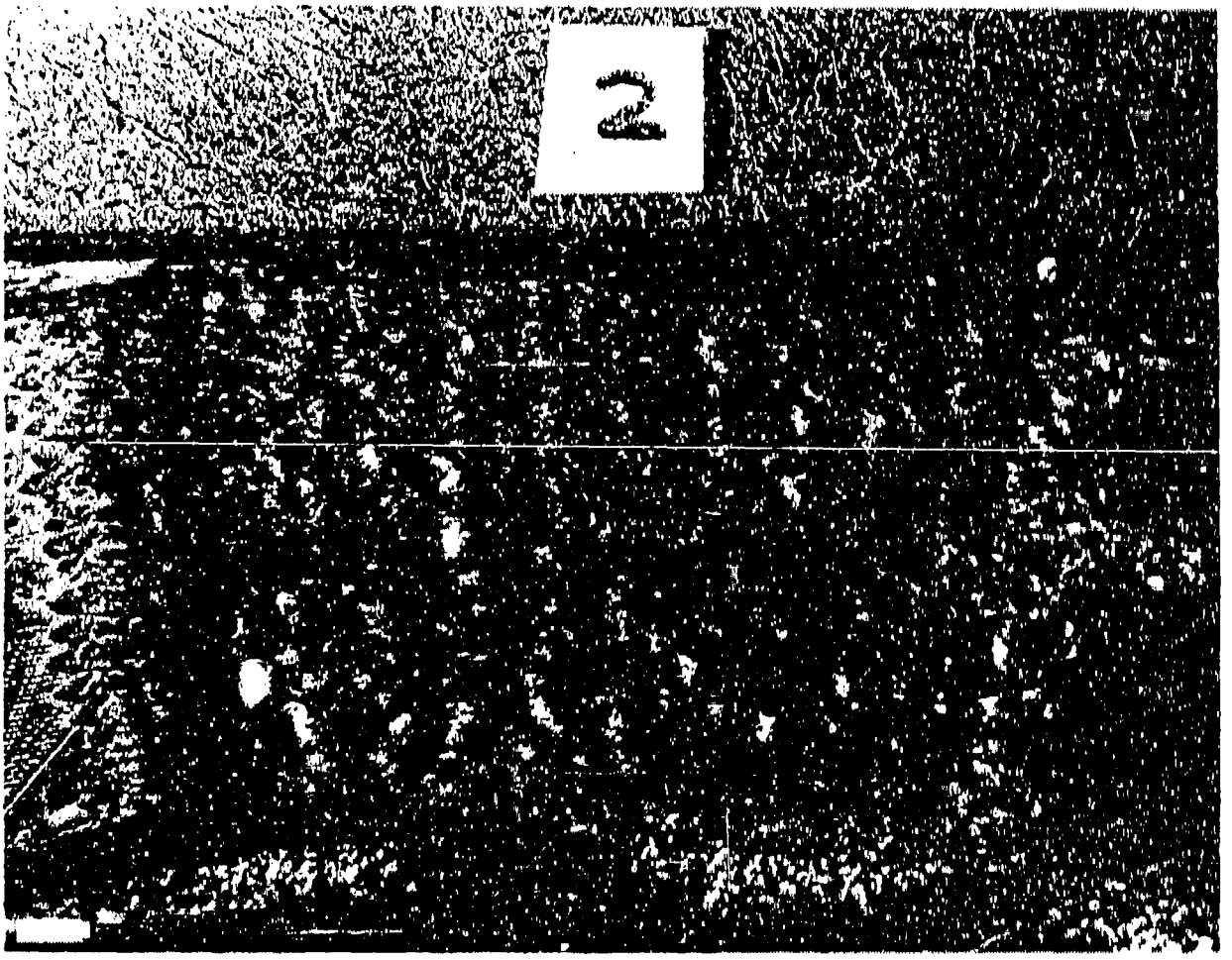

Figure 5-31. Circumferential Burn with Post-Processing

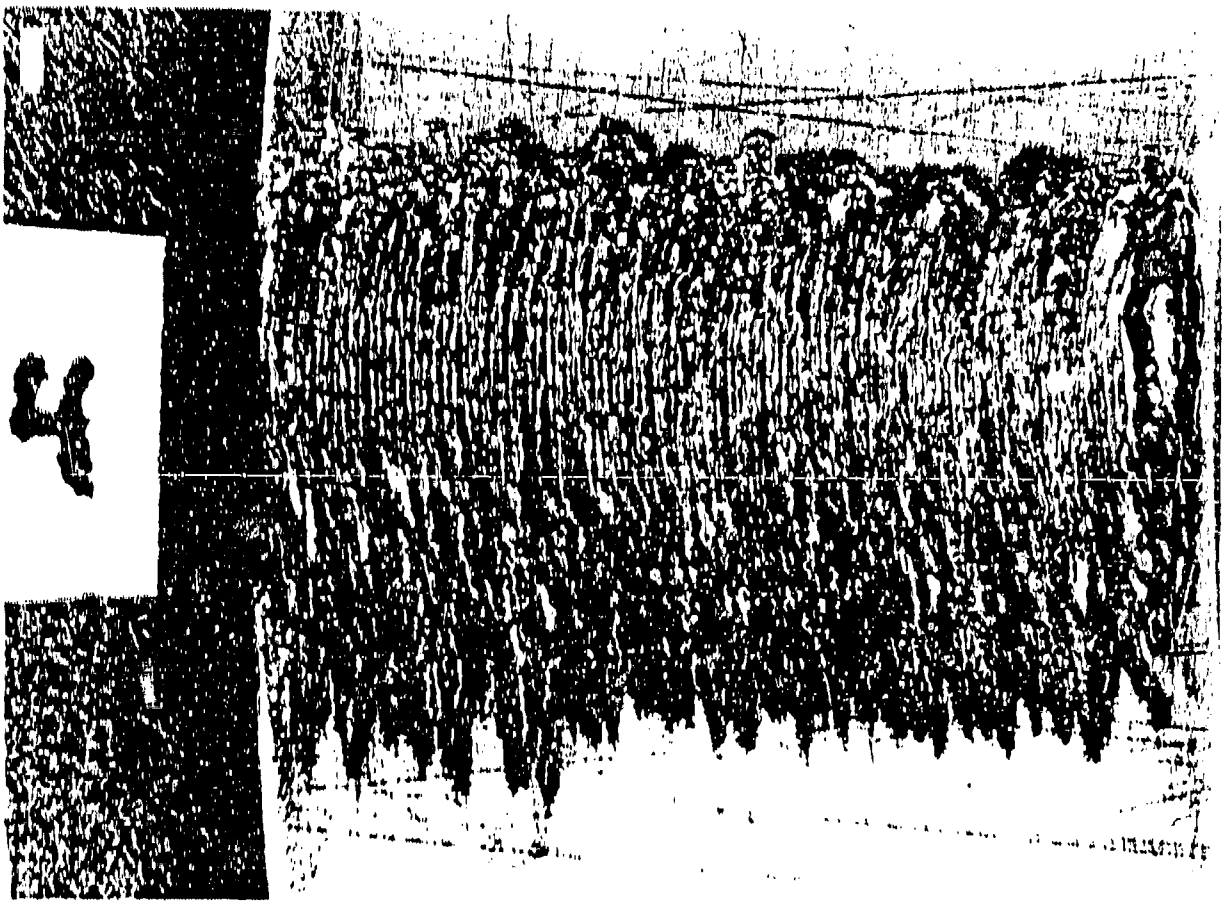

Figure 5-32. Radial Burn with Post Processing--0.005-in Steps

defocused pulses. The impact of post treatment by beam defocusing is very marked.

It has been established that the conditions for optimal surface treating have sound physical rationale. Clearly, the conditions for surface striation elimination or reduction, require that the surface be melted during a pulse. However, despite the melt flow induced by centrifugal accelerations, the most significant requirement is that of a vapor pressure induced melt flow. This requires that the surface reaches vaporization, which is therefore a more stringent criterion than that of reaching melt temperature. This requires a nominal spot size measure of a factor of 2-3 over that used during mass removal.

There appears to be a second reason for a vaporization temperature criterion upon surface post-treatment. With a pulsed irradiation procedure, having partial offsets in both radial and circumferential directions, the impact of defocusing is to dramatically increase the number of thermal cycles to which a given point in the surface is exposed. If the pulse reaches a vaporization condition, a thin surface layer is removed. On cooling, it is possible that oxidation will occur, but subsequent irradiation will remove it. However, failure to induce vaporization of the growing oxide layer allows it to continuously grow during the procedure. It has been observed that failure to reach vaporization during post treatment leads to marked surface discoloration. In terms of the above model, the vaporization limit of 1 oxidation cycle compares with up to 100 cycles in a melt limited case.

5.2.4.4. Multilayer tests. A number of tests, using the Number 2 type step and fire routines, were performed in both single-layer and multilayer conditions. It became apparent that irradiation geometry plays an important role in the behavior of the mass removal process. The major variable is that of the direction of traversing along the vertical, or radial, axis. Figure 5-33 illustrates the impact of inward and outward traversing directions. The vapor jet, where high surface pressure drives the melt splash removal process, is trapped in the step formed between previously irradiated and unirradiated material. This leads to a clearly seen inclination of the jet relative to the optical and rotation axes. For outward traversing, the jet inclines inward towards the center of rotation, whereas for the inward case it inclines away from the center or rotation. The trapping effect of the step has some impact upon the rate of cutting into the surface.

The impact of centrifugally induced melt flow can also be found in some cases. In the case of inward traversing, the melt flow is outwards, away from the step, whereas for outward traversing it is towards the step. In addition, the driver for mass removal is the local irradiation conditions of flux density and fluence. With decreasing radius, the fluence, and thus the mass removal per unit area, increases. All the above effects lead to an increasing burn depth as radial position is decreased. Moreover, in some cases it has been found that excessive local average fluence, arising for example, from multiple pulsing at a

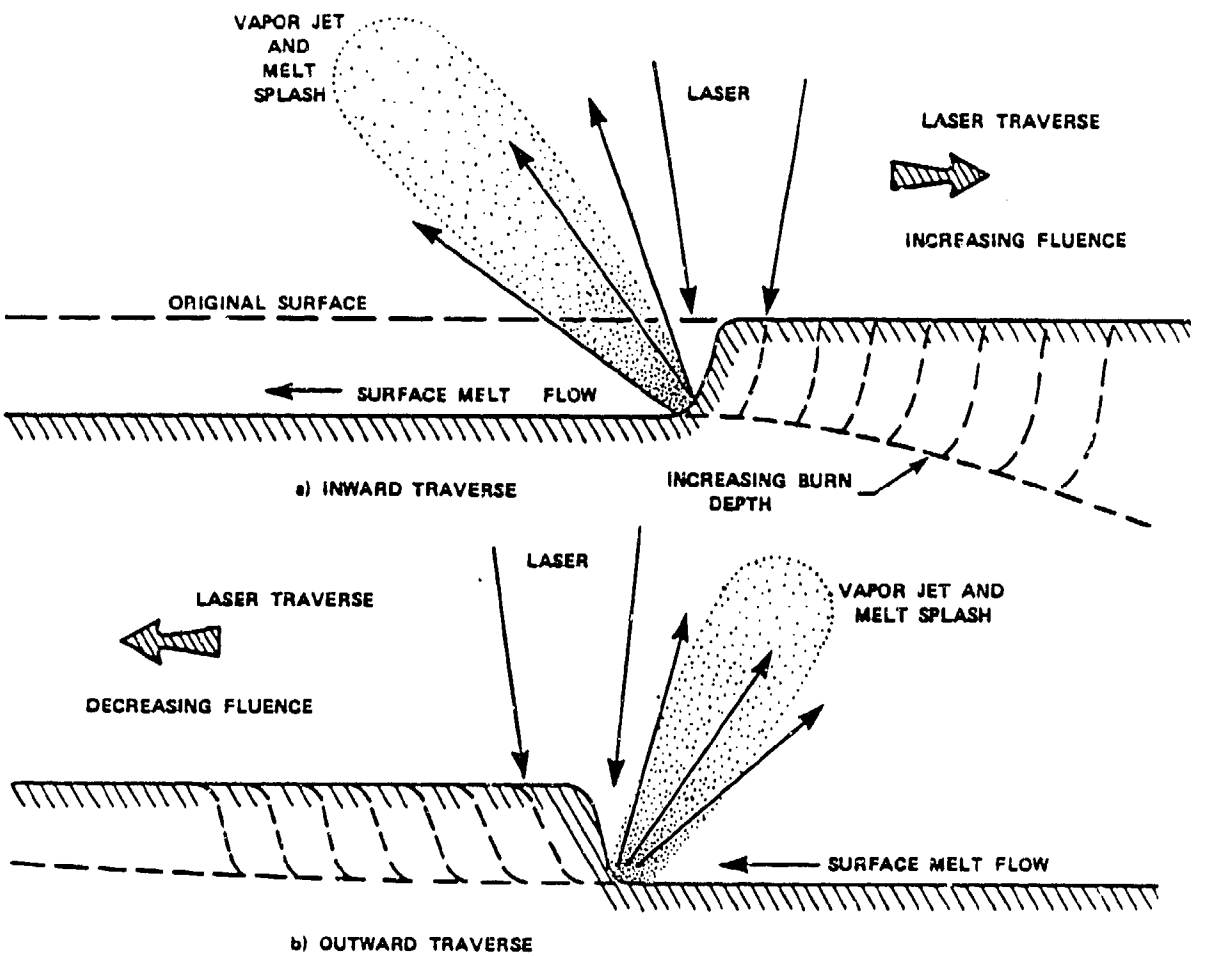

Figure 5-33. Phenomenology of Inward & Outward Irradiation

given location, can lead to significant outward melt flow from the sacrificial ring forming an overhang on the outside edge. Figure 5-34 illustrates these effects. At the inner edge a trench has been formed, through increasing mass removal effectiveness, and melt flow lines, or waves can be seen at the edge of the irradiation zone. This particular burn is an example of a pathological case, as it is also an example of poor surface treatment with excessive oxide build up, as discussed in the previous section 5.2.4.3. The impact of melt flow was minimized if single pulse irradiation at a given location is used between steps. In such a case, the difference between inward and outward stepping direction is minimized. As described in sections 5.2.5.-5.2.7., both inward and outward traversing is used in major mass removal regimes, as this minimizes total irradiation timescales, through reduction in traversing overhead times.

Figure 5-35 shows a rotor with several large multilayer burns in the sacrificial ring. It is to be noted that the circumferential shape of the burn follows a smoothly radiused shape, despite the lack of care and attention to the specifics of circumferential laydown pattern. Figure 5-36 shows the surface of one of these burns; the result of four mass removal passes followed by post treatment of the surface. The circumferential stepping pattern can be seen, similar to that in Figure 5-31.

The desired effects that were postulated from previous modeling studies are comparable to those observed experimentally. The value of post-treatment upon surface quality has been observed and further refinement and improvement appears possible. The overall burn shape appears acceptable from a stress standpoint and is also refineable under full computer control, as opposed to the simple test routines used in these initial experiments. The overall impact of these studies is that significant milestones have been made in understanding the impact of actual required irradiation geometries upon mass removal and cut geometry.

5.2.5. Balancing Tests. Owing to the problem with the counter-based timing system, as described previously, the photodiode-based timing system was used for these tests. The tests were performed on the B-plane of an AGT1500 impeller. The impellers used in these, and subsequent tests, were scrapped components with minor tooling errors. The rims of the impellers were drilled and tapped to accommodate set screws to deliberately control the amount and location of imbalance. The balance machine and icroprocessor were calibrated. This was initially performed using an ASME calibrated rotor, and subsequently through use of an impeller equipped with tapped holes for the addition of calibrated balancing weights.

The rotors were mounted on the balancer and their degree of imbalance adjusted to the desired level. The balancer was then started, the computer given the necessary initiation, and the ensuing procedure observed. The remaining imbalance versus time histories for the four

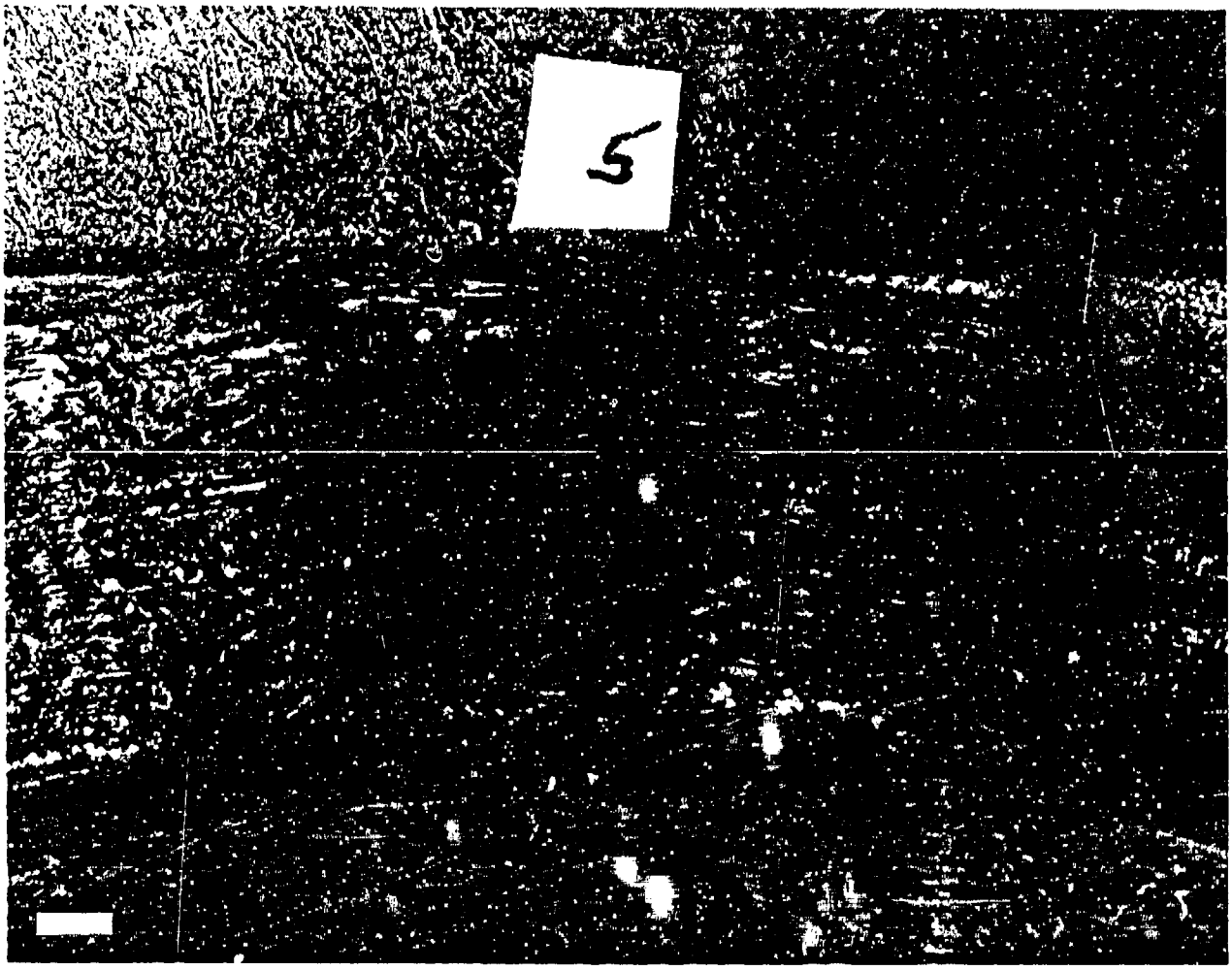

Figure 5-34. Pathological Removal Case with Excessive Flow & Oxidation

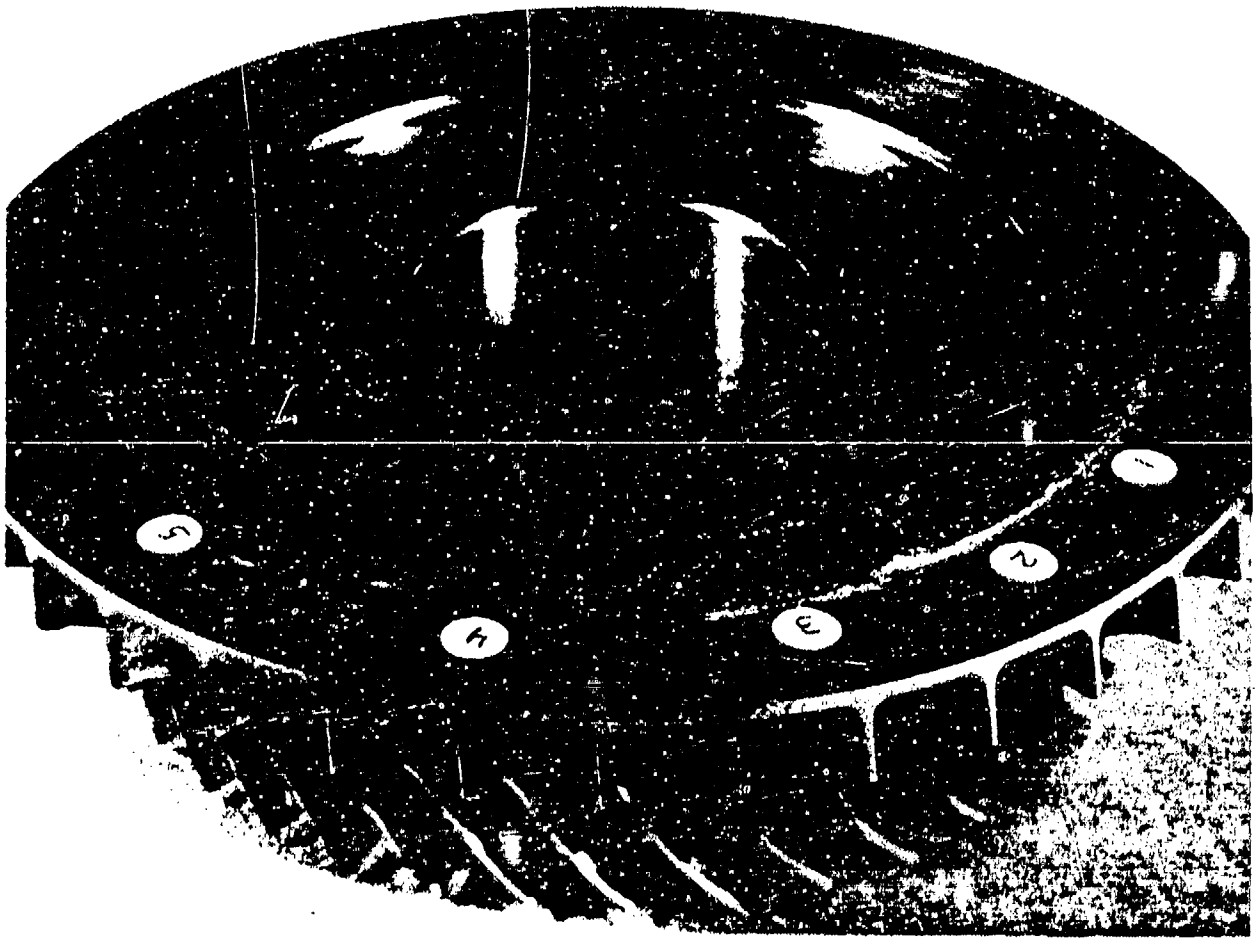

Figure 5-35. Examples of Deep Multilayer Melt Removal

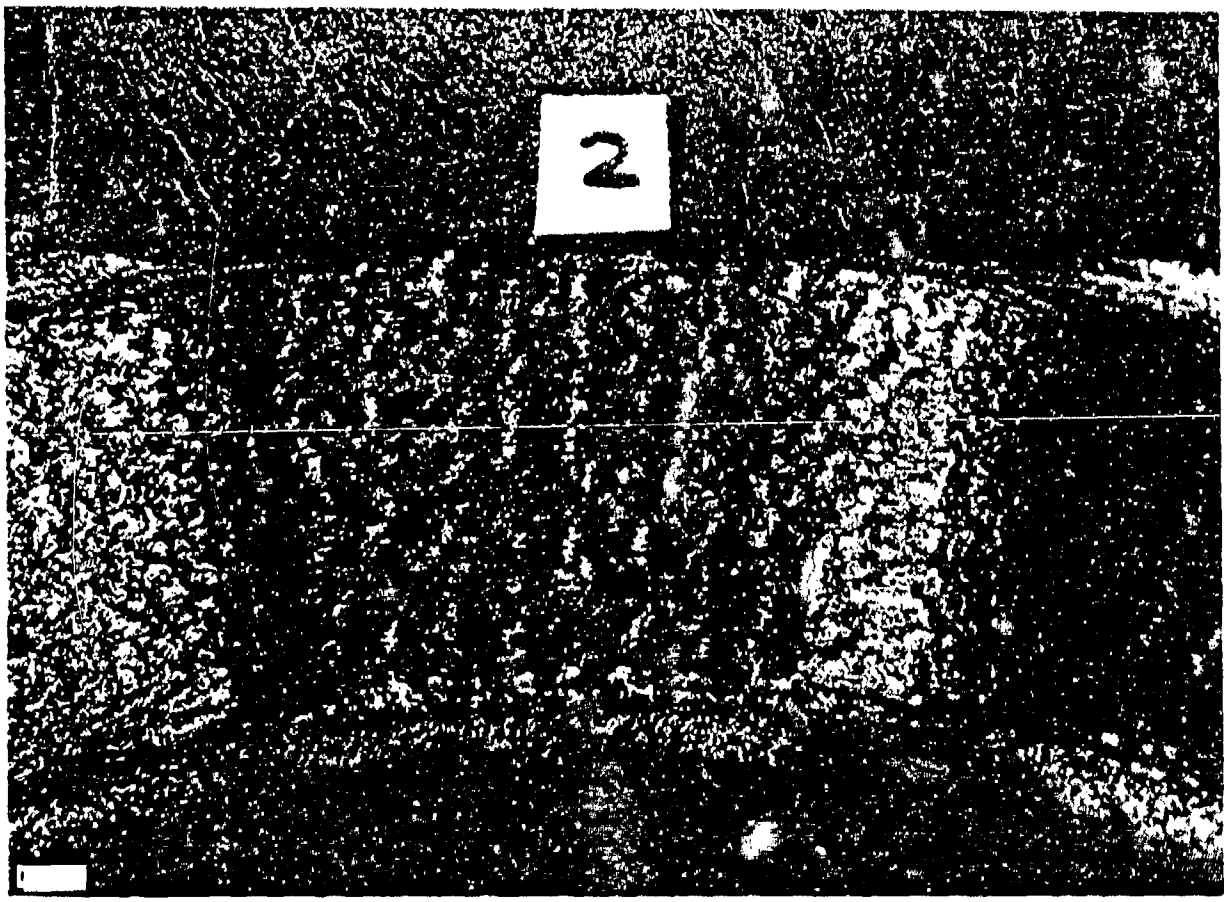

Figure 5-36. Multilayer Melt Removal with Surface Treatment

initial runs are shown in Figure 5-37. The balancing operation was completely automatic, with no operator intervention, and proceeded to a residual imbalance less than the specification for the component (0.5 g-inches). The average value of the residual imbalance during these tests was 0.14 g-inches, with test 4 being the worst case at 0.32 g-inches. As can be seen from Figure 5-37, the quantity of mass removed was considerable, the largest quantity being 19 g-inches. These tests clearly demonstrate the operational capability of the baseline system. The results also indicate room for significant improvement, with respect to conservative stance, with respect to calibration and self-checking during the removal of the first layer, leads to excessive elapsed times. This is a consequence of the procedures for stepping and firing used in this process. The total time for the process may be described by:

$$t_{total} = N_{pulse} t_{rot} + t_{comp} + t_{step} + t_{bal}$$

where:

N_{pulse} is the total number of pulses fired in the process

t_{rot} is the rotation time

t_{comp} is the total computational overhead time

t_{step} is the stepping and repositioning overhead time

t_{bal} is the total balancer reading time

Thus excessive time is taken if the laser is fired only once per step location change.

In addition to the problem with the first layer elapsed time, some variation in mass removal per pulse was observed. Although the balance machine is not capable of resolving the amount of mass removed by any individual pulse, the software keeps track of mass removal over each layer, and therefore, defines an average mass removal per pulse. Some of the variation can also be explained by possible alignment errors. The lack of a coherent and simple solution to the layer-by-layer and test-to-test mass removal variation makes this explanation far from satisfactory, and led to experiments to explain these issues as discussed. The result of the above testing was to upgrade the software and procedures and add a post removal surface treatment operation.

The initial tests demonstrated th workability of the overall system, despite some issues with elapsed time. In consequence, the software was modified to reflect these concerns After having defined a first estimate pulse pattern, the first layer of material is removed carefully. This is because the mass being removed per laser pulse (Δm_p) and the angular offset ($\Delta\theta$) between the photo detector and laser target point are not known accurately. Thus, removal of the first layer must be done carefully as information is being gathered which yields accurate

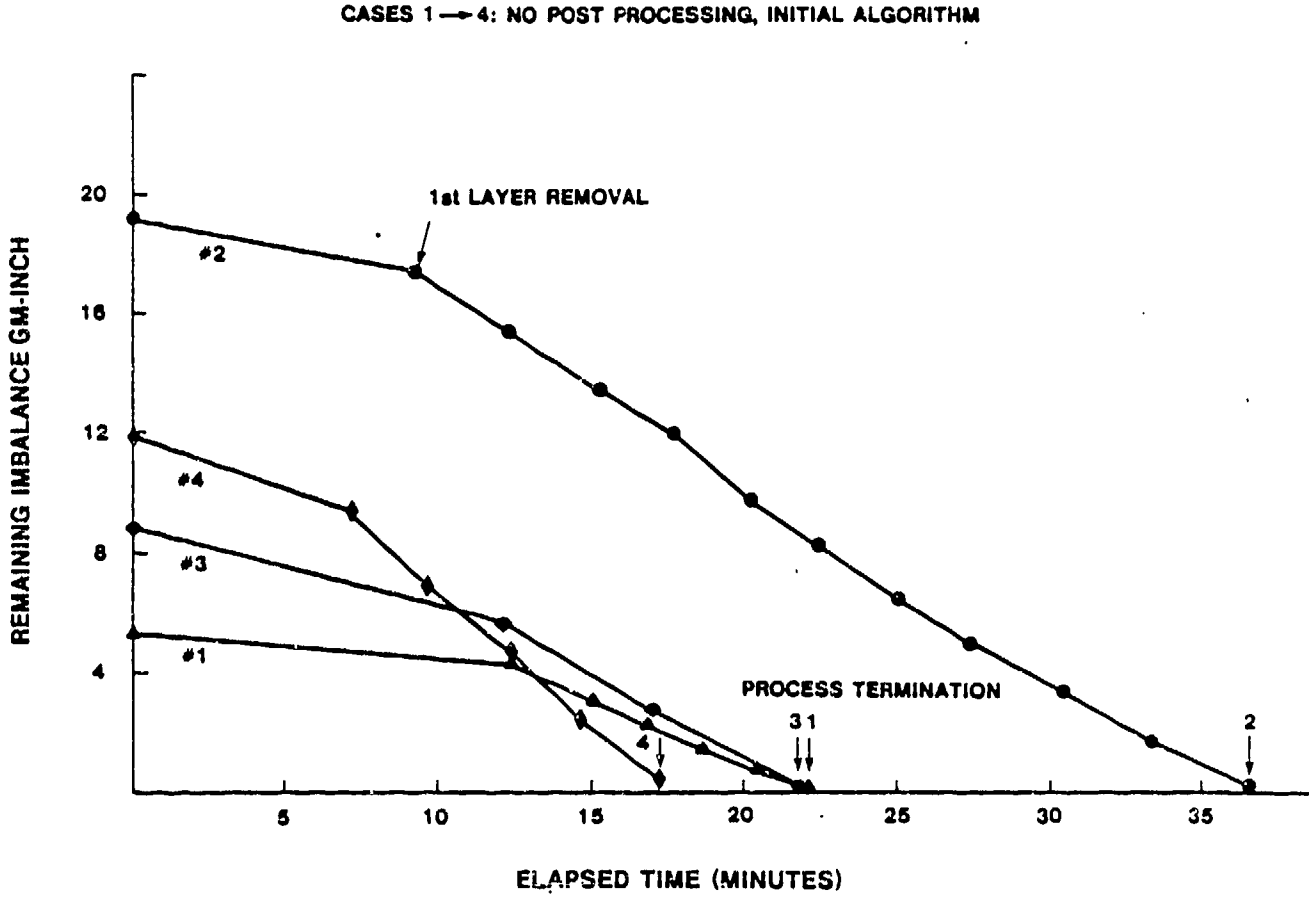

Figure 5-37. Initial Balancing Test Runs

values for Δm_p and $\Delta\theta$. The removal of the first layer is done by applying one or two radial burns at a time.

For the B-plane, a single radial burn is generated by positioning the laser axis at the outer radial edge of the sacrificial ring and repeatedly firing and stepping the laser to the inner radial edge. The first layer removal process begins by applying two radial burns that straddle the radial line defined by the measured imbalance angle, α (see Figure 5-27). These burns are located symmetrically about α and are separated by an amount $\Delta\beta = \ell_p/2R_m$, where ℓ_p is the circumferential length of a single pulse burn, $R_m = (R_i + R_o)/2$, R_i is the radius of the inner edge of the sacrificial ring, and R_o is the radius of the outer edge. In the application of subsequent radial burns, if the current measured imbalance angle is within $\Delta\beta$ of the initially measured value, two radial burns are applied, one on each side of the radial line defined by the initially measured value of α. Each of these radial burns is shifted $\Delta\beta$ relative to the last radial burn applied to that side of the radial line defined by α and in a direction away from the radial line defined by α. On the other hand, if the current measured imbalance angle has shifted by an amount greater than $\Delta\beta$ only one radial burn is applied. This single radial burn is applied to the side of the radial line defined by the initial value that will drive the imbalancing angle back towards the initially measured value of α. The removal of one or two radial burns at a time is repeated until one of the following conditions is met:

(1) The mass moment of the removed material matches or exceeds that given by the first estimate pulse pattern, or;

(2) The number of radial burns matches or exceeds that given by the first estimate pulse pattern.

After one of these conditions is met, the first layer mass removal process is terminated. On the basis of the mass moment imbalance measured before and after removal of the first layer, the actual mass removed per laser pulse (Δm_p) is calculated. This value is used to update the pulse patterns for the remaining layers. By keeping track of the number of radial burns on each side of the radial line defined by the initially measured imbalance angle, the angular offset ($\Delta\theta$) between the photo detector and laser target point can be refined.

The procedure given above works well for determining the mass removed per pulse (Δm_p) but requires an unacceptably long time to remove the first layer of material. The time required to remove the first layer of material is long relative to the removal of subsequent layers of material because the laser axis is being physically moved in the radial direction between laser pulses, whereas subsequent layers are removed by firing the laser at a series of angular locations, stepping the laser in the radial direction, and repeating this sequence. Thus, for subsequent layers, the laser can be fired once per revolution of the turbine component. For the first layer, however, this is not possible; the

laser is fired once every several revolutions. In order to reduce the time it takes to remove the first layer of material, the first layer procedure is not terminated when the mass moment imbalance matches or exceeds 0.5 g-in. The remainder of the first layer is removed in a manner similar to the removal of subsequent layers. A mass moment difference of 0.5 g-in. is sufficient for accurately determining Δm_p and $\Delta\theta$, and reduces the first layer removal time considerably.

5.2.6. Post-Conditioning Process. Figure 5-38 defines the cut geometry and nomenclature relevant to the post-conditioning process. For the B-plane and associated optics (10 cm focal length output lens), the output lens is moved in the X direction away from the burn region floor by 0.2 in. The floor of the burn region is then smoothed by positioning the laser axis at the outer radial edge of the sacrificial ring, firing the laser at a series of angular locations that span the circumferential width of burn region floor, stepping the laser axis inward in the radial edge of the sacrificial ring. This procedure is time efficient.

The edges of the burn region are smoothed next by moving the beam focal point in the X direction away from the burn region floor by the thickness of the layer that was adjacent to the burn region floor; two radial burns are applied, one at each circumferential edge of the burn region; and repeating the X direction step, paired radial burn application sequence until reaching the sacrificial ring surface. The smoothing of the circumferential edges of the burn region is inherently slow because pairs of radial burns are being applied. It is especially time consuming if a large number of layers was needed to remove the required material. Furthermore, a rather large number of laser pulses is being applied to the circumferential ends of the burn region relative to the burn region floor. The post-conditioning time can be reduced significantly by reducing the number of radial burns applied to the circumferential ends of the burn region.

5.2.7. Full Balancing and Post Treatment Demonstration. A series of tests, with the modified first layer algorithm and post treatment, was successfully carried out. The imbalance time histories are shown in Figure 5-39. It can be seen that the first layer removal times have been reduced significantly. The process proceeded to balance in each case, with the post-processing typically requiring 5 minutes. As pointed out in the previous section, this is excessive, mainly as a result of the circumferential end-zone smoothing process employed used for these tests. The average residual imbalance for these tests was 0.2 g-inches. The large values of some of the residual imbalance (0.3 g-inch vs. low values of 0.05 g-inch) is the result of uncertainty in the mass removal per pulse. This will be examined in more detail in a later section. These tests were clearly successful in an overall sense.

The rotor used for these tests is shown in Figure 5-40, with each burn showing post-conditioning of the surface. Some small problems were found with the edge of the sacrificial ring, as had been observed in previous testing. This is primarily an alignment problem, which is

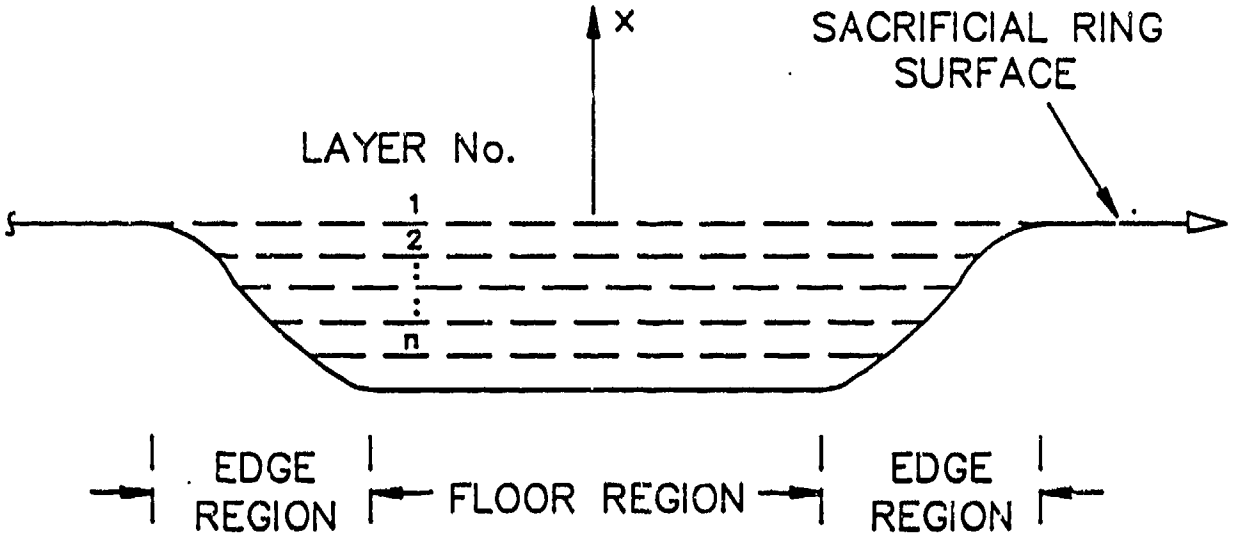

Figure 5-38. Post-Processing Cut Geometry

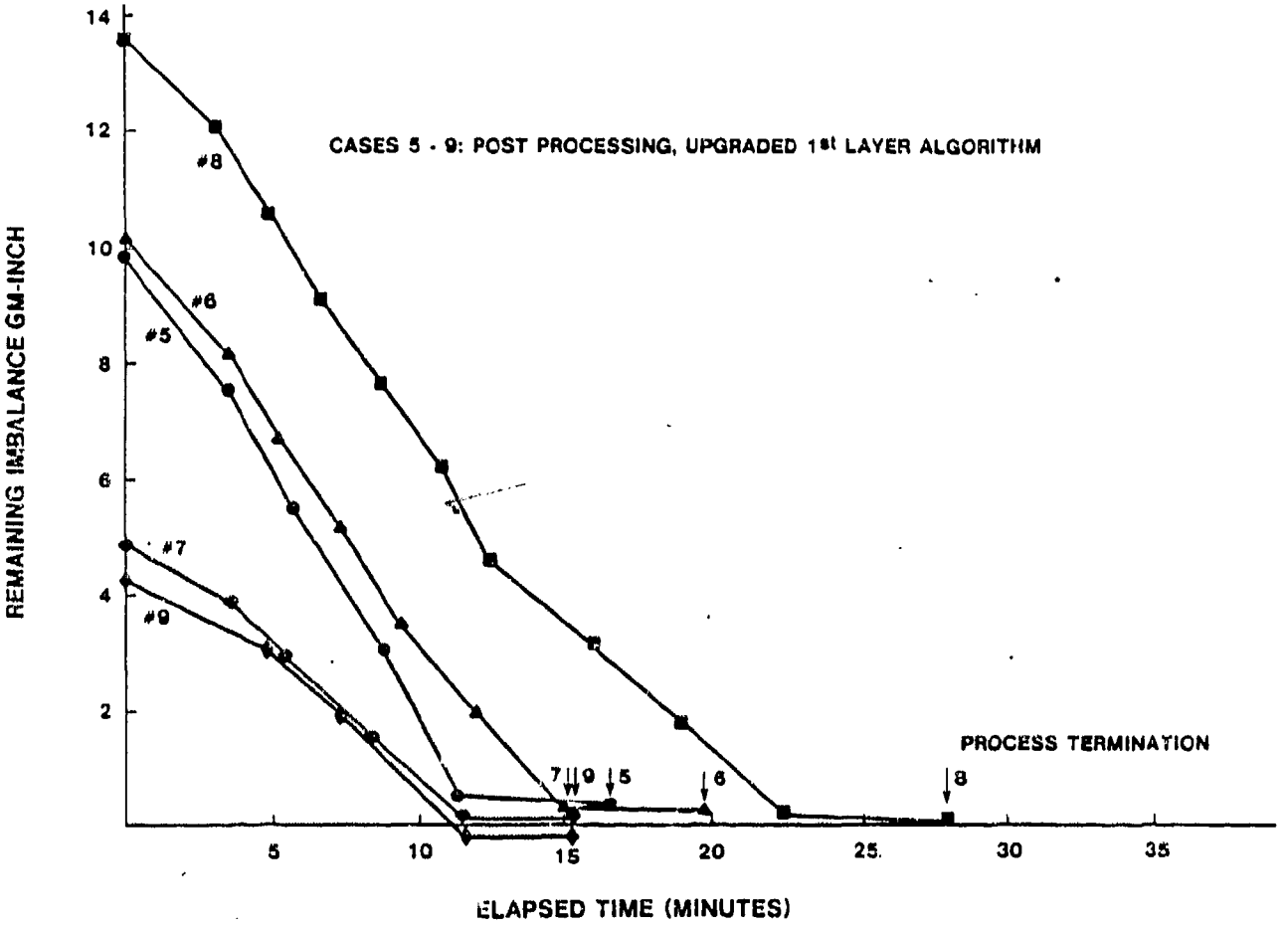

Figure 5-39. Balancing Tests with Post-Processing

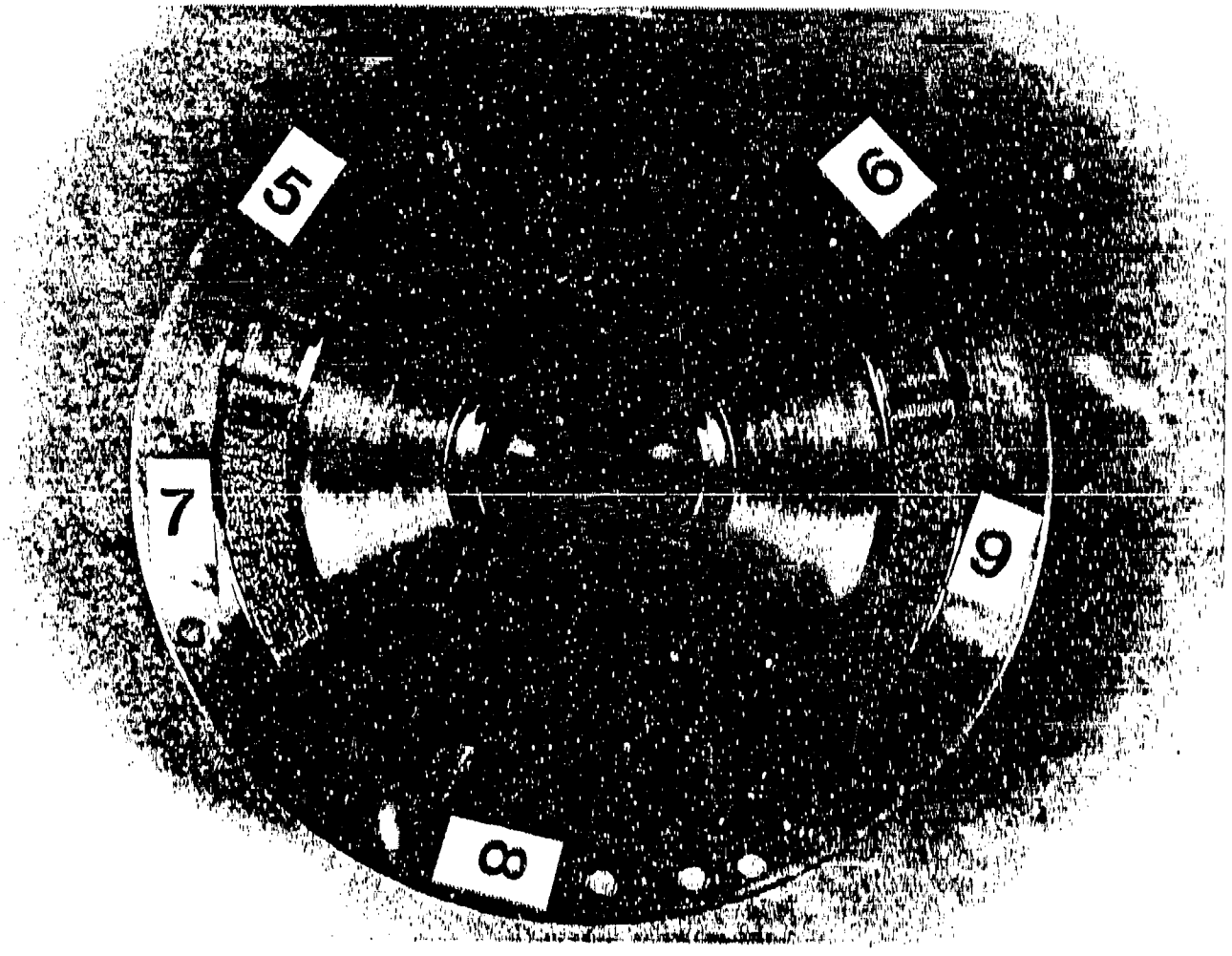

Figure 5-40. Rotor with Examples of Balancing, Runs No. 5-9

solvable with some care and attention. Initially, the modified first-layer calibration scheme worked reasonably well. However, it was subsequently found that the calibration procedure was giving values for Δm_p which were considerably less than those determined from removal of subsequent layers. The problem was traced to the fact that the laser was yielding lower energy per laser pulse at low firing repetition rates (low number of pulses per second) than at higher firing rates.

It was found that variations in pulse energy could be significant under the specific conditions required for laser balancing. The normal mode of operation of the laser is that of fixed repetition frequency for a programmed number of pulses. Under the constraints of laser balancing, the repetition frequency is not fixed, nor is the number of pulses in a burst. Also, the normal mode of operation uses closed shutter prefire (CSP) sequence to establish a thermally stable condition of the laser cavity. The CSP sequence cannot be used under external computer control. Tests were performed to examine the impact of this using a small calorimeter. With Fixed Pulse Forming Network (PFN) voltage conditions, low repetition rate firing and changes in CSP time duration, the laser produced wide variation in pulse energy over a fixed 50-pulse burst for repetition rates ranging from 2 to 15 H_z, which is comparable to the type of burst mode operation defined by the balancing algorithm.

Since the first layer calibration process is performed at a firing rate that is much lower than the firing rate associated with the removal of subsequent layers, the calibration yields very low, unrealistic values for Δm_p. For a given mass moment imbalance, the number of layers of material to actual mass removed per pulse is a factor of two greater than the calibration value forcing the pulse pattern to have twice as many layers as really needed. Since the algorithm updates the pulse pattern for remaining layers after removal of each layer, the update procedure produces layers having large circumferential spacing between laser pulses. This is not satisfactory. Furthermore, the removal time increases because there is a fixed time overhead for each layer.

5.2.8. Large Mass Unbalance Problem. In the balancing tests performed with the previously described algorithm structure, it has been found that the mass removed per laser pulse (m_p) varies from layer to layer. The residual imbalance left after removing all layers of material can be shown to be approximately:

$$\text{residual} = (R\Delta M)_n \times \frac{\Delta (m_p)_n}{(m_p)_n}$$

where $(R\Delta m)_n$ is the mass moment of the last layer of material to be removed, Δ $(\Delta m_p)_n$ is the change in Δm_p between the n-1 and n layers, and $(\Delta m_p)_n$ is the mass per pulse for tne last layer. As can be seen, the residual varies with the mass moment of the last layer and with the normalized variation in Δm_p. The current mass removal algorithm produces values for the number of layers to be removed that are

independent of the initial mass moment imbalance when RΔM is greater than 10 g-in. Based on the expression relating the residual to layer mass moment given above, one sees that the residual imbalance will increase as the total imbalance increases.

Thus, for large imbalances, the mass removal algorithm must be modified so that the mass moment of the last layer is below some imposed value. This can be accomplished by applying the last layer in two parts. During the first pass, every other radial step location is irradiated and, based on the measured mass per pulse, the remaining radial step locations are used to optimize the pulse pattern so as to achieve balance. This is described in the later section describing the enhanced algorithm structure.

5.2.9. Laser Balancing Algorithm: Version Number 2.

5.2.9.1. Approach. As pointed out in previous sections there were several areas of potential improvement in the algorithm structure that offered potential gains, not only in accuracy but in elapsed time to balance. These can be summarized as follows:

(1) First layer calibration and checking of fire angles required too much time, arising out of an excessive stepper overhead. In addition, the problem of pulse energy variation due to low repetition frequency affects mass removal per pulse.

(2) The algorithm allowed for a potentially large number of layers to be generated for the laydown pattern. This introduced excessive stepper overhead.

(3) Residual imbalance errors, due to the variable mass removal per pulse throughout the process, lead to nonzero final imbalance.

(4) Algorithm computational overhead was felt to be unnecessarily high and simplification of the procedure offered benefit to throughput.

(5) For the range of imbalances tested, the burn geometries, although well contoured, were found to be relatively deep and cover small circumferential angles. This may possibly increase the likelihood of stress concentration problems as compared to conventional grinding, where smoothing tends to cover a large arc.

These areas lead to a different strategy being employed in the definition of the procedures for the new algorithm structure. Although the changes are in places quite radical, the overall structure remains unaltered. The changes may be summarized as:

(1) First layer removal is accomplished by an interleaved, two-part removal that eliminates unnecessary stepping and maximizes removal rate while allowing angle calibration and correction.

(2) Last layer removal uses the same interleaving approach to minimize the potential for large residuals through changes in focusing and laser operation.

(3) The number of layers to be removed is kept fixed and the pulse overlap varied to maintain the overall characteristics of the mass removal process.

(4) It was felt, that the arc length of the layer should be increased in order to reduce the total depth of the burn at moderate and small imbalances. This would have minimal impact on mass removal/pulse. Both A-plane and B-plane irradiation menus were implemented in an improved algorithm structure. The irradiation geometries have been illustrated in Figure 5-41. Thus, the traversing terminology used in subsequent sections reflects the differences describing A-plane and B-plane irradiations. Laser trigger timing will control the circumferential position in the A-plane and B-plane. The stepper is used to control radial position in the B-plane and axial position in the A-plane. The generic use of lateral translation reflects the use of stepper controlled motion, whereas circumferential translation (or angular position) implies time delay.

5.2.9.2. Overall burn geometry. The number of layers to be used in the balancing procedure is taken from nominal overlaps and assumed mass removed per pulse. The rationale behind this, is that it allows a given part geometry to have an assigned set of limits that maintains a high mass removal rate and minimizes the computational and stepper overhead. Thus, for example, the revised B-plane algorithm allows for a maximum of 4 or 5 layers as opposed to the 10 or more layers that were used in previous testing. The overall uniformity of the process is achieved by altering the circumferential overlap to account for variations in mass removed per pulse. This variation in mass removal per pulse averages out of two mechanisms; firstly, minor changes in focus position with respect to the surface will lead to changes in pulse removal efficiency. Secondly, the operating procedure for balancing (i.e., circumferentially overlapped burns followed by stepping) does not allow the laser to operate in a steady state mode. The short train of pulses on a circumferential sweep does not allow the laser rod to reach thermal equilibrium, and thus caused the laser power output to vary to some degree. Consequently, the mass removal per pulse in different layers may vary slightly.

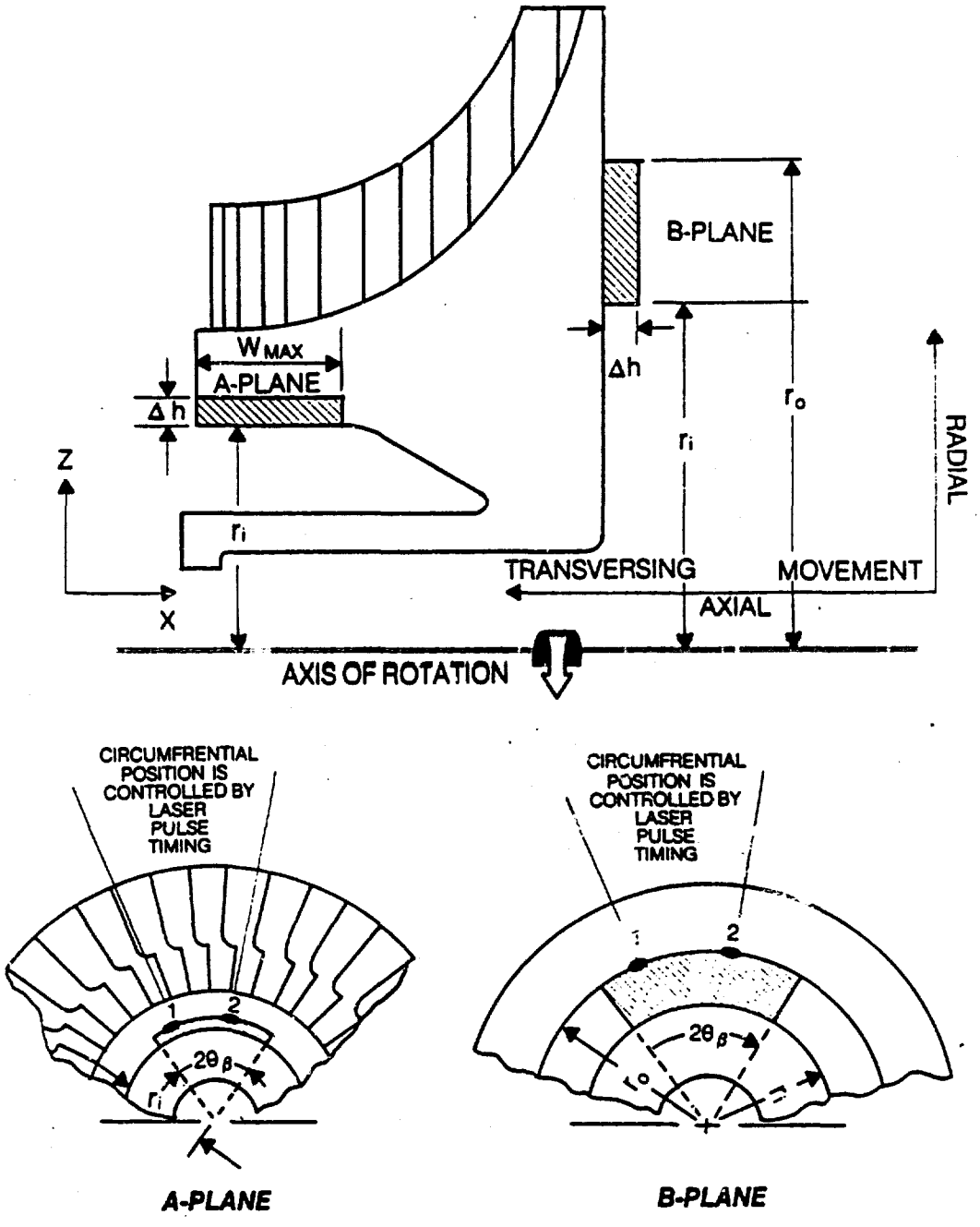

Figure 5-41. Effects of Traversing Movement & Pulse Timing on Irradiation Geometry

The circumferential length of the overall burn is controlled by means of two-part dependent parameters (Figure 5-42). These define the maximum length of a single-layer burn and the minimum length of a maximum allowable burn depth. Again, as with the previous version for the algorithm, this results in three regimes of burn geometry (Figure 5-43). As can be seen, this can allow a smaller depth burn at moderate (2.0 gm-in) imbalances than the previous method.

5.2.9.3. First layer removal. The method of removal involves an interleaving of angular burn strips. This is illustrated in Figure 5-44. The lateral traversing (either radial or axial) is accomplished in two parts. Having established the required overall burn geometry, based upon the past defined geometric limits and the measured imbalance, the first layer overlapping is defined for the initial estimated mass removal per pulse. The lateral and circumferential burn location matrix is then divided into two parts. The odd-numbered locations in the lateral direction are used to remove the first half of the layer. Upon doing so, the balancer is read and the characteristics of the removal process defined.

The potential error in firing angle is calculated by analyzing the imbalance vectors. This allows the new center point firing angles to be calculated and a correction angle to account for error in the first half removal. The correction angle is then applied to the second half of the burn location matrix. The pattern to be removed, if part of a multilayer burn, is then taken directly from the initial burn matrix. However, if the removal is for a small initial imbalance, with only one layer to be removed, the pattern is updated to account for the actual mass removed per pulse. This requires a new pulse overlap for circumferential location to be used in order to remove the remaining imbalances, as well as a new correction angle to reduce the final vector imbalance to zero.

5.2.9.4. Intermediate layer removal. There are up to three intermediate layers removed depending on the mass imbalance region selected. The amount of material removed in each layer is varied by the amount of pulse overlapping. After each intermediate layer, the mass per pulse is updated and calculations done to update the overlapping, as required and described in Section 5.2.9.2.

5.2.9.5. Last-layer removal. The last-layer removal process uses the same approach as described for the first layer. The mass per pulse calculated during the first half removal is used, along with any small angle correction, to obtain as near zero a residual imbalance as possible. The same lateral burn location matrix as that of the first layer is used with the changing of circumferential overlap accounting for changes in mass per pulse.

5.2.9.6. Algorithm integration. Although the second algorithm version encompasses a large fraction of the original version, a key feature of

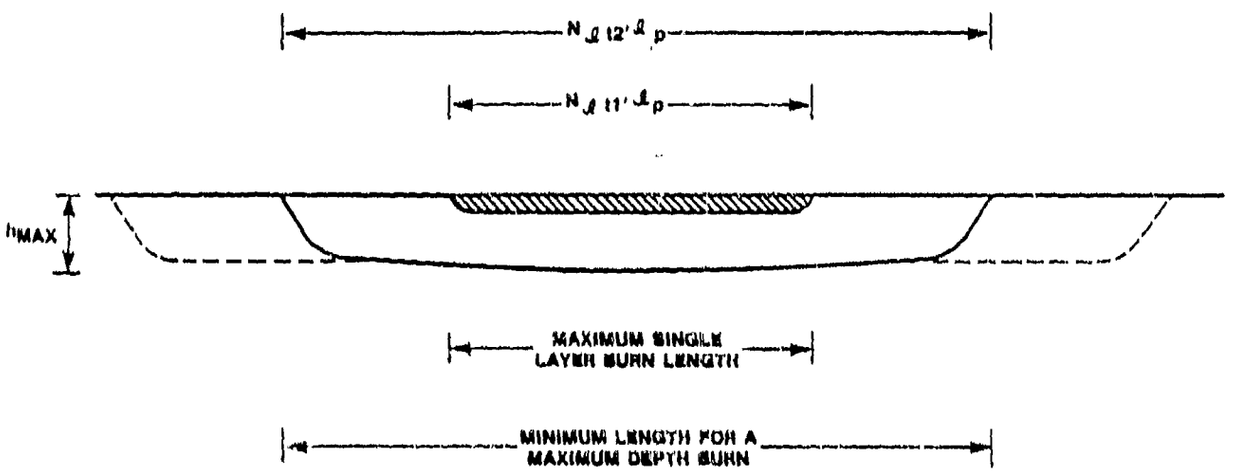

Figure 5-42. Modified Burn Geometry Definition

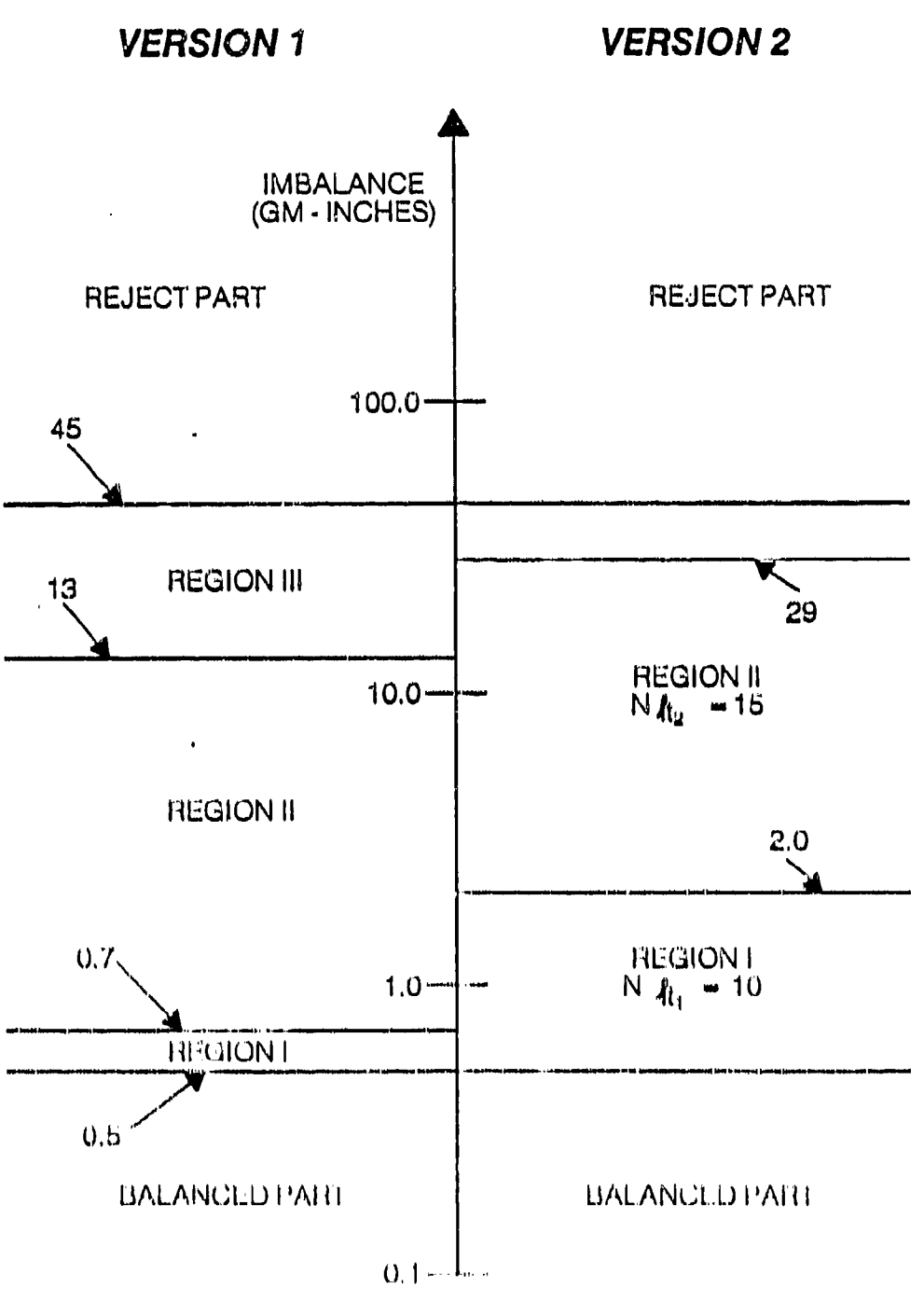

Figure 5-41. Comparison of Algorithm Mass Removal Regimes

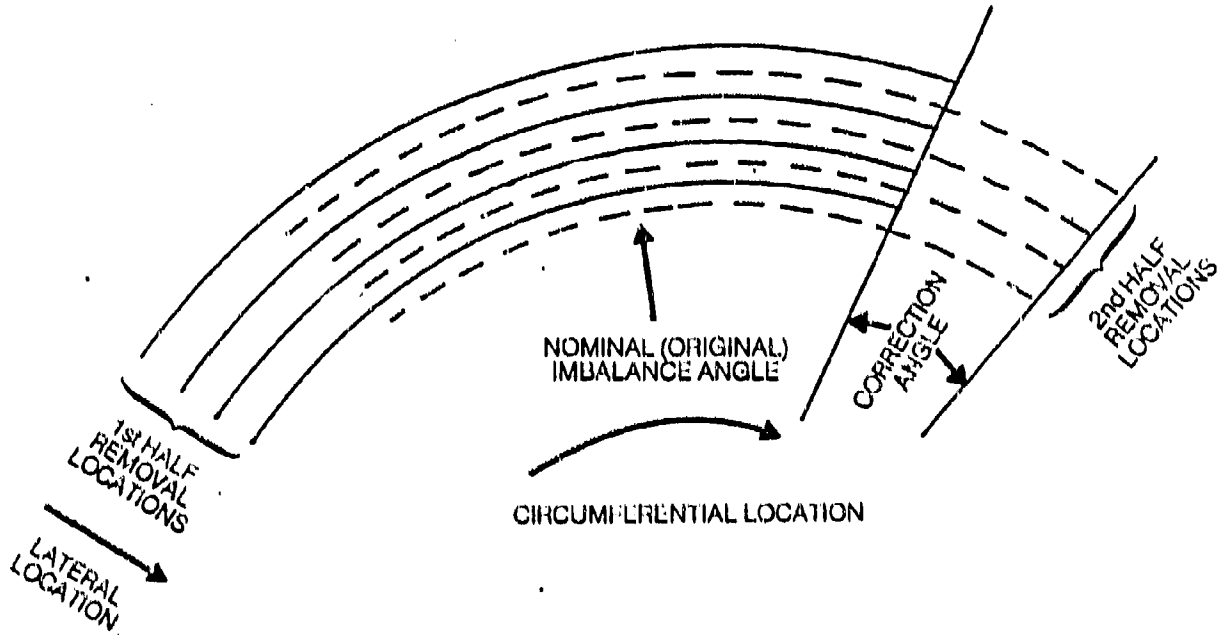

Figure 5-44. Modified First Layer Removal

the software integration is that of menu driven selection of a component with its associated geometric parameters. For the purpose of this program, the conceptual framework of this structure has been implemented and the specific requirements for such an integrated approach to work are relatively straightforward, but necessitate that the calculations of imbalance and mass removal, optics motion control and laser firing can be correctly performed under internal software code selection.

The approach taken to effect this process is that of use of a simple set of logic controlling operations. The data file for each part and configuration for balancing contains a pair of control variables, "jgeom" and "jplane." "jgeom" is intended to allow the operating software to determine the specific geometric requirement of mass removal and motion control of that part, i.e., step radially within axial steps, etc. "jplane" defines which specific type of mass removal configuration is required i.e., A-plane, B-plane or any other. This, in principle, allows a matrix of possible control decision points in the SW subroutines, that can be used to direct the HW routines which become a closed set with no need for any modifications or variation. The structure, as implemented for the impeller, uses only a small fraction of the possible matrix, but the structural concept is fully realized in terms of being operational for the specific program goals. It is possible to extend the software to a larger number of configurations and parts with small and easily implemented changes in a few of the key SW subroutines.

The specific goals of this program necessitate balancing of both A- and B-planes of the compressor impeller. The geometry of motion control and mass-imbalance description are very different. This can be seen in Figure 6-41. Thus, for example, the imbalance, as defined by a mass removal zone, is given by,

$$(R\,\Delta m) = 2/3\ \rho w_{max} \sin(\theta_B)\ [(r_1+h)^3 - r_1^3] \qquad \text{(A-plane)}$$

$$= 2/3\ \rho(\Delta h) \sin(\theta_B)\ [r_0^3 - r_1^3] \qquad \text{(B-plane)}$$

where:

w_{max} is the burn width in the axial direction for the A-plane

θ_B is the burn half angle

r_1 is the inner burn radius

r_0 is the outer burn radius

Δh is the burn depth

Clearly there are significant differences between these two formulations especially when they have to be translated into the areas of relevance to traverse motion and firing angle.

Thus each balancing plane is characterized by logical decision points, as defined by "jgeom" and "jplane," as to which expressions for burn depth, imbalance and required mass removal are used in each subroutine. Furthermore, the actual definition of the firing and stepping routines have to reflect these geometric changes. Thus, the A-plane single layer stepper direction is along the rotation axis, which is defined as the X-axis in optics coordinates, whereas the direction for the B-plane is the radial or optical Z-axis. The stepping and firing routines are, therefore, different. The approach taken to make this an easily implemented structure is that of nearly identical subroutines, each of which controls stepper motion in a given optical axis direction during the firing process for a layer. Thus, subroutine FAXY controls the A-plane removal, by motion in the X direction during firing, with refocusing between layers being in the Y direction, and FAZX controls B-plane removal, with Z-axis stepping and X-axis refocusing.

The final variable in the firing specification is the time delay offset angle, as required by the specific laser burn location relative to the photodiode trigger location. As this differs for each plane of the rotor, it is selected from the component data files.

The above structure allows the system to operate correctly upon the desired configuration purely on the basis of menu selection at the initiation of the procedure, with all logical control being implemented internally to the software.

5.2.9.7. Balancing demonstration. A rotor was balanced on both A- and B-planes using the new algorithm. The rotor in question had typical imbalances on both planes; 1.0 g-inches on the A-plane and 2.3 g-inches on the B-plane. It was balanced within specification in both cases. The time histories of the process is shown in Figure 5-45. The post-processing smoothing of the surface can be seen to account for a significant fraction of the total time, especially for the relatively small initial imbalances, which required only a one-or two-layer removal process. The mass removal rates in these cases were smaller than expected, as a direct result of laser performance degradation. The laser flashlamps were reaching the end of their normal lifetime (10^6 shots) and power levels were down by approximately 40 percent. This significantly reduced the mass removal rates, as the melt splash removal mechanism is closely coupled to the vapor induced overpressure generated by the high flux densities at the surface. This clearly raises the issue of process optimization through lifetime monitoring of laser performance and also that of laser power requirements for the most effective use of the laser-balancing process.

The test clearly indicates the successful application of the process on the compressor impeller. The new algorithm, with an extended burn zone length, leads to a much better appearing post-processed surface on the B plane. The A-plane is not without its problems. As stated earlier, the A-plane suffers from an optical access problem, which resolved

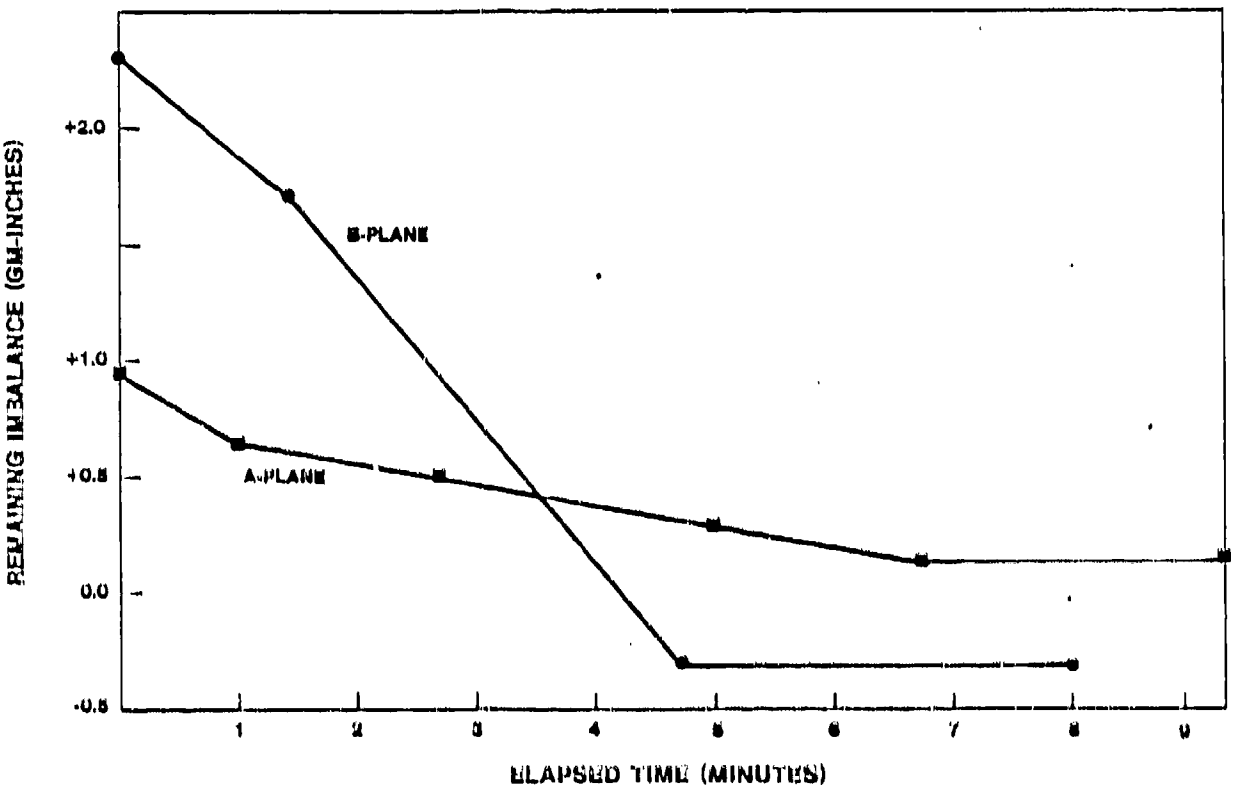

Figure 5-45. A-Plane and B-Plane Balance Time History

itself into two potentially troublesome issues with respect to efficient and uniform mass removal. A consequence of the A-plane irradiation geometry is that the alignment of the entire optical and balancing mechanical systems has to be very tightly toleranced. The removal zone is 0.5-inch long along the rotation axis. As the depth of field is typically 0.08-inch, it can be seen that relatively small axis offset angular errors can cause shifts in focal location with respect to the surface. If this issue is considered in association with the off-axis target impingement angle and the vibrational sensitivity of the A-plane burn location, it can be seen that the potential exists for significant problems with efficient mass removal. The process is also potentially unstable, with an initial alignment error leading to progressively worse mass removal effectiveness with increasing overall burn depth. Some problems with this have been experienced, and although, with care, the magnitude of the problem can be reduced, it is an inherent problem with the geometry of the impeller A-plane as mounted on the existing arbor. Typically, the alignment problem leads to progressively worse removal rate; therefore, the part unbalance improves with time, but at a diminishing rate. The part unbalance then gets no worse, but balancing has to be aborted as it does not progress. The system software has included within its structure an automatic abort condition if the total unbalance increases between successive measurements of the balance microprocessor.

5.2.10. System Performance Evaluations. In view of the overall issue of system economics and utility, it is necessary to evaluate the magnitude of overall elapsed times for a range of imbalances. Based upon the data base and an evaluation from dummy test cases, the contribution of the various elements of the system to total time has been evaluated. These elements are laser firing (based upon total integrated delay between pulses), stepper motion, computational overhead and balancer reading. A plot of this is shown in Figure 5-46 for B-plane mass removal. It can be seen that the overhead is a significant fraction of the total time at low imbalances. The post-processing smoothing can also be seen to be a substantial fraction of the total time. Clearly, the computational time has been made sufficiently low that further effort to improve algorithm computational efficiency is unnecessary. However, both stepper motion and balancer reading are significant sources of overhead. Motor upgrade may reduce the traverse times, and, if possible, an upgrade of BP2020 microprocessor performance could produce a more rapid reading of the imbalance data. Despite these overhead contributions, the total elapsed timescales are certainly very attractive. Figure 5-47 illustrates this for B-plane mass removal for the impeller. The three curves represent per pulse mass removals of 0.5, 1.0 and 1.5 mg (Δm). The lowest value is typical of present system performance based on typical flashlamp lifetime. The higher values for Δm would be typical of a 400-W system as opposed to the present 200-W system. The highest value is most likely, as the regime of operation of the present system is not optimum from the standpoint of mass removal efficiency. The key features of the evaluations is that

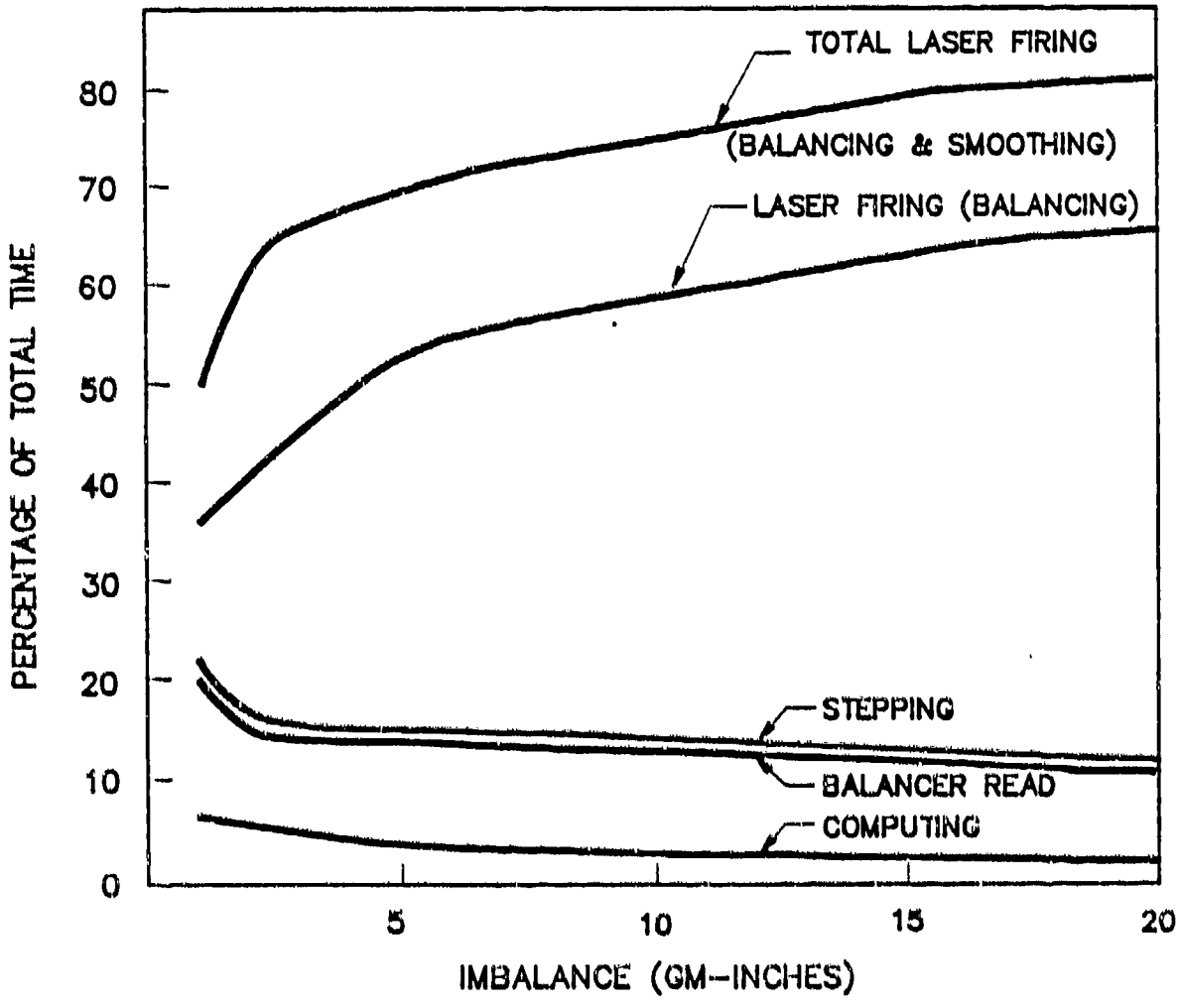

Figure 5-46. Contribution of System Elements to Total Time

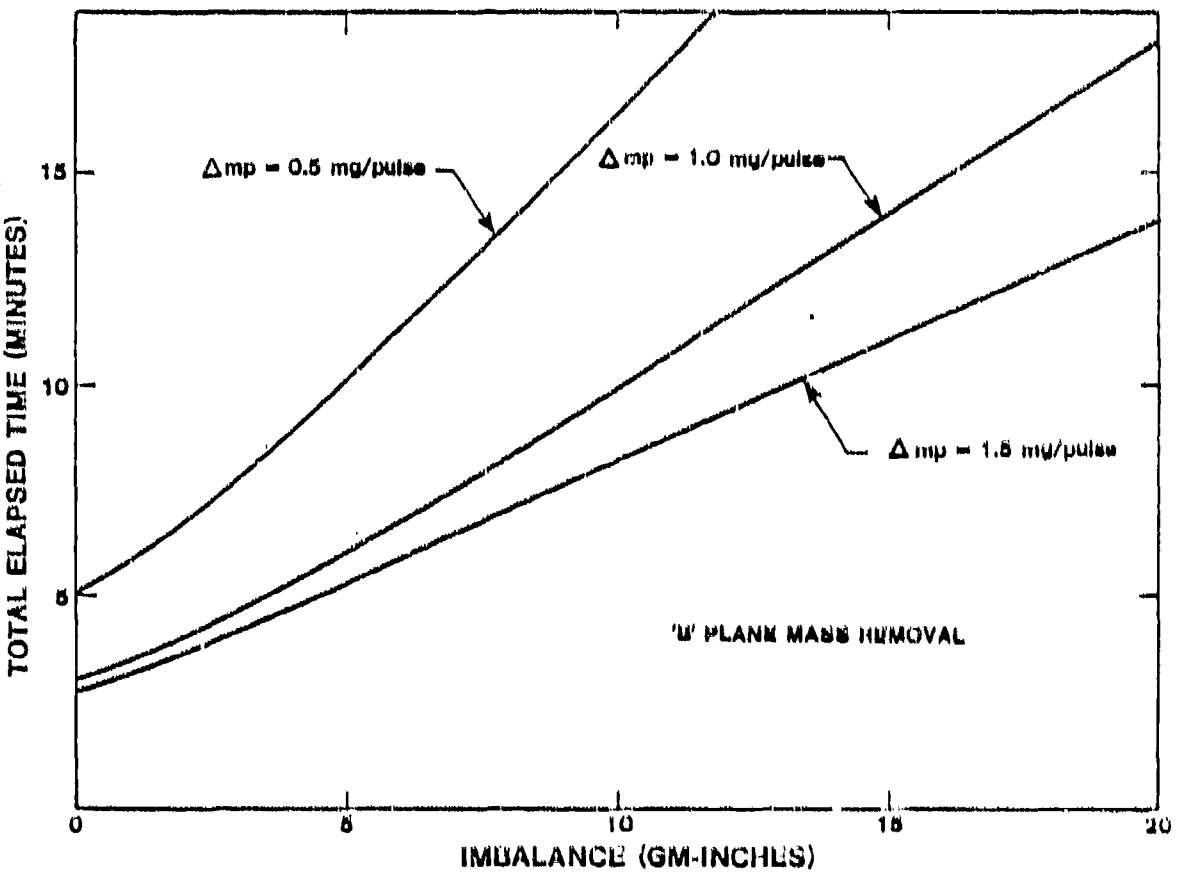

Figure 5-47. Process Efficiency for Different Laser Power Levels

the time scales for balancing of typical imbalances (2-4 g-inches) is significantly lower then the presently achievable hand grinding times (15 minutes) by factors of between 2-3 with the 200-W system and is projected to be 3-5 for the larger 400-W system.

5.3. Materials Testing

5.3.1. Objective. To evaluate material properties, that part integrity is not compromised by selected laser irradiation techniques.

5.3.2. Methodology. During initial efforts at irradiating the impeller, many different material removal conditions were executed, involving different beam diameters, pattern overlap, and post-conditioning. Initially, many different irradiation patterns were applied to test impeller B-planes, as well as "straight section microsection bars." (Straight section microsection bars were not for fatigue testing, but had the same center section diameter, so that many laser irradiation patterns could be applied, at a surface speed equivalent to the fatigue specimens). The straight section specimens were cut apart and examined for microstructural changes. The micro-section studies were completed on a SEM, a Nikon macro-camera, and a Metallograph.

The impeller and straight section microsection bars were examined with the objective of determining the laser parameters which resulted in a microstructure, that displayed the least indication of stress-risers and voids. The irradiation parameters were then duplicated and applied to the fatigue test specimens. Figure 5-48 shows the microstructure of the specimens, which were selected for life cycle testing.

All life cycle testing was carried out on Lycoming Smooth Fatigue Specimens, P/N TE-25217 (see Figure 5-49), under the following environmental conditions:

A.	Temperature	=	400°F.
B.	Frequency	=	2.0 hz
C.	Area ratio	=	1.0.

Two sets of laser irradiation conditions were selected to be repeated on the remaining fatigue samples. Both irradiation samples showed similar microstructures within the laser affected zone, when compared to an impeller segment with a minimum of voids and stress risers in its recast layer.

The two fatigue samples selected as comparable to acceptable impeller conditions, were straight microsection bar Number 2, Ring Number 2 and straight microsection bar Number 5, Ring Number 3. Four samples of each of these specimens were reproduced and fatigue tested at 160KSI. The results were plotted as part of Material Lab Report MR 4668. Even though both irradiation conditions produced good looking recast layers, they differed significantly in one major characteristic i.e., one

IMPELLER SECTION #5

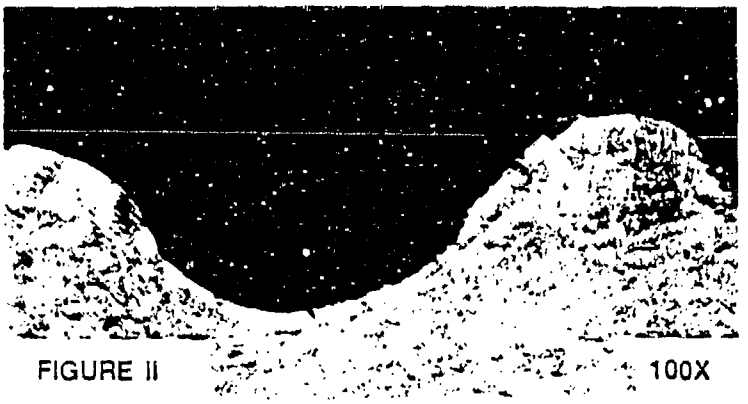

TEST BAR SECTION
BAR #2, RING #2

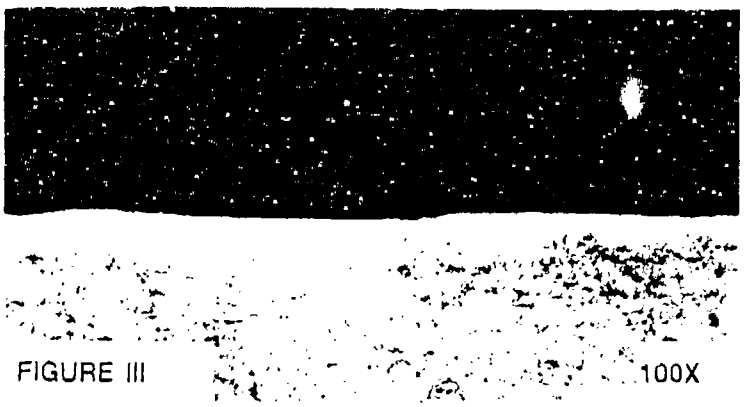

TEST BAR SECTION
BAR #5, RING #3

Figure 5-48. Microstructure of Laser Balanced Specimens

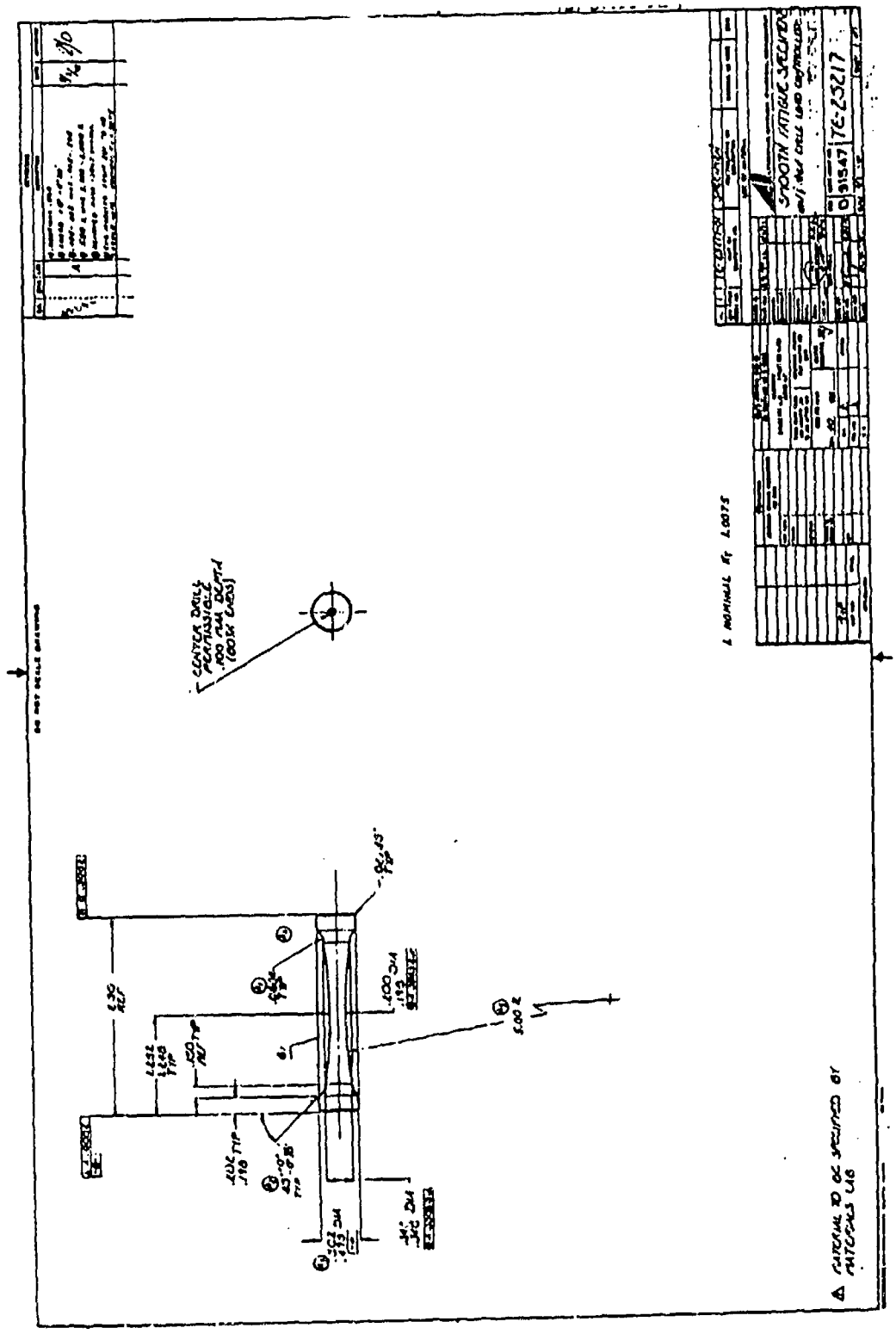

Figure 5-49. Lycoming Smooth Fatigue Specimens

fatigue sample was highly notched and the other was not. However, both configurations were tested initially, in an attempt to understand the effect of the notch.

These data indicated that a notch, caused by material removal, would have a major detrimental effect on the strength of the fatigue specimen (an effect due to geometry, which was seen as incomparable to the irradiated impeller).

It was concluded, that examination of the laser affected zone without a notch, was the appropriate test of the additional Fatigue Samples as well. Therefore, all subsequent laser irradiated Fatigue Samples were produced without a notch.

Additional fatigue samples were prepared, by hand grinding, as well as hand grinding and polishing, for comparison to existing techniques. The grinding and polishing operation was accomplished using Norton Grind Wheel MW-1500-4 (coarse) and MW-1500-1 (fine), which were dressed to have an OD axial radius of .335 inches. The fatigue specimens were mounted on a lathe and spun at 3000 rpm. With an air-driven motor spinning the grinding wheel, a circumferentially ground band was applied around the middle of the fatigue specimen (approximately .004 inches deep, as show in Figure 5-50). An additional quantity of fatigue samples were additionally polished.

A raw data inventory of test bars is provided in Table 5-1. It is a tabulation of the experimental data.

5.3.3. Summary of Results. During the contract, various tests were completed relative to life cycle fatigue. The test report numbers are:

- MR 0446 dated: Oct 22, 1987
- MR 0448 dated: Feb 25, 1988

Copies of the reports can be found in the Addendum.

Data indicates, that the laser irradiation test specimens fall within the range of test values for the hand ground and polished samples. It appears that reproduction of these irradiation conditions on another impeller, of similar geometry and material, would not have a significant detrimental effect on structural integrity.

5.4. Final Demonstration on 12/17/87

5.4.1. Aberrant Behavior Cause. The system demonstration failed due to its inability to balance an impeller within its specification tolerance of 0.5 gm-in. Subsequent investigation by the Everett Technical Staff, in collaboration with the Gilman Technician, produced the following observations.

Table 5-1. Raw Data Inventory

FATIGUE SPECIMEN INVENTORY

CONDITION	TEST NO.	STRESS	CYCLE TO FAIL	REMARKS
1	7531	130000	20920	MULTI-SURF ORIGIN
1	7450	160000	11520	MULTI-SURF ORIGIN
1	7532	130000	15010	MULTI-SURF ORIGIN
1	7453	160000	10580	MULTI-SURF ORIGIN
1	7533	110000	37290	MULTI-SURF ORIGIN
1	7524	150000	10300	DOUBLE SURF ORIGIN
1	7534	110000	34050	DOUBLE SURF ORIGIN
1	7528	140000	13760	MULTI-SURF ORIGIN
1	7535	90000	1051100	RETIRED
1	7530	140000	12520	DOUBLE SURF ORIGIN
1	7536	90000	1000010	RETIRED
1	7454	160000	12420	MULTI-SURF ORIGIN
1	7537	100000	137300	DOUBLE SURF ORIGIN
1	7529	140000	20470	DOUBLE SURF ORIGIN
1	7526	150000	11980	MULTI-SURF ORIGIN
1	7452	160000	13880	MULTI-SURF ORIGIN
1	7525	150000	10090	MULTI-SURF ORIGIN
2	7543	140000	16190	MULTI-SURF ORIGIN
2	7547	110000	45780	DOUBLE SURF ORIGIN
2	7483	160000	10280	MULTI-SURF ORIGIN
2	7548	100000	1051170	RETIRED
2	7541	140000	18970	SINGLE SURF ORIGIN
2	7549	100000	1149530	SINGLE SURF ORIGIN
2	7538	150000	13730	SINGLE SURF ORIGIN
2	7491	60000	949774	RETIRED
2	7545	130000	22070	MULTI-SURF ORIGIN
2	7488	80000	362349	DOUBLE SURF ORIGIN
2	7540	150000	16730	MULTI-SURF ORIGIN
2	7539	150000	12070	MULTI-SURF ORIGIN
2	7544	130000	19020	MULTI-SURF ORIGIN
2	7542	140000	15780	MULTI-SURF ORIGIN
2	7546	110000	35860	MULTI-SURF ORIGIN
2	7485	120000	23130	MULTI-SURF ORIGIN
3	7458	160000	330	SINGLE SURF ORIGIN
3	7457	160000	350	SINGLE SURF ORIGIN
3	7455	160000	300	SINGLE SURF ORIGIN
3	7459	160000	390	SINGLE SURF ORIGIN
4	7306	160000	31610	MULTI-SURF ORIGIN
4	7312	160000	27770	MULTI-SURF ORIGIN
4	7310	160000	31090	MULTI-SURF ORIGIN
4	7313	160000	22080	MULTI-SURF ORIGIN
5	7470	160000	7340	MULTI-SURF ORIGIN
5	7471	160000	4340	MULTI-SURF ORIGIN
5	7469	160000	5510	MULTI-SURF ORIGIN
5	7468	160000	3150	MULTI-SURF ORIGIN

CONDITION 1. LASER IRRADIATED WITH NO MATERIAL REMOVED
CONDITION 2. HAND GROUND AND POLISHED
CONDITION 3. LASER IRRADIATED WITH MATERIAL REMOVED (NOTCHED)
CONDITION 4. NO MACHINING
CONDITION 5. HAND GROUND

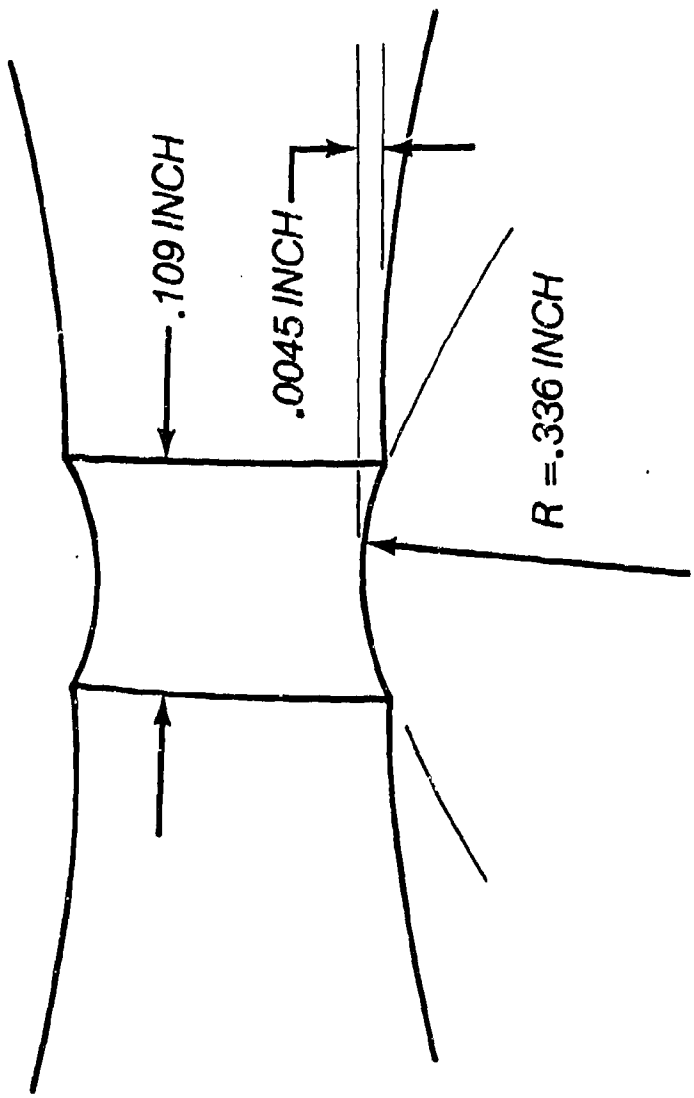

Figure 5-50. Hand Ground Specimen Geometry

- The index mark, for zero angle, is a piece of silver photodiode trigger tape.
- The laser triggered off the leading edge of the tape.
- The BP2020 referenced off the trailing edge.
- The rotational angle error difference was approximately 30^{0}.
- The balance algorithm never was able to correct for the built-in error, resulting in a failed demonstration.

5.4.2. Aberrant Behavior Correction. Steps taken, once the problem areas were defined, were as follows:

- Reduce the arc length of the silvered tape i.e., make it narrow.
- Modify the balance algorithm to reduce balance angle uncertainty i.e., increase sample number.

After incorporating these simple modifications, a successful demonstration resulted on February 24, 1989. A more detailed discussion of the problem, with its associated solution can be found in the Addendum (see report 1016L dated 4/5/89).

5.5. Qualification Test Plan

5.5.1. Purpose. The purpose of this draft plan is to define the test procedures required to qualify the laser balancing procedure for use with parts which are currently balanced by hand grinding on the AGT-1500, T-53, and T-55 engines, such that parts which are laser balanced can be placed in service without modification to the engines or engine operating envelopes.

5.5.2. AGT-1500.

5.5.2.1. Hand Ground Parts. There are 11 parts which are currently balanced by hand grinding. Because of the unusual configuration of the material removal pattern required when balancing part number 3-110-008-, Shaft, 2nd Turbine Rotor, L.P., this part will not be laser balanced. The remaining 10 parts are shown in Table 5-1.

Table 5-2. Candidates for Laser Balance

P/N	Description	Material
3-020-173-	Gear Helical (Planet)	SAE9310
3-020-175-24	Gear Shaft, Sun	SAE9310
3-100-160-21	Compressor Rotor Assy, L.P.	AM355

Table 5-2. Candidates for Laser Balance (continued)

P/N	Description	Material
3-105-100-	Compressor Rotor Assy, H.P.	AM355
3-105-230-	Impeller Assembly	AM355
3-110-010-	Plate & Disc Assy	Waspaloy
3-110-120-	Rotor & Shaft Assy	IN718
3-140-045-	Rotor, 3rd Stage	IN713LC
3-140-047-	Rotor, 4th Stage	IN713LC
3-140-202-	Shaft, Rigid Splined	TIMKEN 17-22 AS

5.5.2.2. Materials. There are five materials of interest:

- 9310 Low Alloy Steel
- TIMKEN 17-22 AS Low Alloy Heat Resistant Steel
- AM355 Stainless Steel
- IN718 Nickel Alloy (Forging)
- IN713LC Nickel Alloy (Casting)
- Waspaloy (Forging)

5.5.2.3. Acceptance Criteria. The acceptance criteria shall be that there shall be no significant reduction in structural integrity when comparing a laser balanced part to a similar part which has been balanced by hand grinding. This shall be measured by:

a. Metallurgical examination of the surfaces of the laser irradiated specimens for surface damage caused by the laser beam as well as the depth and characteristics of the Heat Affected Zone (HAZ) will be performed. Specimens will also be examined for evidence of re-deposition of laser vaporized material during the balancing process. Specimens to be examined include those laser balanced with and without post-treatment (tempering/stress relief) and/or with and without preheat. An assumption has been made that Timken 17-22 AS and SAE9310 low alloy steels will react to laser irradiation in the same manner. Metallurgical examination (surface damage, heat affected zone, and crystal structure) of identically irradiated specimens of the two materials will be performed before deciding whether that assumption is valid and that Timken 17-22 AS and SAE9310 can be evaluated using the same mechanical property data. If not, an additional set of tests will be required.

b. Fatigue testing will be conducted on specimens which have a given amount of material (determined during the analysis phase of the program) removed either by hand grinding and burnishing or by laser vaporization. There shall be one set of fatigue tests for each of the five materials of interest. The hand grinding and laser vaporization shall be performed to simulate actual balancing operations. The

fatigue test specimens shall be axially loaded in the strain control mode, with an "A" ratio of 1.0 and 2 cps. The specimens shall be tested at an elevated temperature to simulate the actual temperature in the balance material area when the engine is operating. Approximate temperatures will be: Timken 17-22 AS/SAE9310 -300°F, AM355 - 400°F, IN718 - 900°F, IN713LC - 1000°F, and Waspaloy - 1000°F. Actual test temperatures will be determined during the analysis phase of the program. Cycle count at failure will be recorded and fracture surfaces will be examined to determine the nature and location of fatigue origins. Runout (i.e. retirement if no failure) will be 1,000,000 cycles. There shall be a minimum of 20 specimens for each fatigue curve within a set of fatigue tests. One curve shall be developed for each material for the hand ground and burnished specimens and additional curves shall be developed for various proposed laser balancing cycles. The results shall be plotted as S/N curves and the mean and minimum (minus three sigma) curves for the hand ground and burnished specimens shall be compared to the data for the laser vaporized samples.

c. Spin Pit testing will be performed at room temperature on selected components. Six laser balanced components will be subjected to 10,000 cycles from 10% to approximately 150% of full speed. The exact speeds will be established, during the analysis phase of the program, to simulate the stresses associated with full speed operation at use temperature. The components will also be pre-stressed axially to simulate additional operating loads beyond the centrifugal loading. The pre-stress loadings will be established during the analysis phase of the program. The six components will be selected to maximize the usefulness of the data obtained from the spin pit testing. At least one component from each material will be tested. In addition, an analysis will be performed to select the component from each material which has the highest stress in the balance area. For example, the components could be:

a) Impeller.
b) Compressor Disk (stage to be determined).
c) Sun Gear Shaft.
d) H.P. Turbine Disc - Stage 1.
e) H.P. Turbine Disc - Stage 2.
f) Power Turbine Disc (T.B.D.).

d Engine durability cycle testing will be performed on an engine which has all of the laser balanced components

installed. It will be subjected to an equivalent 6000 mile/350 hour test cycle.

e. In-service monitoring will be performed on an engine which has all of laser balanced components installed. This will include a standard Aberdeen Proving Ground vehicle test cycle. At the conclusion of these tests, before the final qualification approval is given, several more engines with laser balanced parts will be placed in service in a high usage environment and monitored for several months to be sure that there are no "surprises."

5.5.3. Aviation Engines.

5.5.3.1. Hand Ground Parts. The RFQ specifies two parts for laser balancing. These are:

1-100-720-42	T-53 Rotor Assembly	(AM355)
2-100-180-18	T-55 Impeller	(6-4Ti)

5.5.3.2. Materials. The materials are:

AM355 Stainless Steel
6-4 Titanium Alloy

5.5.3.3. Acceptance Criteria. The aviation engines, T-53 and T-55, because they are man rated, will require additional testing. Since the T-55 impeller is a titanium alloy, an additional set of material fatigue tests would have to be run. In addition, the spin pit testing for man rated engine components will require more cycles than the AGT-1500 test. Although a qualification procedure is listed, it is strongly recommended that titanium alloy parts not be considered for laser balancing at this time because of the high risk. There are too many problems (such as major changes in crystal structure) which can occur when titanium is heated (whether in the presence of oxygen or not). There may be "unknown unknowns" which occur during the laser balancing process, the results of which might not appear during the qualification tests but which could cause part failure in use.

a. Metallurgical examination of the laser irradiated samples similar to paragraph 5.5.2.3.a. will be performed.

b. Fatigue testing will be performed in a manner similar to paragraph 5.5.2.3.b. The AM355 data from paragraph 5.5.2.3.b. may be acceptable for the T-53 Rotor Assembly. Testing of a titanium alloy will be more complex. Because of titanium's known sensitivity to oxygen, besides the standard set of fatigue data, additional data may have to be taken as a function of oxygen partial pressure. One worry with titanium is that a failure in the shielding gas supply may damage a part during the balance procedure or,

even worse, may lower the properties of the part without giving a visual (or other easily detectable) indication that the part has been damaged. Therefore, additional fatigue tests will have to be run with titanium to determine the effect of the use of a shielding gas. Again, the test will be at use temperature, approximately 400°F, with the actual test temperature determined during the analysis phase of the program.

c. Spin pit testing will have to be performed for either 25,000 or 50,000 cycles (to be determined by analysis). As in paragraph 5.5.2.3.c., the exact rotational speeds and pre-stressed loading conditions will be determined by analysis.

d. Engine durability testing will be performed through a standard 150 hour and a 1,000 cycle test.

e. In-service monitoring of several additional high usage engines, such as those on aircraft at the Aviation Center and School at Fort Rucker, will also have to be performed. This monitoring will take place for approximately 6 months, as in paragraph 5.5.2.3.e., to avoid "surprises."

5.5.4. Acceptance. Acceptance of this process for implementation both for producing a new part and rework of an existing part during overhaul will occur after all tests for a given part have been satisfactorily completed.

5.6 Implementation Plan

5.6.1. Review of Issues. As a consequence of the building, testing, and demonstration of the current system, several lessons have been learned. These lessons can be divided into two groups:

- Those pertaining to the short-term improvement and implementation; and
- Those pertaining to a long-term evolutionary application of the technology.

5.6.1.1. Short-term issues. Several requirements of the optical system for short-term implementation of the laser balancing technology have been addressed, as a result of testing this prototypical system. It has become clear that the alignment and focusing procedures need upgrading. This is a result of an initial desire to control costs and eliminate some optical system complexity. However, this has proven to be a false economy. The upgrade requires changes to the optics, necessitating a two-wavelength reflective coating on the mirrors so that the He-Ne alignment laser is not attenuated as dramatically as it is at present. The alignment of the He-Ne beam also requires two video cameras and

displays so that alignment can be done outside of the safety enclosure. Additionally, the focusing of the beam on the target surface requires a telescope assembly to be added to the laser. This system is augmented by a simple remote viewing CRT, so that focusing can be performed from the computer control console. Without these remote viewing enhancements, the procedure would be too cumbersome and time consuming for a production environment.

An additional short-term optical system enhancement issue is the use of a double focusing traverse assembly as opposed to two separate traverse assemblies, for the A-plane and B-plane. Data appears to favor the latter.

The lack of these features has been of some detriment to laboratory demonstration of the system, but are necessary in the production environment.

5.6.1.2. Long-term issues. There are several issues, namely:

- The system performance can be improved by the use of a higher power laser. This would ensure mass removal efficiencies from mass removal sites. The present system can be increased to a 400-W power level, giving a throughput factor increase of at least two. This would also be reflected by increased system capable costs.

  The use of a higher power system has advantages in the long term. Not only is time to balance a component reduced significantly, but the higher power system should be a more efficient process in terms of mass removal per unit of required energy. The present technology base for Nd:YAG lasers would allow for the laser size to be easily increased from 200-W up to significantly higher pulse energies. No obvious problems can be foreseen at this time with such a change in power, except those of Laser-Computer interfacing, should another vendor be selected.

- System costs could be reduced by the employment of the concept of laser timesharing. It is possible to set up two or more balancers and control systems, which would share the output of one or more lasers. This would allow for mounting and aligning the part on a machine, while another component is being balanced.

  The layout shown in Figure 5-51 is compatible with both an increase in laser power and the implementation of timesharing. Timesharing of the laser between two balancers and control systems is possible by use of a simple "handshake" circuit that defines which laser trigger circuitry is connected to the laser.

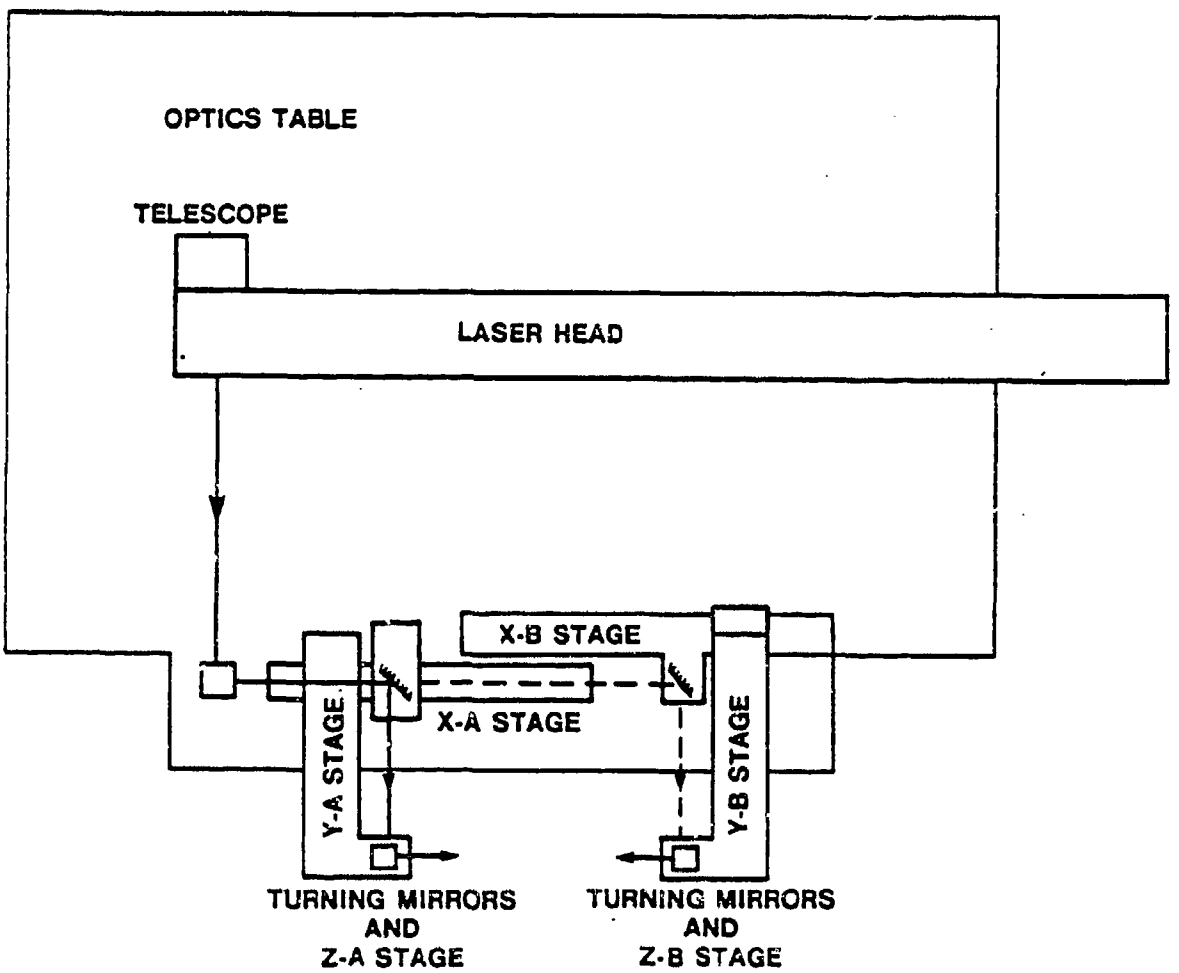

Figure 5-51. System Layout with Two Optical Traverse Assemblies

- Productivity and output uniformity would be greatly affected by the development of automatic focusing. This could be accomplished through the use of an optical feedback control system, to precisely locate the surface with respect to the laser focus. This can reduce some of the problems of setup, as well as reduce the time to perform the task. In the long term, this can affect the efficacy of a fully automatic part handling, loading and balancing system. The automatic focusing system can be used in three areas. The first is the assurance of good initial focus. This second is the reading of the burn depth while removing material, therefore, maintaining a good focus throughout the process. The third is especially helpful in a depot environment where previously balanced parts can have their surfaces measured while rotating to find "keep-out" zones of previously machined areas.

5.6.2. System Layout. Figure 5-52 shows the physical orientation and dimensions of the existing laser balancer system at ARL (Avco Research Laboratory). The important idea presented is that great flexibility is possible, regarding the layout of the enclosure and the various components. Either short-or long-term implementation plans can benefit from a repacking of the optics bench and optics system. The bench can be replaced with a much more compact bench that can stand on the floor and hold the laser head, the optics system and the vacuum and air cooling system. This repackaging would reduce the enclosure size significantly.

5.6.3. System Requirements. Service requirements include:

- 280 ft^2 floor space
- 12.5 kW electricity
- 600 gal/hr Water
- 125 psi oil free shop air

5.6.4. Training. Initial operator and management OJT would take four man-weeks on-site training. At least one person should attend the standard laser training course given by the manufacturer. This training would allow engineering and manufacturing personnel to assimilate the technology, optimize productivity, and add new components as well as incorporate upgrades.

5.6.5. Maintenance and Repair. Maintenance must be carried out by personnel with a broad range of skills, involving, for example: laser, computer, and facility repair. Adequate spare parts should be maintained within the various disciplines.

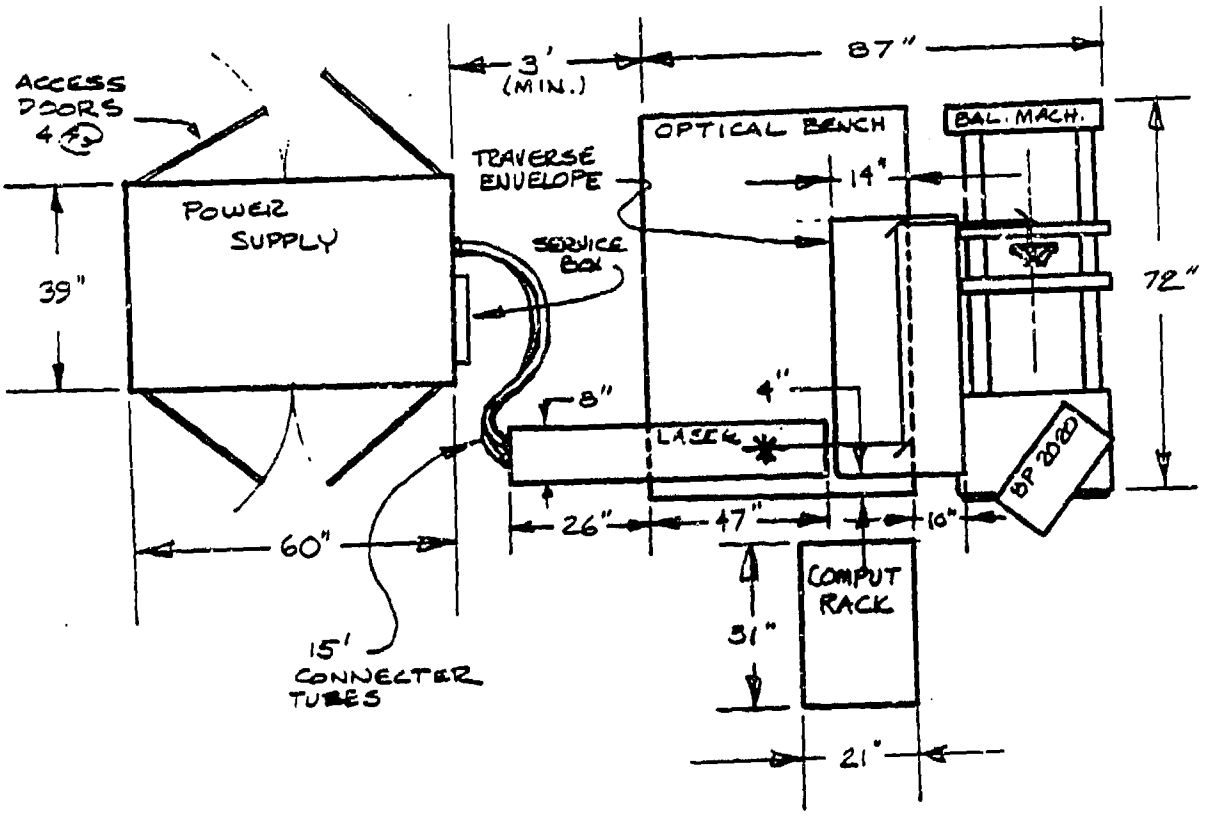

Figure 5-32. Existing System Layout

5.6.6. Proposed Additional Modifications to Present System. Incorporation of a two-head optical assembly would allow rapid switching from A- to B-plane. This will reduce dead time during the transitions between the two balance planes, and reduce operator intervention in the procedures. As a result, apart from initial fine tuning of the focus and alignment of the beams, the operator needs only to initiate the balance procedure via the computer keyboard. Another, more important reason, is that for larger diameter components, the traversing system does not have enough reach to move around the component.

The incorporation of the two-head traverse system requires some thought in order to avoid interference of the two assemblies (Figure 5-51). This would require that the present Y-stage and Z-stage assemblies be simplified to minimize weight and size. The Y-stage could be replaced with a purely manual adjustment (assuming the A-plane can be mounted on a more appropriate arbor such that the focusing has no Y-axis component to it). The mirror traverse could be replaced by a pneumatic slide system. The current X stage may be used as the X_B stage and a new stage employed as the X_A stage. A new Y (if needed) and Z stage are required for the additional assembly.

An additional motor control board and two drive boards are necessary in order to control the three additional traverses unless the Y-axis and M-axis requirements are bypassed as described above. The replacement of the current motor control board with a newer model that incorporates the linear encoder function would improve the reliability and repeatability over the current system.

5.6.7. Rotor Arbor. A major issue in the implementation of the laser-balancing technology is the effective handling of geometric limitations, as defined by optical and balancer hardware. The balancing of the A-plane has not been as easy as originally thought, due to the constraints imposed by the rotor arbor design. The arbor, with current balancing techniques, has no impact upon the ease of obtaining a good fast balance. With laser balancing, it is possible that the arbor design can affect overall balance performance. Therefore, a significant design change is suggested, which will ease the geometric constraints upon optical access. The present arbor and impeller configuration is shown in Figure 5-53. A possible configuration for implementation of a more accessible and stable balancing operation is shown in Figure 5-54. This is basically a reversal of a part upon the arbor to yield a greater accessibility to the laser. The shortness of the arbor on the A-plane side of the rotor allows for end-on targeting. The subtended angle of the optical cone of laser radiation is typically 9° - 11°. With the postulated configuration, an allowable angle of 18° is possible. Thus, the impingement of the laser at the apex of the vertical axis of the rotor is available whereas, with previous standard arbors, access is difficult and sensitive to arbor movement.

5.6.8. Summary. The large number of different component and assembly geometries needed for engines necessitates that efficient production

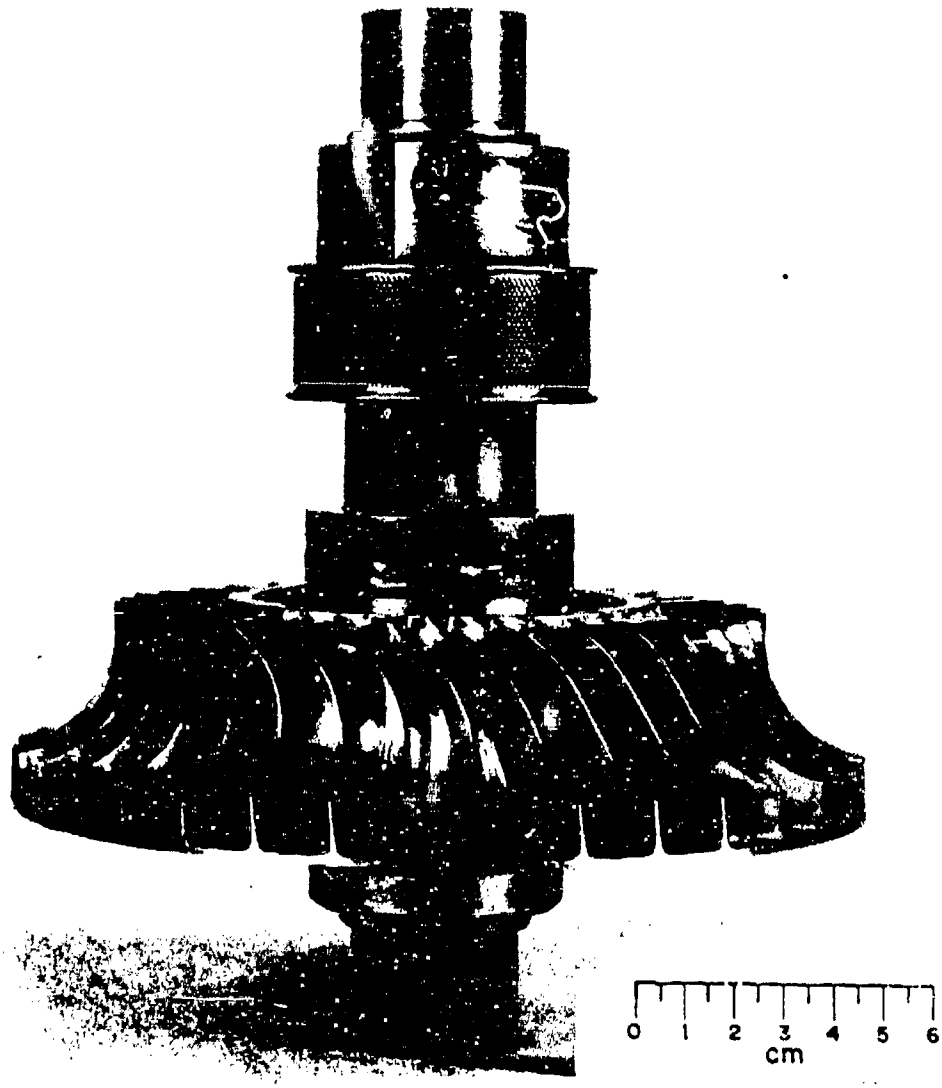

Figure 5-53. Rotor Mounted on Existing Arbor

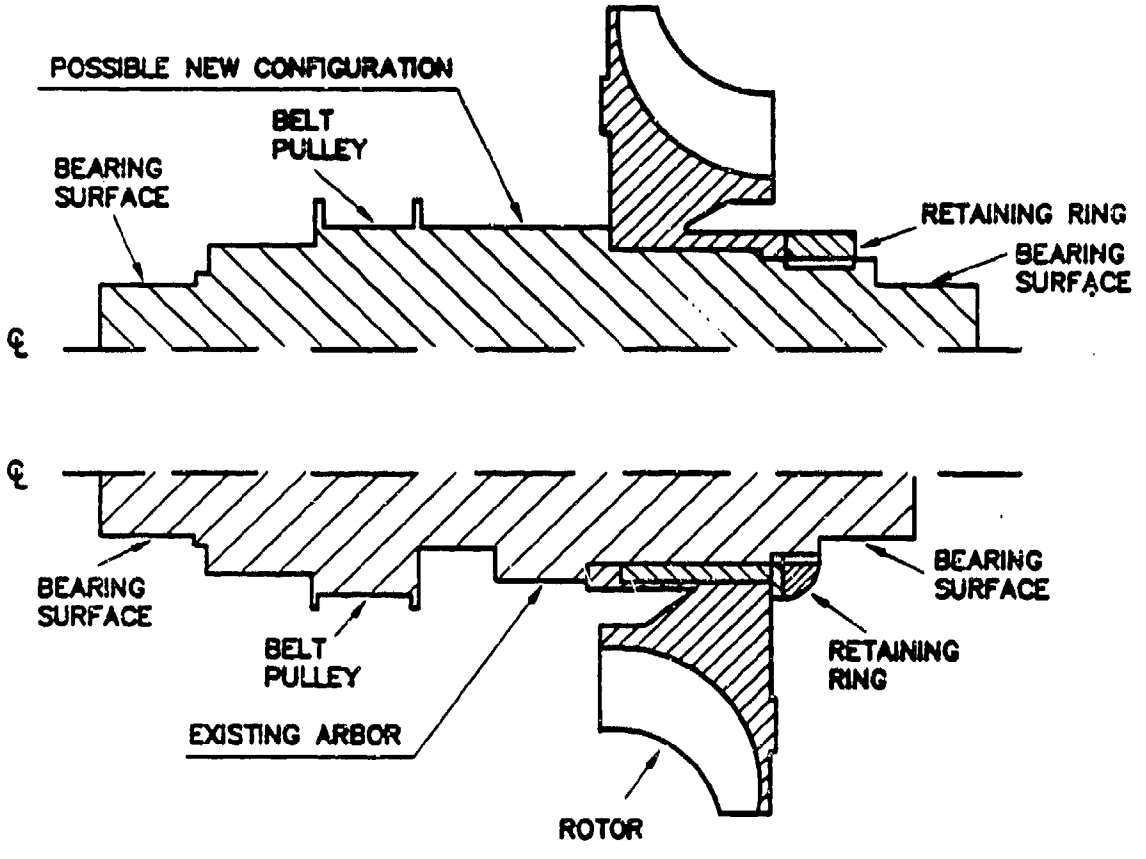

Figure 5-54. Arbor Configurations

uses different balancer configurations and different balance machine types. It is much easier to use a specific balancer for a given part, at least for a significant production run, than to be constantly changing geometries between each use of the balancer. The most effective use of the laser can be obtained if it is being used at as high a rate as possible. The installation, calibration, alignment, and removal procedures of a part take significant time. If another part can be balanced using the laser while this is being performed, productivity can be enhanced and unit costs reduced. If multi-tasking of the laser systems is used, with a range of balancer types and setups, it allows for flexibility and optimization of productivity to account for downtime of a specific laser system. This, of course, presupposes the use of several laser systems in the production balance room.

In the same view, the setup and alignment timescales can be reduced by implementing an automatic focusing system. This allows the target surface to be located at the point of maximum effectiveness for mass removal. This can be implemented through use of a system such as is shown in Figure 5-55. This has the advantage of being optically straightforward, using the He-Ne alignment laser as a probe for focusing and, additionally, providing possible real-time data on degree of out-of-focus displacement. This would allow the system to evaluate the new surface position when doing multilayer burns where significant surface recession takes place. The focus of the burned area is of course different from that of the pristine balance plane surface. With the part rotating it becomes necessary to differentiate between these locations in real time. Such a system can perform this function, in addition to providing data of actual burn geometry that can be used as a diagnostic of algorithm and balancer performance.

5.7. Cost Plan

5.7.1. Project Cost. The total contract award was $615,120.

5.7.2. Equipment Cost. The cost of the equipment obtained and used during this contract is itemized below:

• Balance Machine	$39,000.00
• PC Computer, Software & Interface Bds.	$ 7,614.00
• 250 Watt Nd YAG Pulse Laser	$79,000.00
• Optics & Beam Delivery Equipment	$15,223.67
• Periphery Equipment	$22,409.03

5.7.3. Implementation Costs (1987 $ Projections). In order to install the system, special facility revisions must be completed.

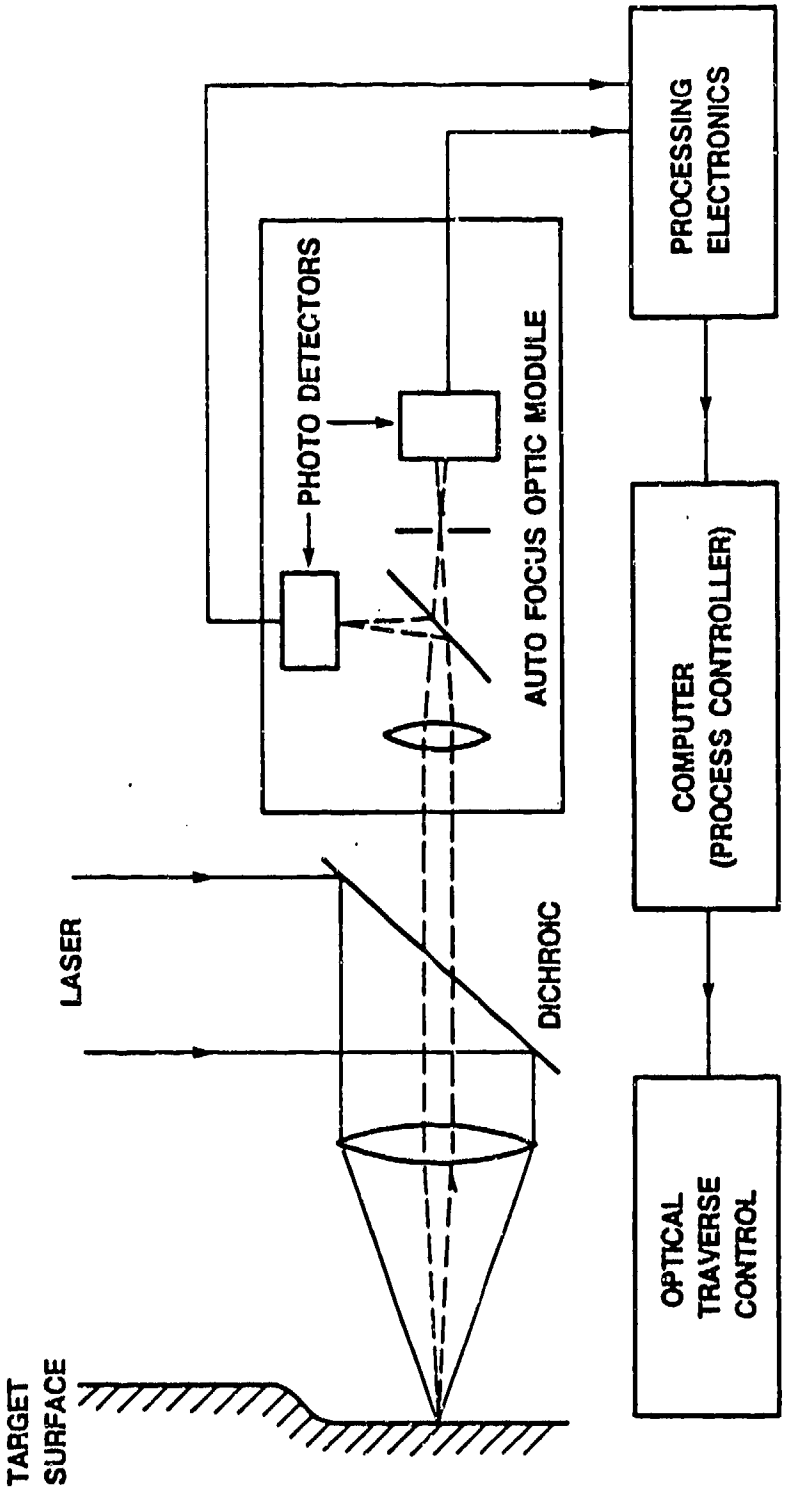

Figure 5-55. Auto-Focusing System Concept

- Laser Balance Room must be Class I enclosure.
- Laser Balance Room access safety interlocks, must be installed.

The total for implementing the system at SAEP is shown in the following table:

Freight from Everett	$ 2,000.00
Building Site Preparation	$60,000.00
Installation and Start-Up	$46,960.00
Training (exclusive of Everett Training Support)	$ 5 360.00

5.7.4. Enhancements to System. Enhancements to operating the equipment in a production environment, fall into two categories, specific costs of which, are detailed in separate proposals.

5.7.4.1. Mandatory enhancements. It is necessary that the following items be incorporated into the Balance Machine Units, before operation of the prototype unit in production.

- Remote Focusing System
- Double Coated Optics
- New Arbor Configuration.

5.7.4.2. Recommended enhancements. It is recommended that the following items be incorporated into the Balance Machine Unit to minimize hands on operation:

- Alignment Video Cameras (includes two cameras and monitors).
- Packaging for production.

* (See Paragraph #5.4 for Implementation Plan)
* Projected costs, exclusive of Engineering support and financial factors. (G&A, CAS, etc.)

ADDENDUM

MATERIALS TESTING REPORTS

MR 0446
October 22, 1987

AVCO LYCOMING DIVISION
STRATFORD, CONNECTICUT

MATERIALS AND PROCESS TECHNOLOGY LABORATORIES

SUBJECT: EVALUATION OF LASER BALANCING PARAMETERS RELATIVE TO RECAST LAYER CHARACTERISTICS OF AM355

SUMMARY:

An AGT1500 Impeller, S/N 84J-053 was sent to Avco Everett Research Laboratory (AERL) to perform laser balancing experiments using various laser parameters. After several experiements were performed, the impeller was returned to Textron Lycoming for metallurgical evaluation and documentation relative to the recast layer/heat affected zone. Evaluation of the recast layer/heat affected zone from fifteen (15) sections of the impeller revealed such defects as voids, moderate to severe grooving and variations in the thickness of the recast layer itself along with a decrease in hardness in the recast layer vs base metal. On the basis of these observations, it was concluded that stress risers could develop as a result of these defects, especially, if some of the more severe parameters are used to remove material in balancing. It is therefore recommended that if the laser method of balancing AGT1500 Impellers is used, defects such as voids and grooves must be kept to an absolute minimum.

Prepared by: P. M. Follo

P. M. Follo
Sr. Materials Engineer
Materials Testing Laboratory
Materials Technology Laboratories

Approved by: Louis J. Fiedler

Louis J. Fiedler
Director
Materials & Process Technology Laboratories

MR 0446
October 22, 1987

MATERIALS AND PROCESS TECHNOLOGY LABORATORIES

SUBJECT: EVALUATION OF LASER BALANCING PARAMETERS RELATIVE TO RECAST LAYER CHARACTERISTICS OF AM-355.

BACKGROUND:

An AGT1500 Impeller, S/N 84J-053 (Figure A), was sent to Avco Everrett Research Laboratory (AERL) to perform laser balancing experiments using various laser parameters. After several experiments were performed, fifteen (15) in all, the impeller was returned to the Textron Lycoming Materials Laboratory for microstructural documentation and evaluation. The evaluations were performed to determine the metallurgical surface conditions resulting from each set of parameters relative to the recast layer/heat affected zone. The task was conducted in support of contract number DAAE07-85-C-R/63, Advanced Balancing/Machining Techniques.

DISCUSSION:

An AGT1500 Impeller submitted to the Textron Lycoming Materials Laboratory by AERL was radially sectioned through fifteen (15) locations that contained laser burns created under various conditions. Each section was then nickel plated for edge retention, mounted in a thermoplastic media, metallographically polished and electrolytically etched in a solution of 10% Hydrofluoric Acid (HF) in water to reveal the recast layer produced by the laser treatment. Each polished and etched sample was then examined by optical microscopy and photographs were taken to document the thickness (Table 1) and general characteristics of each recast layer (Figures 1-15). To further characterize conditions, microhardness measurements were taken of the recast layer and compared to the base metal (Table 2). Also, four (4) test samples that revealed low hardness readings were heat treated at 800°F for two (2) hours to determine whether the low hardness properties could be restored (Table 2).

LASER PARAMETERS:

The following is a list of laser parameters and comments supplied to Textron Lycoming by AERL. Each set of test parameters is associated with the optical photographs in Figures 1-15:

TEST #	CONDITION	COMMENTS
1	θ=13.1 deg. One radial burn 100 Pulses/radial burn Δr/wp=0.32	Rough surface finish
2	θ=24.2 deg. One radial burn 50 pulses/radial burn Δr/wp=0.64	Rough, more noticeable grooving
3	θ=35.2 deg. Two identical radial burns 50 pulses/radial burn Δr/wp=0.64	
4	θ=46.2 deg Two radial burns 1st. @ z=0mm 2nd. @ z=0.15mm 50 pulses/radial burn Δr/wp=0.64	Second radial burn pattern shifted relative to first by 0.13mm in radial direction.
5	θ=57.3 deg. One radial burn 33 pulses/radial burn Δr/wp=0.95	Noticeable surface ripples
6	θ=68.3 deg. Three idential radial burns, 33 pulses/radial burn Δr/wp=0.95	Very clear rippling
7	θ=79.4 deg. Three radial burns 1st. layer @ z=0mm 2nd. layer @ z=.13mm 3rd. layer @ z=.25mm 33 pulses/radial burn Δr/wp=0.95	Second radial burn shifted relative to first by 0.13 mm in radial direction. Third radial burn shifted by 0.25 mm relative to first radial burn. Smearing of ripples.
8	θ=92.9 deg. 100 pulses/radial burn Δc/lp=0.40 Δr/wp=0.32	Four radial burns shifted in circumferential direction.

TEST#	CONDITION	COMMENTS
9	θ=106.9 deg. Two radial burns 1st. layer @ x=0mm 2nd. layer @ x=2.5mm 100 pulses/radial burn Δr/wp=0.32	First and second laser overlap identical, but second layer defocused to simulate past conditioning. Rough surface finish.
10	θ=118.0 deg. Two radial burns 1st. layer @ x=0mm 2nd. layer @ x=-5.1mm 100 pulses/radial burn Δr/wp=0.32	First and second layer overlap identical. Second layer defocused to simulate past conditioning. Still in focal zone.
11	θ=129 deg. Two radial burns 1st. layer @ x=0mm 2nd. layer @ x=-7.6mm 100 pulses/radial burn Δr/wp=0.32	First and second layer overlap identical. Second layer defocused to simulate past conditioning. Surface treatment beginning.
12	θ=140.1 deg. Two radial burns 1st. layer @ x=0mm 2nd. layer @ x=-10.2mm 100 pulses/radial burn Δr/wp=0.32	First and second layer overlap identical. Second layer defocused to simulate past conditioning.
13	θ=151.1 deg. Two radial burns 1st. layer @ x=0mm 2nd. layer @ x=-12.7mm 100 pulses/layer Δr/wp=0.32	Same comment as #12
14	θ=162.2 deg. Two radial burns 1st. layer @ x=0mm 2nd. layer @ x=-15.1mm 100 pulses/radial burn Δr/wp=0.32	Same comment as #12
15	θ=173.2 deg. Two radial burns 1st. layer @ x=0mm 2nd. layer @ x=-0.01mm 100 pulses/radial burn Δr/wp=0.32	Same comment as in test #12, plus surface treatment lessening.

NOTES:

wp = Radial width of a single pulse burn (mm).
lp = Circumferential length of a single pulse burn (mm).
r = Offset in radial direction (mm).
c = Offset in circumferential direction (mm).
$\Delta r/wp$ = Normalized radial shift, i.e. offset.
$\Delta c/lp$ = Normalized circumferential shift, i.e. offset.
θ =Angular location of burn.
Radial Burn = For a fixed angular location, fire laser and step in radial direction by $\Delta r/wp$.
Circumferential Burn = For a fixed radial position, fire laser and step circumferentially by $\Delta c/lp$.
Pattern generation for test #8 = For a fixed radial position, fire laser and step circumferentially by $\Delta c/lp$, then step in radial direction by r/wp and repeat.

TABLE #1
Thickness Of Recast Layer

TEST #	RANGE
1	.002 - .006 in.
2	.015 - .006 in.
3	.001 - .004 in.
4	.003 - .005 in.
5	.015 - .005 in.
6	.005 - .120 in.
7	.002 - .008 in.
8	.001 - .007 in.
9	.0005 - .003 in.
10	.0005 - .002 in.
11	.001 - .002 in.
12	.001 - .001 in.
13	.002 - .006 in.
14	.001 - .004 in.
15	.0005 - .003 in.

TABLE #2

Microhardness Measurements (Rc) For Test 1-15

TEST #	RECAST LAYER	AFTER H.T. @ 800°F/2 HRS.	BASE METAL
1	40.5	43.5	41.5
2	38.0	37.0	42.5
3	38.0	39.0	42.5
4	40.0		45.0
5	46.5		49.5
6	43.0		46.0
7	44.5		42.5
8	48.0		49.0
9	51.5		48.0
10	45.0		45.0
11	40.0		43.5
12	38.0	43.0	43.0
13	49.0		43.5
14	51.0		45.0
15	44.0		45.5
	Avg.= 42.4		Avg.= 47.7

CONCLUSIONS/RECOMMENDATIONS:

Visual examination of the recast/heat affected zone revealed such material defects as voids, moderate to severe grooving, and variations in the thickness of the recast layer itself. Also, the microhardness measurements made on each test specimen revealed the hardness (Rc) to be on the average lower in the recast layer then in the base metal. The four samples that were heat treated at 800°F for two (2) hours revealed no significant change in hardness.

As a result of these observations, it is concluded that stress risers could develop as a result of these defects, especially, if some of the more severe laser parameters are used to remove material. It is therefore recommended that, if the laser method of material removal is to be used, defects such as voids and grooves must be kept to an absolute minimum.

jj

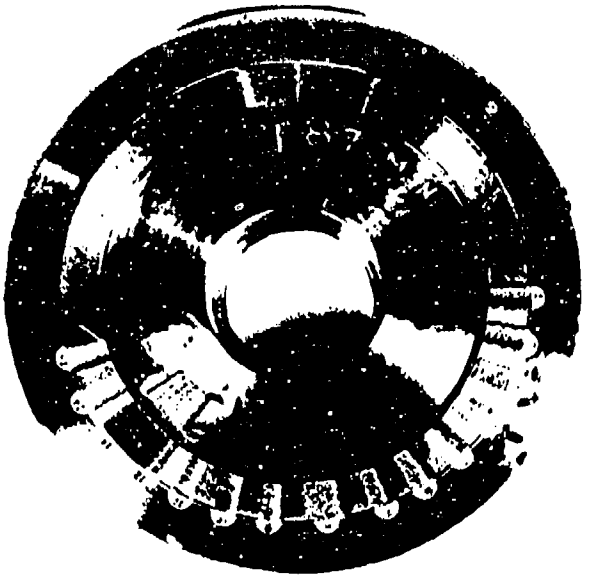

S/N 84J-053 MAG. 0.5

Figure A. Overall of AM355 Impeller showing 15 laser treated sections.

TEST #1 MAG. 100X

Figure 1. Photomicrograph of laser treated AM355 impeller section showing voids in the recast layer and grooving (Test #1). Laser Parameters: θ = 13.1°, One radial burn, 100 pulses/burn, $\Delta r/wp$ = 0.32.

TEST #2 MAG. 100X

Figure 2. Laser parameters: θ = 24.2°, One radial burn, 50 pulses/ burn $\Delta r/wp$ = 0.64.

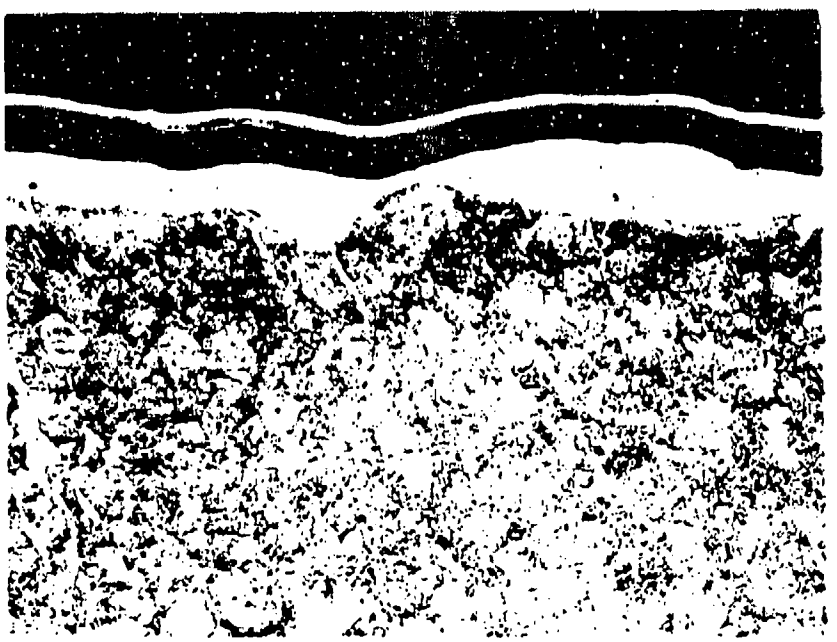

TEST #3 MAG. 100X

Figure 3. Laser parameters: θ = 35.2°, Two radial burns, 50 pulses/ burn $\Delta r/wp$ = 0.64.

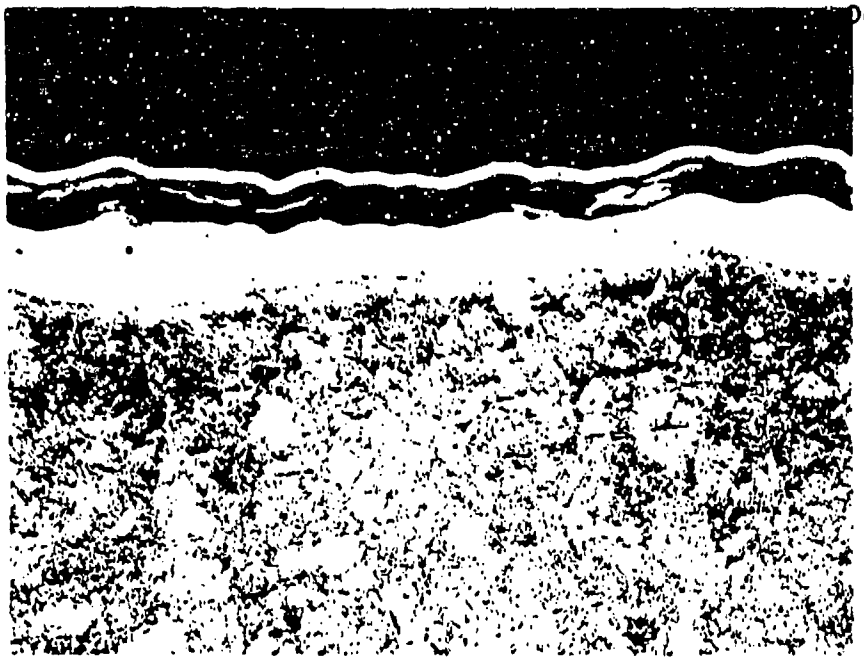

TEST #4 MAG. 100X

Figure 4. Laser Parameters: θ = 46.2°, Two radial burns, 1st @ z = 0, 2nd @ z = 0.15 mm, 50 pulses/burn, $\Delta r/wp$ = 0.64.

TEST #5 MAG. 100X

Figure 5. Laser parameters: θ = 57.3°, One radial burn, 33 pulses/burn $\Delta r/wp$ = 0.95.

TEST #6 MAG.100X

Figure 6. Laser parameters: Θ = 68.3°, Three identical radial burns, 33 pulses/burn $\Delta r/wp$ = 0.95.

TEST #7 MAG. 100X

Figure 7. Laser parameters: Θ = 79.4°, Three radial burns, 1st layer @ z = 0, 2nd layer @ z = 0.13 mm, 3rd layer @ z = 0.25 mm, 33 pulses/burn, $\Delta r/wp$ = 0.95.

TEST #8 MAG. 100X

Figure 8. Laser parameters: Θ = 92.9°, Four radial burns shifted in circumferential direction, 100 pules/burn, $\Delta c/lp$ = 0.40, $\Delta r/wp$ = 0.32.

TEST #9 MAG. 100X

Figure 9. Laser parameters: Θ = 106.9°, Two radial burns, 1st layer @ x = 0, 2nd layer @ x = -2.5 mm, 100 pulses/burn, $\Delta r/wp$ = 0.32.

TEST #10 MAG. 100X

Figure 10. Laser parameters: θ = 118°, Two radial burns, 1st layer @ x = 0, 2nd layer @ x = -5.1 mm, 100 pulses/burn, Δr/wp = 0.32.

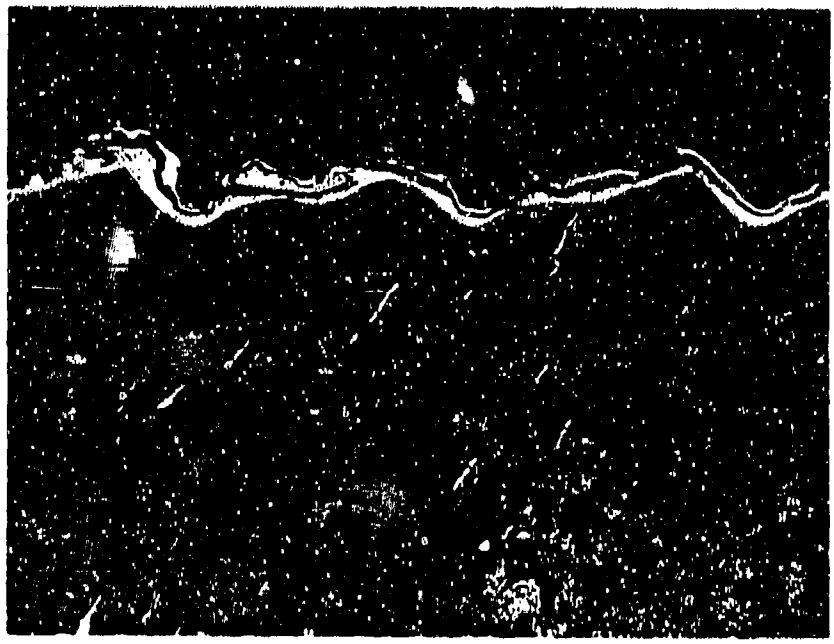

TEST #11 MAG. 100X

Figure 11. Laser parameters: θ = 129°, Two radial burns, 1st layer @ x = 0, 2nd layer @ x = -7.6 mm, 100 pulses/burn, Δr/wp = 0.32.

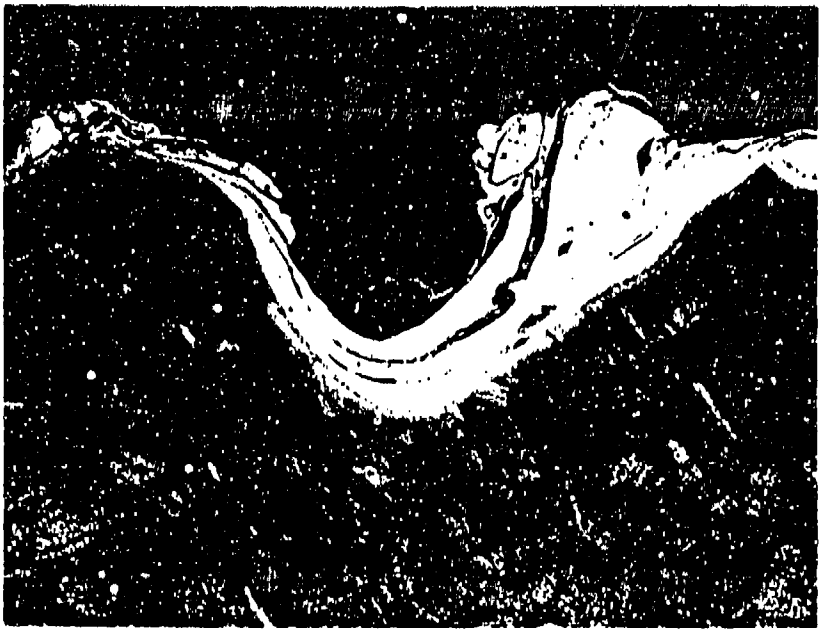

TEST #12 MAG. 100X

Figure 12. Laser parameters: θ = 140.1°, Two radial burns, 1st layer @ x = 0, 2nd layer @ x = -10.2 mm, 100 pulses/burn, $\Delta r/wp$ = 0.32.

TEST #13 MAG. 100X

Figure 13. Laser parameters: θ = 151.1°, Two radial burns, 1st layer @ x = 0, 2nd layer @ x = -12.7 mm, 100 pulses/burn, $\Delta r/wp$ = 0.32.

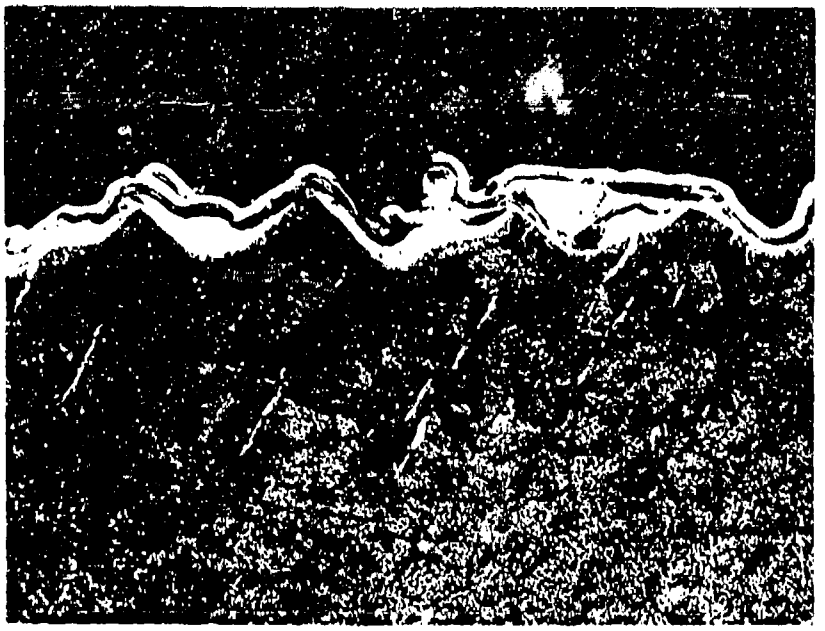

TEST #14 MAG. 100X

Figure 14. Laser parameters: θ = 162.2°, Two radial burns, 1st layer @ x = 0, 2nd layer @ x = -15.2 mm, 100 pulses/burn, Δr/wp = 0.32.

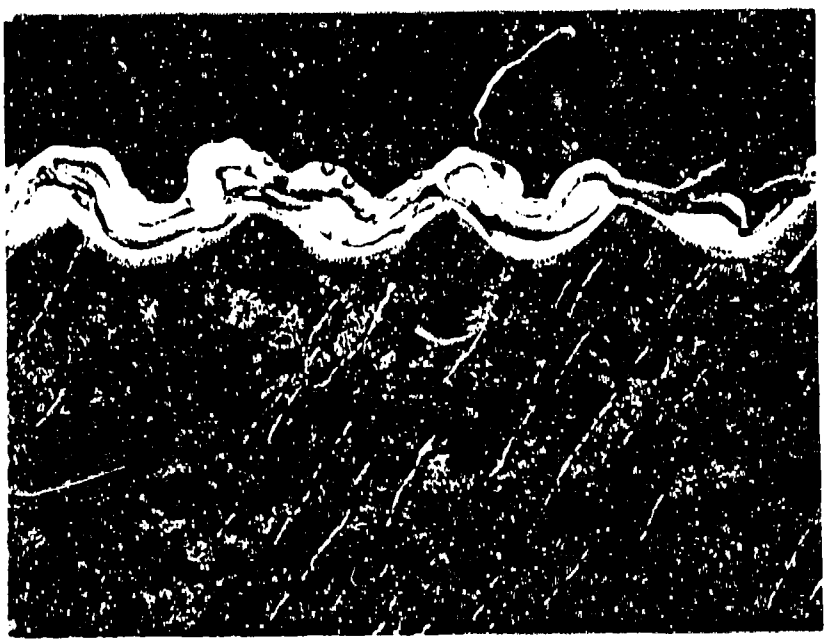

TEST #15 MAG. 100X

Figure 15. Laser parameters: θ = 173.2°, Two radial burns, 1st layer @ x = 0, 2nd layer @ x = -0.01 mm, 100 pulses/burn, Δr/wp = 0.32.

TEXTRON Lycoming

MATERIALS AND PROCESS TECHNOLOGY LABORATORIES

Subject: FATIGUE TESTING OF LASER TREATED VS HAND GROUND/BURNISHED AM355 TEST SPECIMENS.

Summary:

Load control fatigue test specimens were sent to Avco Everett Research Laboratory (AERL) for them to perform a laser balancing treatment on the gauge section in order to simulate conditions that might result from laser balancing an AGT1500 impeller. The task was conducted in order to compare base line AM355 fatigue data against data generated from the laser treated and hand ground/burnished specimens. Samples prepared by these techniques were tested by the Textron Lycoming Materials Laboratory under load control at 400 deg.F, with an "A" ratio of one (1.0) and a frequency of 2 Hz. Evaluation of the test results revealed that a similar fatigue debit was created by both the laser treated and hand ground/burnished methods when compared to base line AM355 fatigue.

Prepared By: P.M. Follo
P.M. Follo
Sr. Materials Engineer
Materials Testing Laboratory
Materials Technology Laboratories

Concurred By: R.E. Wilson
R.E. Wilson
Materials Testing Manager
Materials Technology Laboratories

Approved By: Louis J. Fiedler
Louis J. Fiedler
Director
Materials & Process Technology Laboratories

TEXTRON Lycoming

MATERIALS AND PROCESS TECHNOLOGY LABORATORIES

Subject: FATIGUE TESTING OF LASER TREATED VS HAND GROUND/BURNISHED AM355 TEST SPECIMENS.

References: MR0446 - EVALUATION OF LASER BALANCING PARAMETERS RELATIVE TO RECAST LAYER CHARACTERISTICS OF AM355

BACKGROUND:

Load control fatigue test specimens (Figure 1) were sent to Avco Everrett Research Laboratory (AERL) to perform a laser treatment on the gauge section of each specimen (Figure 2). The task was conducted in order to simulate conditions used to laser balance AGT1500 impellers and assess the magnitude of the fatigue debit created as a result of laser treatment. The laser parameters for these tests were chosen from preliminary data acquired previously to keep defects such as grooves and voids to a minimum (similar to Figure 4, MR0446). No attempt was made to eliminate the recast/heat affected zone characteristic of laser burns. A second set of test specimens (Figure 3) was prepared by Textron Lycoming using the conventional hand grinding/burnishing technique adapted for current balance operations per blueprint requirements. To produce a possible worst case, several specimens were tested in the as ground condition without burnishing (Figure 4). After all test specimens were prepared, the Textron Lycoming Materials Laboratory conducted low cycle fatigue tests on each specimen. The testing was conducted in support of contract number DAAE07-85-C-R163, Advanced Balancing/Machining Techniques.

Discussion:

Laser treated, hand ground and hand ground/burnished test specimens were subjected to low cycle fatigue testing to determine the fatigue debit created as a result of surface damage caused by the laser technique of material removal vs hand grinding. Each test was performed at 400 deg. F, with an "A" ratio of one (1.0) and a frequency of 2 Hz. The results of each test are summarized in table (1,2,3). Plots of the laser treated and hand ground/burnished data are presented on Figure 5 and 6. Scanning Electron Microscope (SEM) photomicrographs are presented in Figures (7,8,9) revealing a typical fracture surface with multiple surface origins created as a result of each material removal condition. A failed test specimen was also sectioned longitudinally through the fracture surface, metallographically prepared and etched in 10% Hydrofluoric Acid (HF) in water to reveal the recast layer/heat affected zone (Figure 10) produced by the laser treatment.

Evaluation of fatigue data presented in tables 1, 2 and 3 revealed that the fatigue life of the laser treated and hand ground/burnished test bars falls between the design data curves for a smooth bar (Kt = 1.0) and a

test bar containing a notch factor of 3.5 Kt (Figure 11). The as hand ground test samples revealed a significant reduction in fatigue life and are only shown here as a possible worst case for comparison purposes only. The laser balancing parameters used in this evaluation, were chosen to create the least amount of damage possible keeping the surface free of voids, grooves and as thin a recast layer as possible. It is not known, relative to the tests performed to date, what effect various recast layer thicknesses have on fatigue life nor has any attempt been made to evaluate the other parameters presented in MR0446.

CONCLUSION/RECOMMENDATIONS:

Evaluation of the test results revealed that a nominal 35% fatigue debit was created as a result of laser treatment. It is, however, concluded that this debit is insufficient to disallow the process, especially, if balancing is performed in low stress areas of the part. To further understand the laser method of material removal and its effects on engine componenet life, a more exact correlation is recommended to be made between the component and fatigue test bar. For the interim, it is recommended that Structural Integrity use the notch fatigue curve (Kt = 3.5) to estimate the fatigue debit due to ground/burnished or laser balanced surfaces.

TABLE 1
LASER TREATED TEST BARS

Test #	Max Stress (Ksi)	Cycles To Failure
7450	167	11520
7452	173	13880
7453	173	10580
7454	163	12420
7524	150	10300
7525	150	10090
7526	150	11980
7528	140	13760
7529	140	20470
7530	140	12520
7531	130	20920
7532	130	15010
7533	110	37290
7534	110	34050
7537	100	137300
7535	90	1000000 nf
7536	90	1000000 nf

nf = no failure

TABLE 2
HAND GROUND/BURNISHED TEST BARS

Test #	Max Stress (Ksi)	Cycles to Failure
7483	160	10280
7538	150	13730
7539	150	12070
7540	150	16730
7541	140	18970
7542	140	15780
7543	140	16190
7544	130	19020
7545	130	22070
7485	120	23130
7546	110	35860
7547	110	45780
7548	100	1000000 nf
7549	100	1000000 nf

nf = no failure

TABLE 3
HAND GROUND TEST BARS

Test #	Max Stress (Ksi)	Cycles To Failure
7468	160	3150
7469	160	5510
7470	160	7340
7471	160	4340

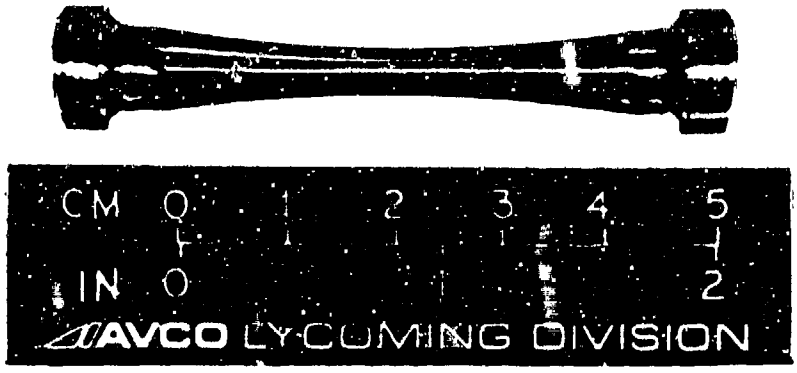

Mag. 1.5X

Figure 1. Overall view of AM355 Load Control/Low cycle fatigue test bar.

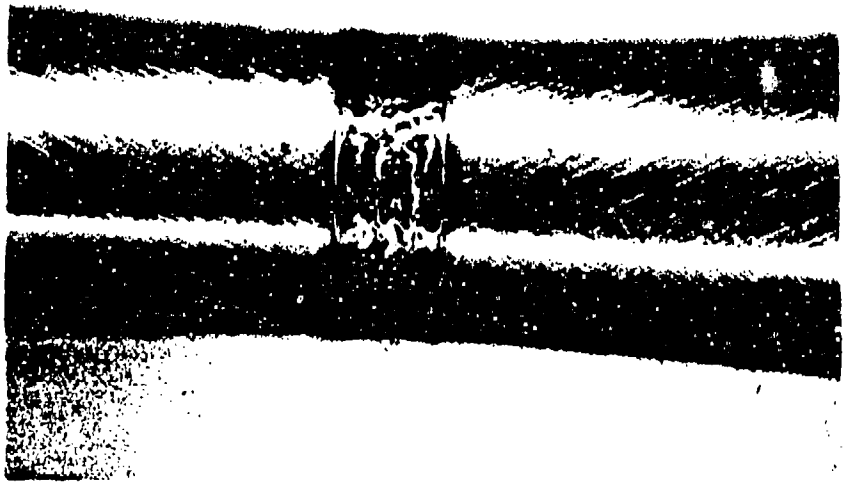

Mag. 10X

Figure 2. Laser treated AM355 fatigue test bar.

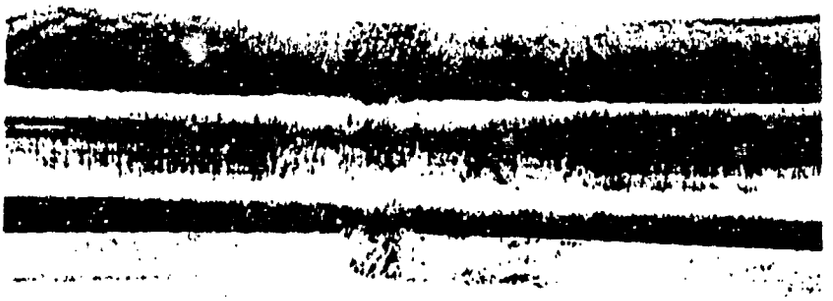

Mag. 10X

Figure 3. Typical hand ground/burnished AM355 fatigue test bar.

Mag. 15X

Figure 4. Typical as ground AM350 fatigue test bar.

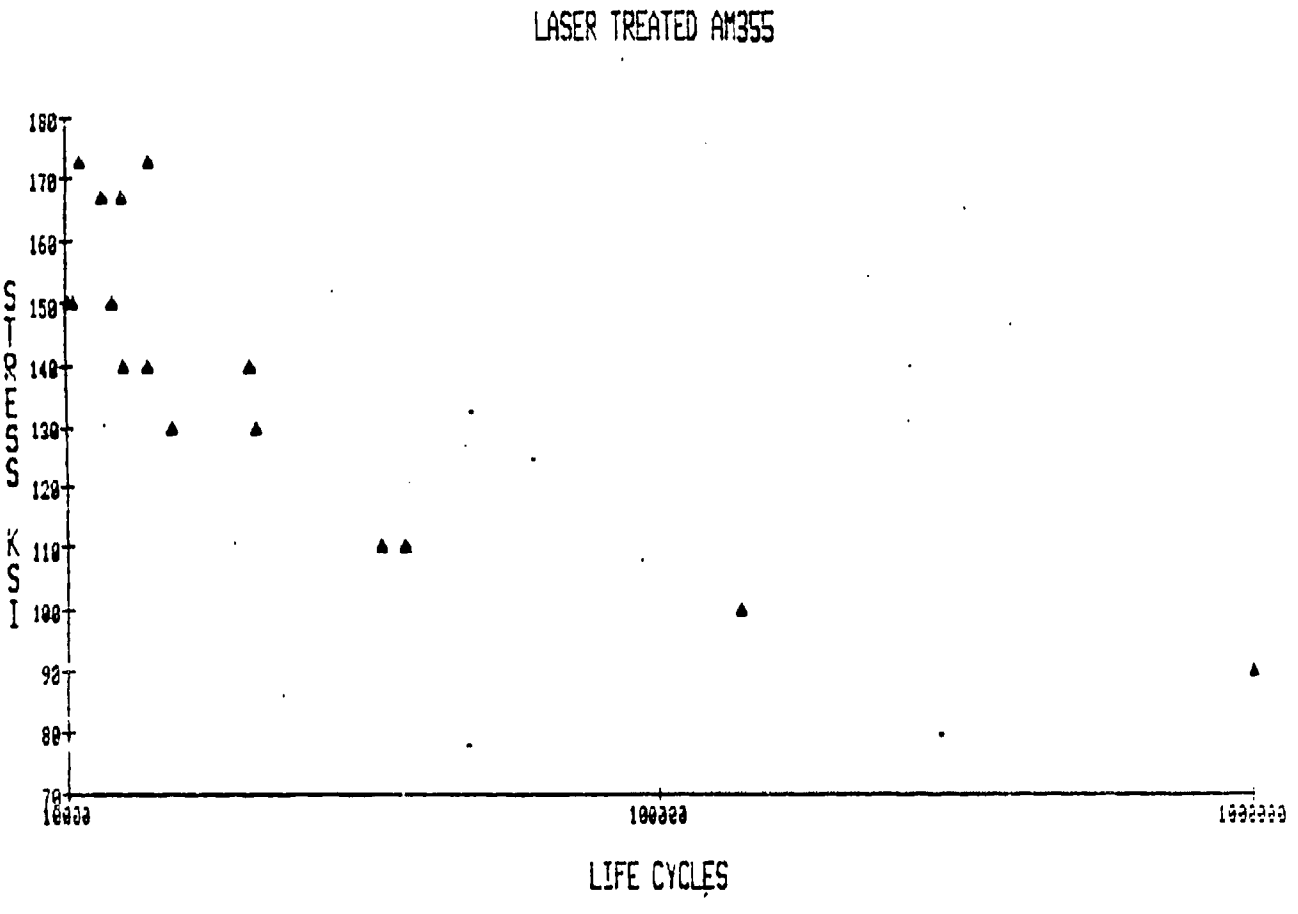
LASER TREATED AM355
STRESS KSI
180
170
160
150
140
130
120
110
100
90
80
70
100000
LIFE CYCLES

FIGURE 5

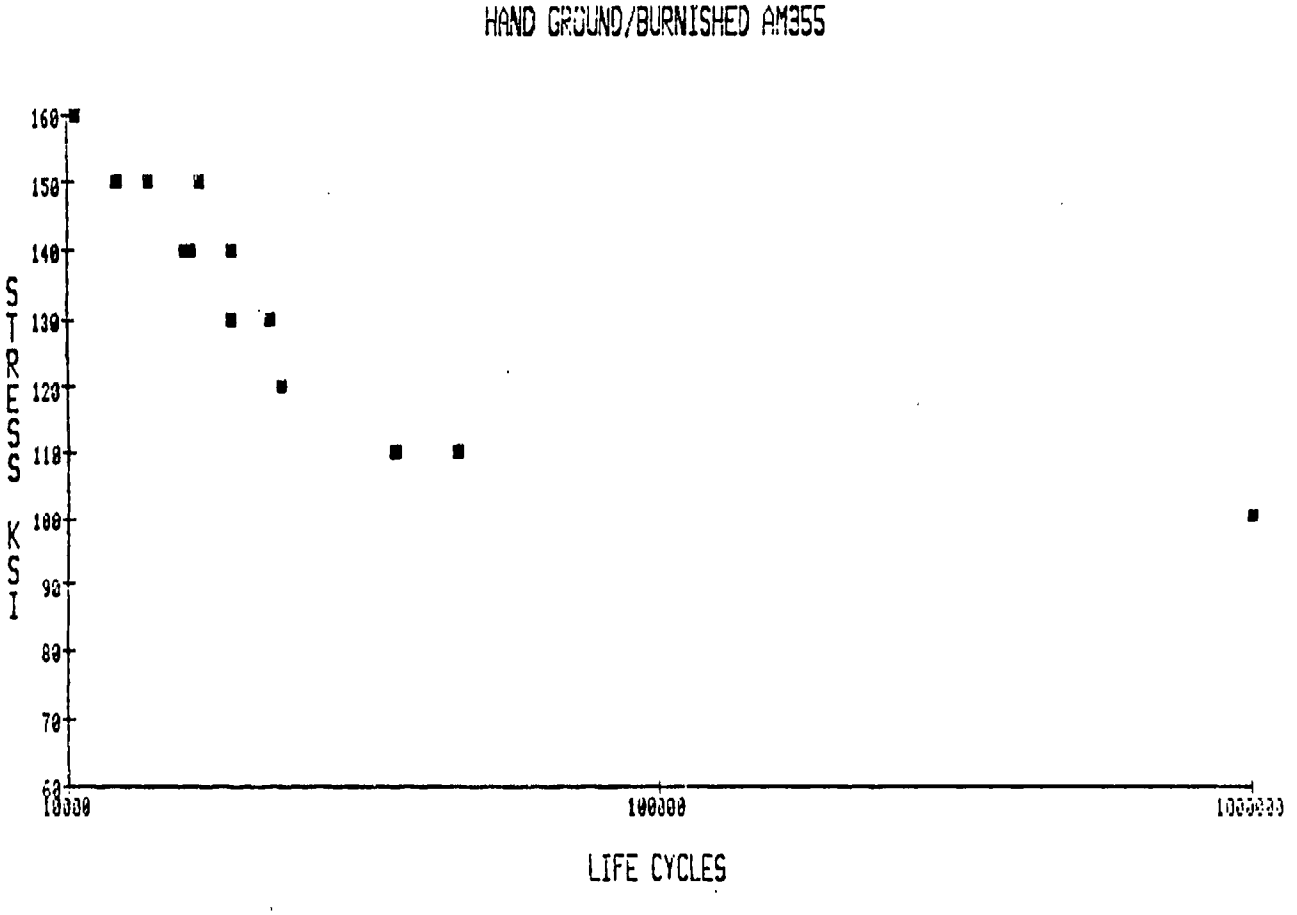
HAND GROUND/BURNISHED AM355
STRESS KSI
160
150
140
130
120
110
100
90
80
70
60
10000
100000
1000000
LIFE CYCLES

Figure 6

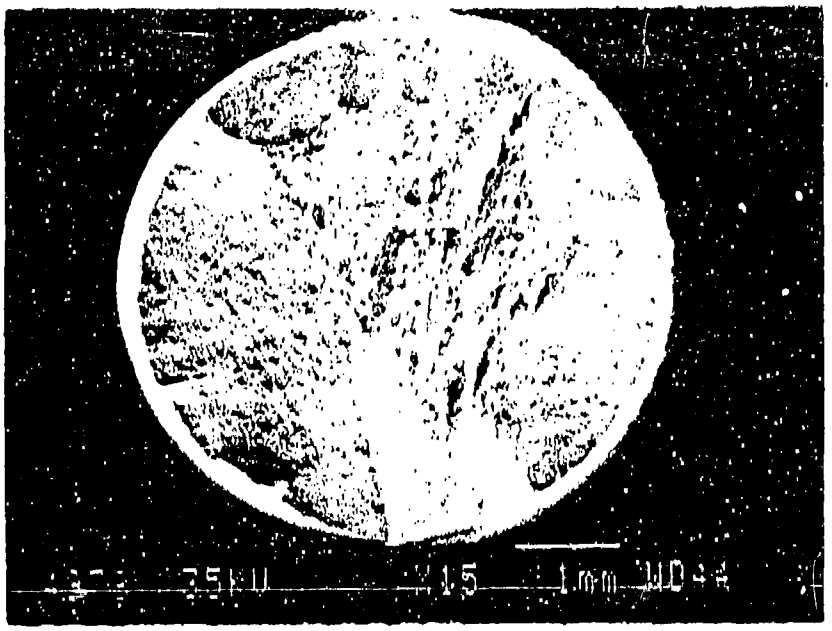

Mag. 15X

Figure 7. SEM photograph of the fracture surface of a laser treated test bar.

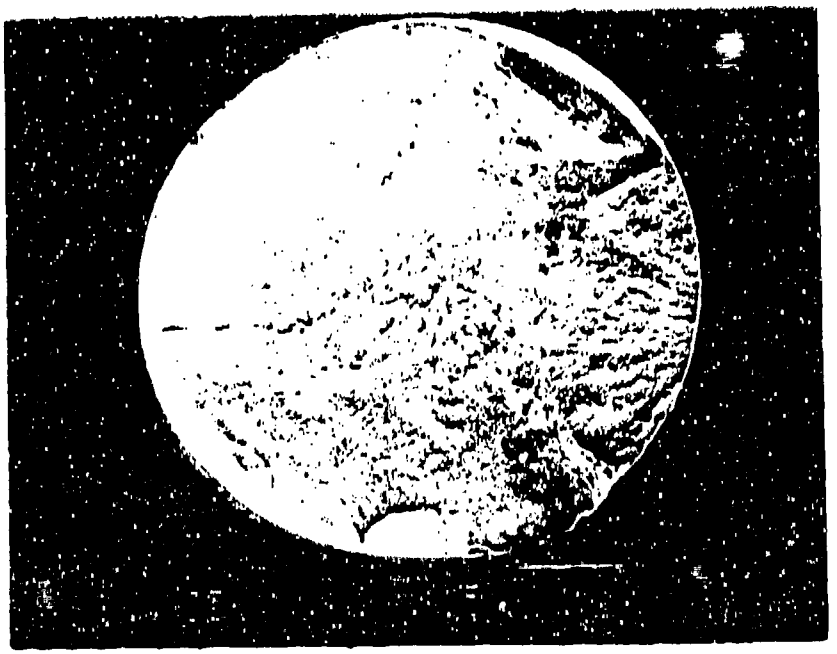

Mag. 15X

Figure 8. SEM photograph of the fracture surface of a hand ground/ burnished test bar.

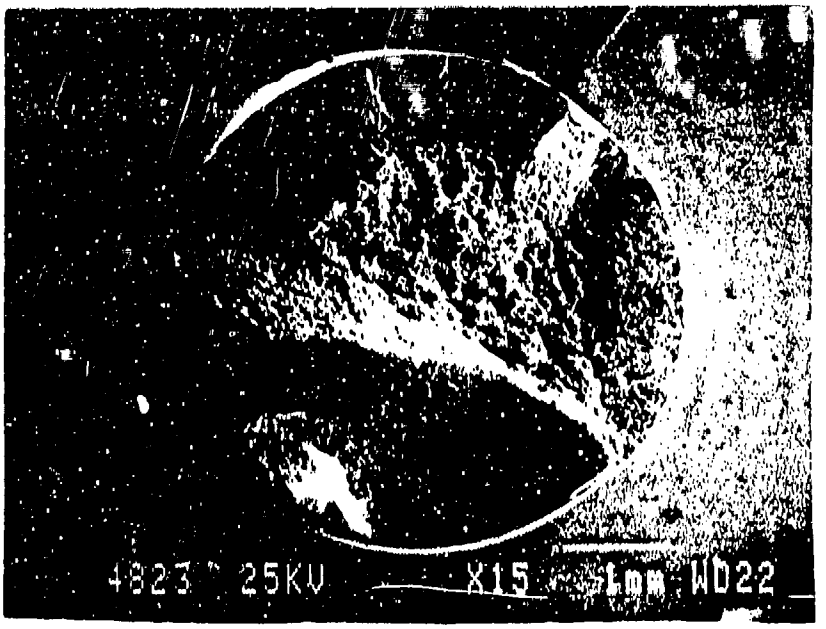

Mag. 15X

Figure 9. SEM photograph of the fracture surface of a hand ground test bar.

Mag. 100X

Figure 10. Optical photomicrograph of a metallographically prepared failed AM355 test bar showing the recast/heat affected zone near the fracture surface.

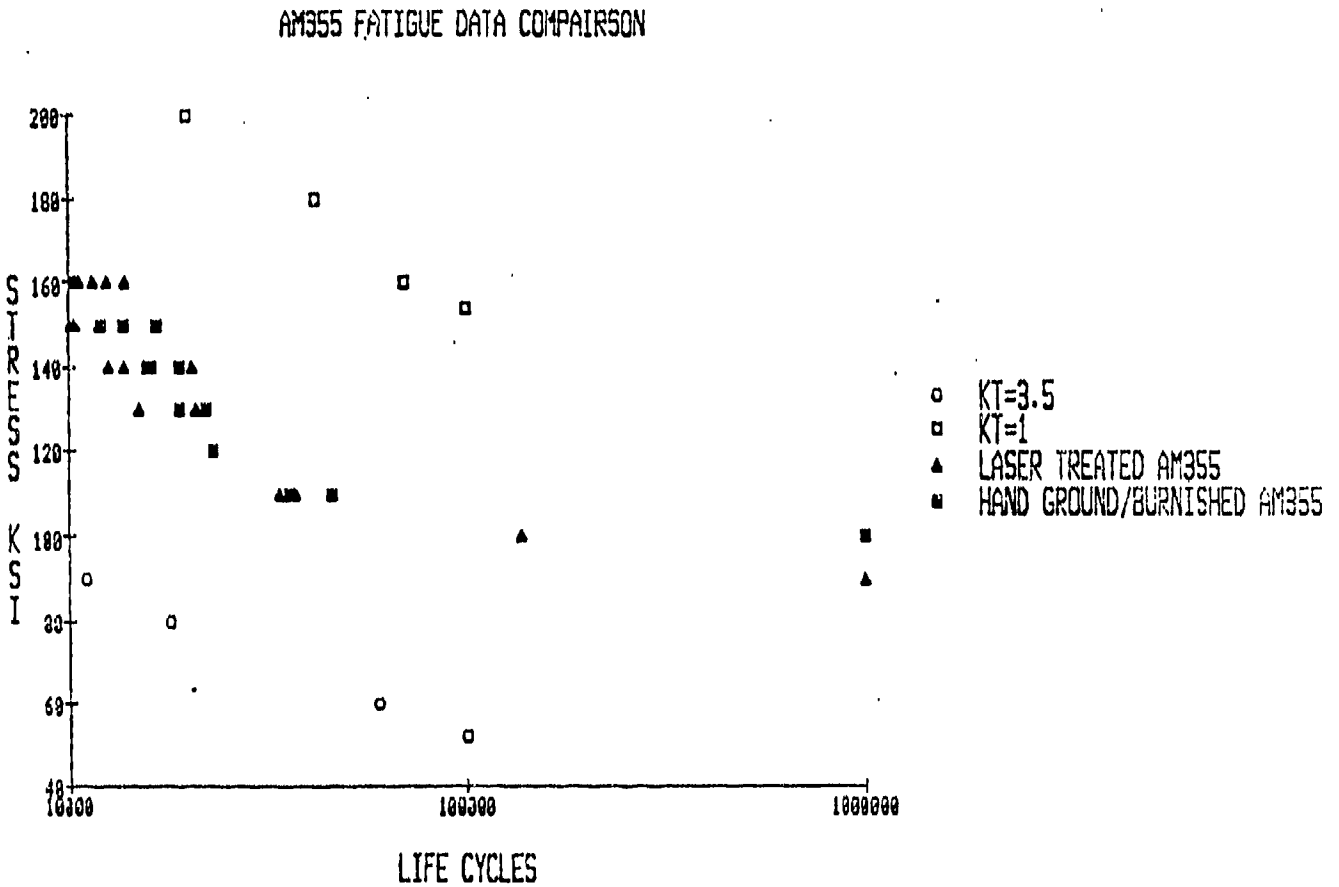
AM355 FATIGUE DATA COMPAIRSON
STRESS KSI
200
180
160
140
120
100
80
60
40
10000
100000
1000000
LIFE CYCLES
KT=3.5
KT=1
LASER TREATED AM355
HAND GROUND/BURNISHED AM355

Figure 11

LASER-BALANCING SYSTEM ABERRANT BEHAVIOR AND SUBSEQUENT CORRECTIVE ACTION

H.M. Eppich
Avco Research Laboratory, Inc.
April 5, 1989

Figure 1 shows the unbalance vector behavior observed during the 17 December 1987 demonstration. This demonstration failed since the residual unbalance (0.92 gm-in) was greater than the specified tolerance (0.5 gm-in). The consistent counterclockwise rotation of the unbalance vector after removal of each layer of material implies that the laser was not firing at the correct angle. The firing angle error has been estimated to be approximately -11°. This erroneous firing angle offset resulted in the failure of the system to produce a balanced component. Speculations on how this error was introduced follow immediately.

On 15 December 1987, one of the two days allocated to prepare the system and a presentation for the 17 December 1987 demonstration, the system exhibited inconsistent behavior during preparation balancing trials. The behavior of the system on 15 December 1987 was similar to that observed during the 17 December 1987 demonstration, yielding similar results, yet was much more erratic than system troubleshooting tests conducted after 17 December 1987 indicated. For this reason, it is argued that the aberrant behavior observed on 15 and 17 December 1987 may have unrelated origins, and that the corrective steps taken on 16 December 1987 removed the origin of the 15 December 1987 problem, but introduced another problem which led to the demonstration failure on 17 December 1987. It has become apparent that the origin of the problem encountered on 15 December 1987 will never be resolved. Troubleshooting tests

and balance machine calibrations performed immediately after the 17 December 1987 demonstration and just prior to the 24 February 1989 demonstration, however, provide a fairly clear indication of the source of the aberrant behavior encountered on 17 December 1987.

After encountering difficulties on 15 December 1987, the Gisholt balance machine was recalibrated on 16 December 1987, with special attention given to unbalance angle definition. As part of this procedure, the silvered photodiode trigger tape on the balance arbor was replaced, and the two photodiodes, which trigger off the silver tape on the arbor and thereby provide angular position references, were repositioned to the specified photodiode/arbor clearance. This last adjustment may have fixed the problem encountered on 15 December 1987, because it has been learned subsequently that photodiode/arbor clearance can affect laser triggering repeatability/accuracy.

Balancing trials conducted on 16 December 1987, subsequent to the calibration and adjustments outlined above, produced B-plant residual unbalances within specification (< 0.5 gm-in), but the firing angle correction determined during removal of the first layer of material was found to be quite large (> 10°) for each of these trials. Since the system was producing residual unbalances within specification and time was running out, the decision was made to perform the final demonstration with the system as operating. In retrospect, the 17 December 1987 final demonstration should have been postponed until all system peculiarities had been resolved, which was emphasized subsequently by the outcome of the final demonstration.

Preliminary troubleshooting tests conducted after the failed 17 December 1987 demonstration suggested that the Gisholt balance machine seemed to be the most likely source of the problem. Based on the results of a thorough checkout and calibration of the Gisholt balance machine and BP-2020 electronics unit, it was concluded that the balance machine was and had been performing fine.

During its checkout, the Gisholt service technician pointed out that the balance machine BP-2020 electronics unit was set up to trigger off the trailing edge of the silvered tape attached to the balance arbor as it passed by the photodiode. The ARL personnel responsible for calibrating the Gisholt balance were not aware of this subtlety, and had assumed that the balance machine electronics triggered off the leading edge of the silvered tape. Since the arc length of the silvered tape corresponds to approximately 30°, this oversight introduced an initial angular error, with respect to laser firing angle, of 30°.

This is illustrated more clearly by referring to Viewgraph 23 which is attached and follows Figure 1. When calibrating the balance machine, a known mass is attached to the impeller at a known radial and angular location. When ARL personnel calibrated the machine on 16 December 1987, a known mass was attached to the impeller on a radial line passing through the leading edge of the silvered tape, and its angular location was specified as 0°. Since the balance machine triggers off the trailing edge, which is really the 0° angular reference point, the leading edge of the silvered tape corresponds to a balance machine referred angle of approximately 330°, due to the finite length of the silvered tape. Since the laser triggers off the leading edge of the silvered tape, which was intended to be the 0° reference point, the laser was actually firing 30° from the true unbalance location. Hence, a firing angle error of approximately 30° was imposed on the procedure at the beginning of the 17 December 1987 demonstration. Although the balance algorithm tried to compensate for this, it could not accurately, which resulted in the failed demonstration.

The reason the algorithm could not accurately compensate will be discussed shortly, but first the remedy for the discrepancy between laser and balance machine trigger references will be explained. Rather than resetting the balance machine BP-2020 electronics unit so that it triggers off the leading edge of the silvered tape, which is possible, an equally effective and very simple solution was to reduce the arc length of the silvered tape so that the angular difference between leading and trailing edges is negligible. This approach, which is shown in the bottom sketch in Viewgraph 23, proved satisfactory and was used during the successful 24 February 1989 demonstration.

The reason the balance algorithm could not recover from the large initial firing angle error now follows. If R_o is the initial unbalance, ΔR the unbalance reduction due to removal of the first half of the first layer of material, $\Delta\theta$ the uncertainty associated with the unbalance angular location reported by the balance machine, and $\Delta\theta_c$ the uncertainty in the computed firing angle correction determined by the algorithm from unbalance changes resulting from removal of the first half of the first layer of material, the firing angle correction uncertainty can be shown to be $\Delta\theta_c \approx (R_o/\Delta R)\ \Delta\theta$. For the 17 December 1987 demonstration $R_o/\Delta R \approx 16$, so there was considerable uncertainty in θ_c, which is the correction that must be applied to all firing angles to guarantee that the laser is firing at the true angular location of the unbalance.

In prior versions of the balance algorithm, the firing angle correction was updated after removal of each layer of material. In which case $\Delta\theta_c^i = (R_i/\Delta R_i)\ \Delta\theta$, where i is the index of the layer of material just removed. Upon approaching the last layer of material to remove $R_i/\Delta R_i \rightarrow 1$. Hence the uncertainty in the correction angle decreases substantially as the bal-

arcing process nears completion. The updating of the firing angle correction after removal of each layer of material was not included in the current version of the balance algorithm. It was felt that it was not needed, which was based on observed balance process behavior, and as an attempt to reduce computational overhead. As it exists now, the firing angle correction is computed only once. This is done after removal of the first half of the first layer of material, and is utilized during the remainder of the balancing operation.

The reason the 17 December 1987 demonstration failed was the result of the angle error introduced due to improper calibration of the balance machine, which was large (~ 30°); the inability of the balance algorithm to accurately resolve the firing angle correction (θ_c), which was needed to compensate for the angle error introduced by improper balance machine calibration; and elimination of the code that updates the firing angle correction after removal of each layer of material. If the code that updates the firing angle correction had not been eliminated, the 17 December 1987 demonstration would not have ended in failure. Now that a better appreciation of its importance has been obtained, this code should be part of any future balance algorithm.

Two corrective action steps were taken prior to the 24 February 1989 demonstration. First, the balance machine was properly calibrated, making sure the balance machine and laser were being triggered off the same point on the silvered tape attached to the balance arbor. This was done by reducing the arc length of the silvered tape to the point where the angular difference between the leading and trailing edges was negligible. Second, the uncertainty in the firing angle correction was reduced, which was done in the following way. As indicated above, the uncertainty in the firing angle correction (θ_c) is $\Delta\theta_c \approx (R_o/\Delta R)\,\Delta\theta$. The uncertainty $\Delta\theta_c$ can be reduced, therefore, by reducing the uncertainty in $\Delta\theta$. In the current version of the balance algo-

rithm, each time a new value for the unbalance angle is required, the algorithm reads from the balance machine BP-2020 display n sequential, discrete values. The unbalance magnitude and angular location used by the algorithm is the average over the n readings. The uncertainty ($\Delta\theta$) in the angular location of the unbalance ($\Delta\theta$) decreases, therefore, as the number of readings (n) is increased. For the 17 December 1987 demonstration, a value of n = 3 was used, whereas a value of n = 6 was used for the 24 February 1989 demonstration.

Implementing these two simple changes produced outstanding laser balancing process performance, which resulted in very successful demonstrations on 24 February 1989. Viewgraph 22 of the 24 February 1989 presentation is attached also, which provides a summary of problem, reason, and corrective action taken regarding the 17 December 1987 demonstration.

View Graph 22

ABERRANT BEHAVIOR OBSERVED DURING DECEMBER 1987 DEMONSTRATION

- PROBLEM: RESIDUAL IMBALANCE (1 GM-IN.) > 0.5 GM-IN.
- REASON: COMBINATION OF EFFECTS
  - IMPROPER BALANCE MACHINE CALIBRATION INTRODUCED A $20\text{-}30^{0}$ ANGLE ERROR
  - MODEST INITIAL IMBALANCE, R_0 ~ 9 GM-IN.
  - CORRECTION ANGLE UNCERTAINTY SCALES AS:

    $$\Delta\theta_C \approx (R_0/\Delta R)\,\Delta\theta \ , \ R = \text{IMBALANCE MOMENT}$$

  - CORRECTION ANGLE UPDATE HAD BEEN REMOVED FROM ALGORITHM
- CORRECTIVE ACTION:
  - PROPER BALANCE MACHINE CALIBRATION
  - REDUCED UNCERTAINTY IN $\Delta\theta$
  - IN FUTURE, INCLUDE θ_C UPDATE PROCEDURE

17 Dec. 1987 B-Plane Balance
Demonstration Failure

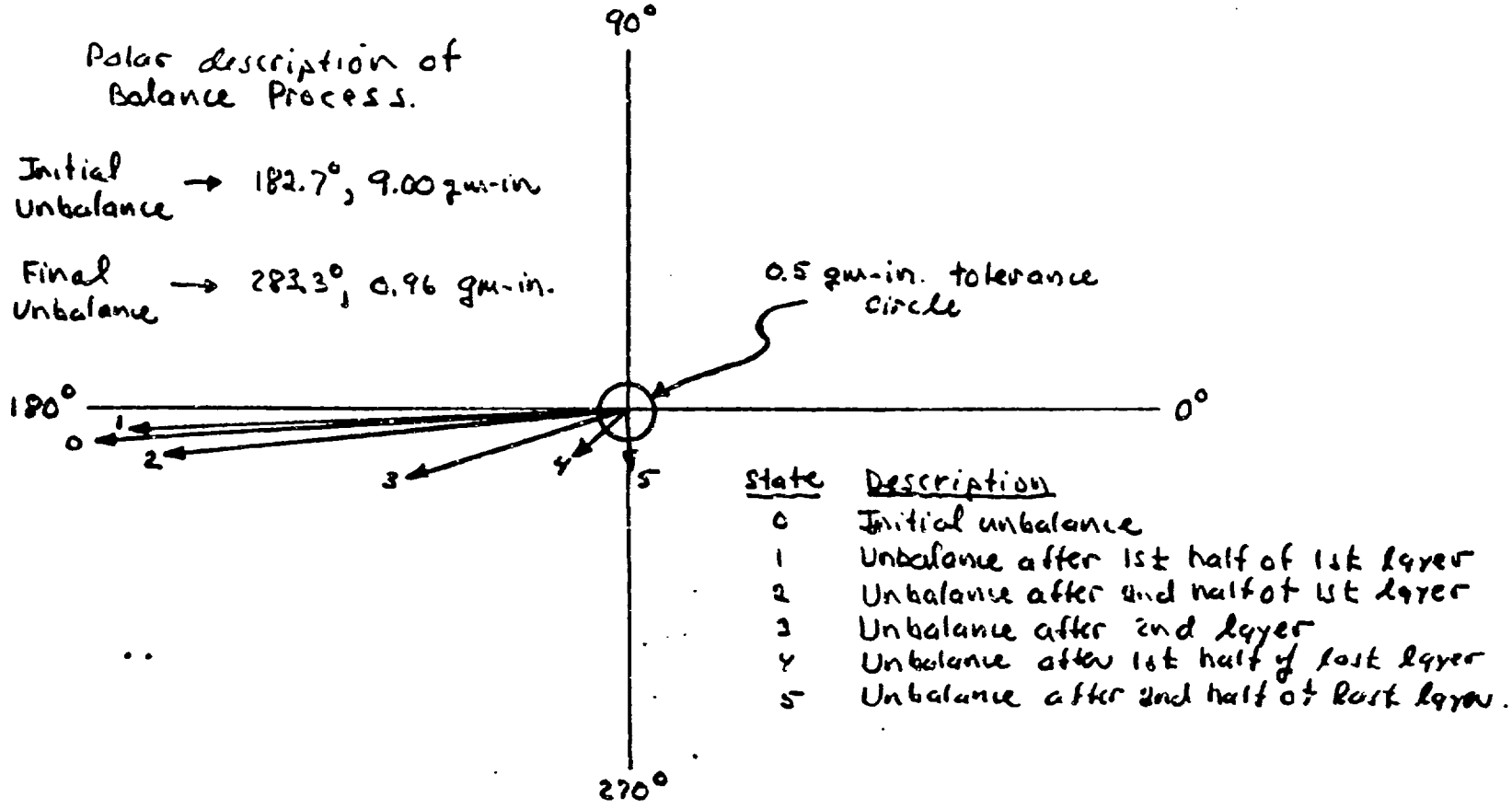

Figure 1. Behavior of unbalance vector during 17 Dec 1987 Balance demonstration.

View Graph 23

BALANCE MACHINE CALIBRATION PROBLEM

- BALANCE MACHINE USES TRAILING EDGE

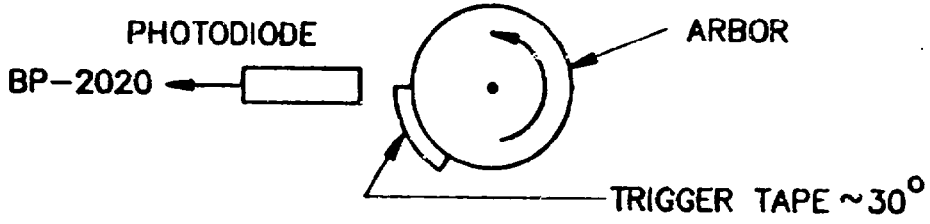

- LASER SYSTEM USES LEADING EDGE

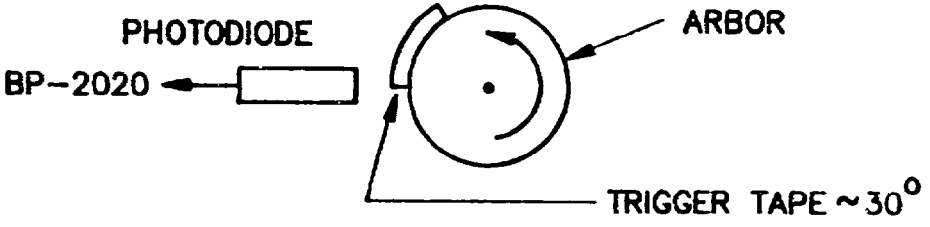

- SIMPLE SOLUTION: REDUCE ARC LENGTH OF TRIGGER TAPE

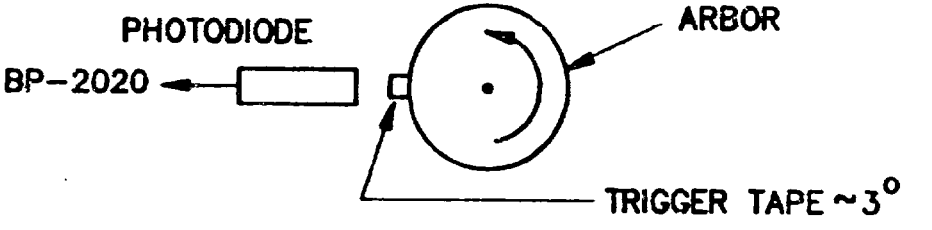

DISTRIBUTION LIST

Commander 44
U.S. Army Tank-Automotive Command
ATTN: AMSTA-TMM
Warren, MI 48397-5000